



Measurement of b -quark fragmentation properties in jets using the decay $B^\pm \rightarrow J/\psi K^\pm$ in pp collisions at $\sqrt{s} = 13$ TeV with the ATLAS detector

The ATLAS Collaboration

The fragmentation properties of jets containing b -hadrons are studied using charged B mesons in 139 fb^{-1} of pp collisions at $\sqrt{s} = 13$ TeV, recorded with the ATLAS detector at the LHC during the period from 2015 to 2018. The B mesons are reconstructed using the decay of B^\pm into $J/\psi K^\pm$, with the J/ψ decaying into a pair of muons. Jets are reconstructed using the anti- k_t algorithm with radius parameter $R = 0.4$. The measurement determines the longitudinal and transverse momentum profiles of the reconstructed B hadrons with respect to the axes of the jets to which they are geometrically associated. These distributions are measured in intervals of the jet transverse momentum, ranging from 50 GeV to above 100 GeV. The results are corrected for detector effects and compared with several Monte Carlo predictions using different parton shower and hadronisation models. The results for the longitudinal and transverse profiles provide useful inputs to improve the description of heavy-flavour fragmentation in jets.

Contents

1	Introduction	3
2	The ATLAS detector	4
3	Data and Monte Carlo samples	5
4	Object and event selection	6
5	Signal extraction	9
6	Unfolding to particle level	13
7	Systematic uncertainties	15
8	Results	19
9	Summary and conclusions	23

1 Introduction

The fragmentation of heavy quarks is a crucial aspect of quantum chromodynamics (QCD). Detailed studies and precision measurements of the heavy-quark fragmentation properties allow a deeper understanding of QCD. Furthermore, reliable modelling of the fragmentation is of great importance for measurements of the production of Higgs bosons [1, 2], top quarks [3, 4] and their associated production [5, 6], whose hadronic decays predominantly feature heavy quarks. Uncertainties related to the modelling of the fragmentation processes of b -quarks into hadrons are significant in the most precise top quark mass determinations [7–11], and are also the subject of theoretical study [12–15]. This subject has been studied in e^+e^- collisions for charm [16–19] and bottom quarks [20–24]. In hadron–hadron collisions, measurements of observables sensitive to the heavy-flavour fragmentation functions have been reported for D^* mesons [25–27], D^0 mesons [28] and J/ψ quarkonia [29].

The Monte Carlo (MC) predictions used at the LHC are tuned to describe the measurements in e^+e^- collisions at relatively low centre-of-mass energies. Therefore, new measurements of b -quark fragmentation can be used to improve the MC simulation at LHC energy scales.

This analysis presents a measurement of the fragmentation of b -quarks into charged B mesons using the ATLAS full Run 2 dataset, containing 139 fb^{-1} of pp collisions at $\sqrt{s} = 13 \text{ TeV}$. To this end, the B^\pm meson is reconstructed using the decay chain $B^\pm \rightarrow J/\psi K^\pm \rightarrow \mu^+\mu^- K^\pm$. The procedure is similar to those in previous ATLAS measurements involving $B^\pm \rightarrow J/\psi K^\pm$ final states [30, 31]. Jets are reconstructed using the anti- k_r algorithm with radius parameter $R = 0.4$. The reconstructed B mesons are matched to jets and the longitudinal and transverse momentum profiles, z and p_T^{rel} , are defined as

$$z = \frac{\vec{p}_B \cdot \vec{p}_j}{|\vec{p}_j|^2}; \quad p_T^{\text{rel}} = \frac{|\vec{p}_B \times \vec{p}_j|}{|\vec{p}_j|},$$

where \vec{p}_B is the three-momentum of the B hadron and \vec{p}_j is the three-momentum of the jet. The longitudinal profile, z , quantifies the fraction of the jet momentum carried by the B meson in the direction parallel to the jet axis. On the other hand, the transverse profile, p_T^{rel} , quantifies the momentum of the B meson in the direction orthogonal to the jet axis. These variables are sensitive to the fragmentation function $D_q^h(x, Q^2)$, which is defined as the probability of a quark q to fragment into a hadron h with an energy fraction x at a scale Q [32, 33]. The measurement is performed in different intervals of the jet transverse momentum, which provides a probe of the scaling of the fragmentation functions. Furthermore, as discussed in the following, these observables are also sensitive to the contributions of gluons producing a $b\bar{b}$ pair. Since, in many cases, $b\bar{b}$ pairs arising from the splitting of high- p_T gluons are not resolved into two different jets, the reconstructed B meson carries a smaller fraction of the jet energy, resulting in a flatter distribution of z and p_T^{rel} compared to jets with a single hard-scattering b -quark.

The paper is structured as follows. Section 2 is dedicated to the description of the ATLAS detector. A summary of the MC samples and the dataset used throughout the analysis is included in Section 3, and the object and event selection is described in detail in Section 4. Section 5 is dedicated to the estimation of the purity corrections, while a discussion of the subsequent corrections for detector effects is found in Section 6. The uncertainties affecting this measurement are discussed in Section 7 and the results are presented in Section 8. Section 9 provides the summary and conclusions.

2 The ATLAS detector

The ATLAS detector [34] at the LHC covers nearly the entire solid angle around the collision point.¹ It consists of an inner tracking detector surrounded by a thin superconducting solenoid, electromagnetic and hadronic calorimeters, and a muon spectrometer incorporating three large superconducting toroidal magnets with eight coils each.

The inner-detector system is immersed in a 2 T axial magnetic field and provides charged-particle tracking in the range $|\eta| < 2.5$. The high-granularity silicon pixel detector covers the vertex region and typically provides four measurements per track, the first hit normally being in the insertable B-layer installed before Run 2 [35, 36]. It is followed by the silicon microstrip tracker, which usually provides eight measurements per track. These silicon detectors are complemented by the transition radiation tracker (TRT), which enables radially extended track reconstruction up to $|\eta| = 2.0$. The TRT also provides electron identification information based on the fraction of hits (typically 30 in total) above a higher energy-deposit threshold corresponding to transition radiation.

The calorimeter system covers the pseudorapidity range $|\eta| < 4.9$. Within the region $|\eta| < 3.2$, electromagnetic calorimetry is provided by barrel and endcap high-granularity lead/liquid-argon (LAr) calorimeters, with an additional thin LAr presampler covering $|\eta| < 1.8$ to correct for energy loss in material upstream of the calorimeters. Hadronic calorimetry is provided by the steel/scintillator-tile calorimeter, segmented into three barrel structures within $|\eta| < 1.7$, and two copper/LAr hadronic endcap calorimeters. The solid angle coverage is completed with forward copper/LAr and tungsten/LAr calorimeter modules optimised for electromagnetic and hadronic measurements respectively.

The muon spectrometer comprises separate trigger and high-precision tracking chambers measuring the deflection of muons in a magnetic field generated by the superconducting air-core toroids. The field integral of the toroids ranges between 2.0 and 6.0 T m across most of the detector. A set of precision chambers covers the region $|\eta| < 2.7$ with three layers of monitored drift tubes, complemented by cathode-strip chambers in the forward region, where the background is highest. The muon trigger system covers the range $|\eta| < 2.4$ with resistive-plate chambers in the barrel, and thin-gap chambers in the endcap regions.

Interesting events are selected to be recorded by the first-level trigger system implemented in custom hardware, followed by selections made by algorithms implemented in software in the high-level trigger [37]. The first-level trigger accepts events from the 40 MHz bunch crossings at a rate below 100 kHz, which the high-level trigger reduces in order to record events to disk at about 1 kHz.

An extensive software suite [38] is used in the reconstruction and analysis of real and simulated data, in detector operations, and in the trigger and data acquisition systems of the experiment.

¹ ATLAS uses a right-handed coordinate system with its origin at the nominal interaction point (IP) in the centre of the detector and the z -axis along the beam pipe. The x -axis points from the IP to the centre of the LHC ring, and the y -axis points upwards. Cylindrical coordinates (r, ϕ) are used in the transverse plane, ϕ being the azimuthal angle around the z -axis. The pseudorapidity is defined in terms of the polar angle θ as $\eta = -\ln \tan(\theta/2)$. Angular distance is measured in units of $\Delta R \equiv \sqrt{(\Delta\eta)^2 + (\Delta\phi)^2}$.

3 Data and Monte Carlo samples

The dataset used in this analysis comprises the data taken from 2015 to 2018 at a centre-of-mass energy of $\sqrt{s} = 13$ TeV. After applying quality criteria to ensure good ATLAS detector operation [39], the total integrated luminosity used in this analysis is 139 fb^{-1} [40, 41]. The uncertainty in the combined 2015–2018 integrated luminosity is 1.7% [40], obtained using the LUCID-2 detector [42] for the primary luminosity measurements. The measurements of the fragmentation properties are unaffected by this uncertainty, given that they are normalised to the total cross section, thus cancelling out the contribution of the luminosity uncertainty. The average number of inelastic pp interactions produced per bunch crossing for the dataset considered, hereafter referred to as ‘pile-up’, is $\langle\mu\rangle = 33.6$.

Several different models of multijet production are used in this analysis. The MC samples were generated using the PYTHIA 8 [43, 44], SHERPA [45], and HERWIG 7 [46–48] generators. These models differ in the matrix element (ME) calculation, the parton shower (PS) and the hadronisation model (HM). The main features of these samples are summarised in Table 1.

The PYTHIA 8 samples were generated using PYTHIA 8.240. The matrix element was calculated at leading order for the $2 \rightarrow 2$ process. The PS algorithm includes initial- and final-state radiation based on the dipole-style p_T -ordered evolution, including $g \rightarrow q\bar{q}$ branchings and a detailed treatment of the colour connections between partons [43]. The renormalisation and factorisation scales were set to the geometric mean of the squared transverse masses of the two outgoing particles (labelled 3 and 4), i.e.

$$\mu_r^2 = \mu_f^2 = \sqrt{m_{T3}^2 \cdot m_{T4}^2} = \sqrt{(p_T^2 + m_3^2) \cdot (p_T^2 + m_4^2)}.$$

Two different sets of hadronisation and underlying-event parameter values (tunes) were used in the generation of the PYTHIA 8 samples. Two of the samples make use of the ATLAS A14 tune [49], for which the CTEQ6L1 PDF set [50] was used for the ME generation, the PS, and the simulation of multi-parton interactions (MPI). Two additional samples make use of the Monash tune [51], interfaced to the NNPDF2.3LO PDF set [52] for the ME generation, PS and MPI. The hadronisation is modelled using the Lund string model [53, 54] in all samples. The two samples using the A14 tune make use of the Lund–Bowler parameterisation of the fragmentation function [55], differing in the value of the parameter r_b , which controls the shape of the fragmentation function for b -quarks: while the first of them uses the nominal value $r_b = 0.855$, the second one uses the so-called A14-RB tune, for which $r_b = 1.05$, as obtained from a combined fit to LEP and SLD data [20–23]. The two samples using the Monash tune make use of the Peterson [56] and Lund–Bowler [55] parameterisations for the fragmentation functions, where the r_b parameter is set to $r_b = 0.855$ for the Lund–Bowler sample. The PYTHIA 8 sample making use of the A14-RB tune is taken as the nominal MC sample, used across the analysis for unfolding and uncertainty estimation.

The SHERPA samples were generated using SHERPA 2.2.5. The matrix element was calculated at leading order (LO) for the $2 \rightarrow 2$ process, and the default SHERPA CSS dipole PS [57, 58]. Matrix element renormalisation and factorisation scales for $2 \rightarrow 2$ processes were set to the harmonic mean of the Mandelstam variables s , t and u [59]. The CT14NNLO [60] PDF set was used for the matrix element calculation, as well as for the modelling of the PS and MPI. The different SHERPA samples use different hadronisation models. The first one makes use of the SHERPA AHADIC model for hadronisation [61], which is based on the cluster hadronisation algorithm [62], while the second one uses the Lund string model [43, 53, 54, 63] for the modelling of the hadronisation.

Finally, two HERWIG 7 samples were generated at leading order using HERWIG 7.2.1. The matrix element for the $2 \rightarrow 2$ process was calculated at LO with the MMHT2014_{LO} PDF [64]. The renormalisation and factorisation scales were set as

$$\mu_r^2 = \mu_f^2 = \frac{2stu}{s^2 + t^2 + u^2},$$

where s , t and u are the Mandelstam variables [59]. The first sample uses the default HERWIG 7 angle-ordered PS, while the second sample uses a dipole-based PS [65]. For both HERWIG 7 samples, the MMHT2014_{LO} [64] PDF was used for the modelling of the MPI, and the hadronisation was modelled by means of the default HERWIG 7 cluster hadronisation algorithm.

The decays of the B mesons, of particular importance for this analysis, were modelled using the EVTGEN 1.6.0 generator [66] for the totality of the samples described above. The samples simulated using PYTHIA 8 A14-RB, PYTHIA 8 A14, and SHERPA with string hadronisation were passed through the GEANT4-based [67] ATLAS detector-simulation program [68] since they were also used to correct the measurements for detector effects, as described in Section 6. They are reconstructed and analysed with the same processing chain as the data. These fully simulated samples include the effect of multiple pp interactions per bunch crossing, simulated using PYTHIA 8.186 interfaced to the A3 tune [69], as well as the effect on the detector response of interactions from bunch crossings before or after the one containing the hard interaction. In addition, during the data-taking, some modules of the ATLAS hadronic calorimeter were disabled for some periods of time. The resulting non-functioning regions in the hadronic calorimeter were not necessarily included in the simulation for all the samples. However, the effect of removing jets pointing towards these regions has been found to be negligible.

Table 1: Properties of the Monte Carlo samples used in the analysis, including the perturbative order in α_s , the number of final-state partons, the PDF set, the parton shower algorithm, the renormalisation and factorisation scales, the tune and the hadronisation model. Further details can be found in the text.

Generator	ME order	Scales μ_r, μ_f	Parton shower	PDF set	Tune	Hadronisation
PYTHIA 8	$2 \rightarrow 2$ @ LO	$(m_{T3} \cdot m_{T4})^{\frac{1}{2}}$	p_T -ordered	CTEQ6L1	A14 A14-RB	Lund-Bowler Lund-Bowler
				NNPDF2.3	Monash	Lund-Bowler Peterson
SHERPA	$2 \rightarrow 2$ @ LO	$H(s, t, u)$	CSS (dipole)	CT14	–	Cluster model Lund string model
HERWIG 7	$2 \rightarrow 2$ @ LO	$\sqrt{\frac{2stu}{s^2+t^2+u^2}}$	Angle-ordered Dipole	MMHT2014	–	Cluster model

4 Object and event selection

Events are selected using triggers optimised for J/ψ meson identification and selection in its decay into muon pairs [70]. These triggers select events with two muons with $p_T > 6$ GeV. During the 2017 and 2018 data-taking periods, the trigger also required the invariant mass of the dimuon pair to satisfy

$2 \text{ GeV} < m_{\mu\mu} < 9 \text{ GeV}$ and the angular separation between the muons to satisfy $\Delta R_{\mu\mu} < 1.5$. The trigger selection efficiency is about 60%.

The primary vertex of the event is reconstructed as the vertex maximising the value of $\sum p_T^2$ for all tracks originating from it. The reconstruction of B^\pm mesons is done by re-fitting a pair of oppositely charged muons with $p_T > 6 \text{ GeV}$ and $|\eta| < 2.5$ to a common vertex, with a fit quality fulfilling $\chi^2 < 10$. Both muons are reconstructed using information from both the inner detector and the muon spectrometer. They must pass the MEDIUM quality requirements [71, 72], including at least one hit in the precision chambers of the muon spectrometer, and are required to have an invariant mass consistent with the mass of the J/ψ meson, i.e. to lie within the range 2.6–3.6 GeV. Moreover, both muons must spatially match the muon objects used in the trigger selection within $\Delta R = 0.01$. Given the short J/ψ lifetime following the $B^\pm \rightarrow J/\psi K^\pm$ decay, a third track with $p_T > 4 \text{ GeV}$ and $|\eta| < 2.5$ is fitted to a common vertex together with the two muon tracks, requiring $\chi^2/N_{\text{dof}} < 2.0$. In the fit, the invariant mass of the pair of muon tracks is constrained [73] to match the world average value for the J/ψ mass, $m_{J/\psi} = 3096.900 \text{ MeV}$ [74]. Moreover, each of the three tracks in the triplet must have at least one hit in the pixel detector and at least four hits in the silicon microstrip detector, while the invariant mass of the triplet is required to lie within the range 5.0–5.7 GeV. Finally, the pseudo-proper lifetime of the B^\pm candidate, $\tau = m_B L_{xy}/p_T$, where m_B is the PDG value of the B^\pm mass, $m_B = 5279.320 \text{ MeV}$ [74], and L_{xy} is the transverse flight distance from the primary vertex, is required to be above 0.20 ps. The efficiency of this cut has been shown to be well described by the MC simulations, and hence to have only a small impact on the results after the corrections for detector effects are applied. The mass of the charged kaon, $m_K = 493.677 \text{ MeV}$ [74], is assumed for the third track for the sake of calculating the three-body invariant mass.

Jet reconstruction is performed using particle-flow objects [75, 76] as inputs to the anti- k_t algorithm as implemented in FastJet [77, 78] with a radius parameter $R = 0.4$. Muon tracks are not considered in the particle-flow algorithm and, thus, the energy of muons from the B^\pm decay chain is not accounted for in the jet energy. In order to correct for the presence of muons inside the jets, muons passing the same quality requirements as those used in the B^\pm reconstruction are matched to the jet by means of the ghost-association method [79]. This procedure defines objects with infinitesimal energy and the same direction as the track momentum (ghosts), which are then used as inputs to the jet reconstruction algorithm. A track is considered matched to a given jet if the ghost associated with it is clustered inside the jet. The jet four-momentum is then corrected by vectorially adding to it the four momenta of the muons associated with the jet, after subtracting the muon energy loss in the calorimeter. After this correction is applied, the jet energy is calibrated and, in order to ensure full inner-detector acceptance, jets with $p_T > 20 \text{ GeV}$ and $|\eta| < 2.1$ are preselected. The jet calibration procedure includes energy corrections for pile-up, as well as angular corrections. Effects due to energy losses in inactive material, shower leakage, the magnetic field and inefficiencies in energy clustering and jet reconstruction are taken into account. This is done using a simulation-based correction, in bins of η and p_T , derived from the relation of the reconstructed jet energy to the energy of the corresponding particle-level jet. In a final step, an in situ calibration corrects for residual differences in the jet response between the MC simulation and the data using p_T -balance techniques for dijet, γ +jet, Z +jet and multijet final states. In order to reject pile-up jets, the so-called ‘jet vertex tagger’ (JVT) algorithm is used [80]. Moreover, in order to avoid overlaps between jets (and thus, incorrect matchings with B mesons), jets at a distance $\Delta R < 0.8$ from any other jet with $p_T > 20 \text{ GeV}$ are discarded.

The reconstructed B^\pm mesons are then matched to the corresponding jet by requiring both objects to be within $\Delta R = 0.4$ of each other. If there is more than one B meson candidate for a single jet, the one

with lowest χ^2 to the three-track vertex is selected. If any of the three tracks arising from the B^\pm decay is found to lie at $\Delta R > 0.4$ from the jet, its four-momentum is added to the jet four-momentum. The basic object for this analysis is, therefore, a jet containing a B^\pm meson. The selection criteria described above are met by 1 413 684 jets in 1 404 620 events.

To correct the simulation for differences in the muon identification and JVT acceptance efficiencies from those measured in the data, simulated events are weighted using dedicated corrections provided to that end [71, 80]. The differences in the trigger efficiencies between data and the simulation are accounted for as a systematic uncertainty, as described in Section 7.

Figure 1 shows the detector-level distributions of the jet p_T and the p_T of the B^\pm meson within the jet, together with the MC predictions. The data distributions include the purity corrections described in Section 5. While the SHERPA sample with string-based fragmentation describes the jet p_T within 10%, it fails to describe the B meson p_T , with discrepancies of over 50%. The PYTHIA samples with the A14 and A14-RB tunes give similar descriptions of the jet p_T , with differences from data of up to 40% in the tail of the distribution. The differences between the two tunes are clearly observed in the distribution of the B meson p_T , where A14 gives a more accurate description within 10% while A14-RB shows discrepancies of up to 30% in the tail of the distribution.

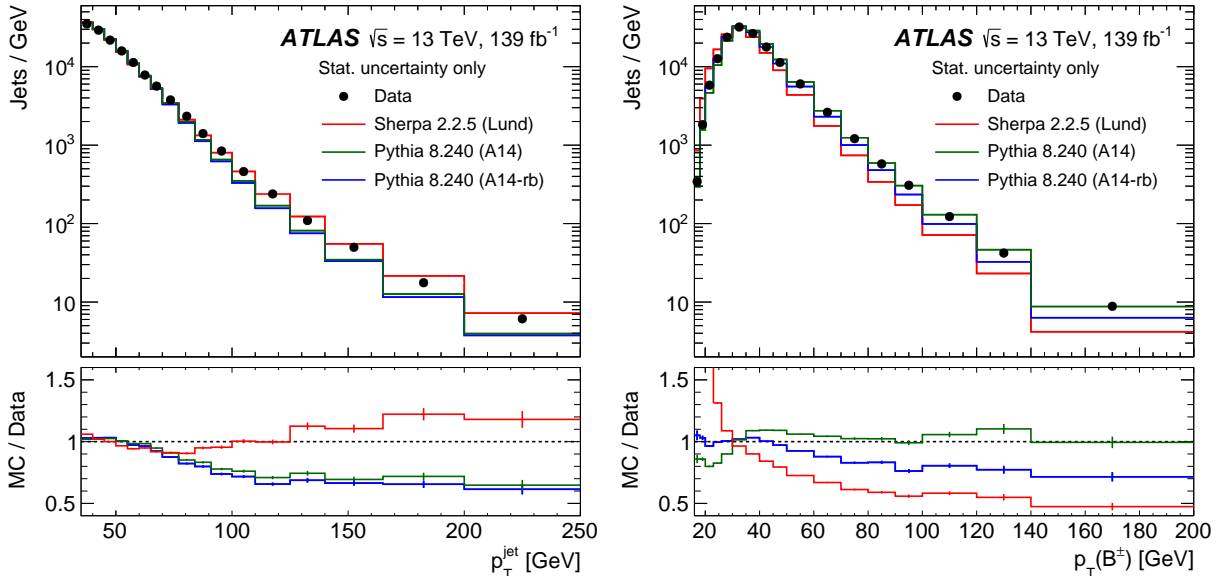


Figure 1: Distributions of the p_T of the selected jets and the B^\pm meson candidates within them, corrected for purity effects, together with MC predictions. The vertical error bars show the statistical uncertainties only.

For the fragmentation measurement, the data are binned in three intervals of the jet p_T , namely $[50, 70)$, $[70, 100)$ and $p_T \geq 100$ GeV. This choice ensures that the bin width is larger than the resolution in the different p_T intervals [75]. For each of these intervals, the z distributions are binned in intervals with a width of 0.07, while the p_T^{rel} distributions use a variable bin width. This choice allows finer binning, while retaining sufficient statistical precision in each bin, as needed for the estimation of the signal purity described in Section 5. The lower limit of the z distribution is extended towards lower values with increasing jet p_T , where a larger fiducial phase space becomes available. The z and p_T^{rel} distributions are nor-

malised to unit area by dividing by the number of entries, allowing the systematic uncertainties to be reduced.

Since the momentum resolution for charged particles is much better than the jet energy resolution, the measured z distribution extends beyond unity. The values larger than one are absorbed as an overflow into the last bin of the z distribution. Similarly, values of z below the lower limit of the first bin are absorbed into the first bin as an underflow, and values of p_T^{rel} above the upper limit of the last bin are absorbed into it as an overflow.

5 Signal extraction

The selected sample of B^\pm meson candidates does not only contain B^\pm mesons, but also backgrounds arising from different sources. For each (p_T, x) bin, with p_T being the jet p_T and $x = z$ or p_T^{rel} , only a fraction $p(p_T, x)$ of the reconstructed entries, referred to as the purity, are real B^\pm mesons. The number of B^\pm mesons, R , reconstructed in a given bin can thus be expressed as

$$R(p_T, x) = N(p_T, x) \times p(p_T, x),$$

where N is the total number of candidates in a given bin. In order to determine $p(p_T, x)$, a binned maximum-likelihood fit to the invariant mass distribution of the B^\pm candidates is performed. The probability density function (pdf) of the model describing the invariant mass distribution can be written as a combination of the signal and background pdfs as

$$\mathcal{F}(m) = \lambda_s \mathcal{F}_s(m) + \lambda_{B_x} \mathcal{F}_{B_x}(m) + \lambda_{B_\pi} \mathcal{F}_{B_\pi}(m) + \lambda_c \mathcal{F}_c(m),$$

where \mathcal{F}_s , \mathcal{F}_{B_x} , \mathcal{F}_{B_π} and \mathcal{F}_c are the pdfs for each of the components, signal or background, and λ_s , λ_{B_x} , λ_{B_π} and λ_c are coefficients representing their relative fractions, and thus $\lambda_s(p_T, x) = p(p_T, x)$. The closure relation $\sum_i \lambda_i = 1$ must be satisfied by these coefficients. Each of the fit components is described below.

- The signal \mathcal{F}_s , arising from the real B^\pm meson contribution, is modelled by a double-Gaussian function

$$\mathcal{F}_s(m|\mu, \sigma_1, \sigma_2, \beta) = \frac{1}{\sqrt{2\pi}} \left\{ \frac{\beta}{\sigma_1} \exp\left[-\frac{(m-\mu)^2}{2\sigma_1^2}\right] + \frac{1-\beta}{\sigma_2} \exp\left[-\frac{(m-\mu)^2}{2\sigma_2^2}\right] \right\},$$

where β is the relative normalisation of the two Gaussian components.

- The misreconstructed background, \mathcal{F}_{B_x} , arising from the decays $B^{\pm/0} \rightarrow J/\psi K^{*\pm/0} \rightarrow J/\psi(K\pi)^{\pm/0}$ and $B^{\pm/0} \rightarrow J/\psi(K\pi)^{\pm/0}$, creates a low-mass structure, displaced from the B^\pm mass. It is modelled by the following function

$$\mathcal{F}_{B_x}(m|b, s) = 1 - \tanh\left(\frac{m-s}{b}\right).$$

- The resonant background \mathcal{F}_{B_π} , arising from the decays $B^\pm \rightarrow J/\psi\pi^\pm$, creates a peaking structure displaced from the B^\pm mass towards higher masses. It is modelled by the sum of a Gaussian and an asymmetric Gaussian function,

$$\mathcal{F}_{B_\pi}(m|\mu_1, \mu_2, \hat{\sigma}_1, \hat{\sigma}_2, \hat{\sigma}_3, \gamma) = \frac{1}{\sqrt{2\pi}} \left\{ \frac{\gamma}{\hat{\sigma}_1} \exp\left[-\frac{(m-\mu_1)^2}{2\hat{\sigma}_1^2}\right] + (1-\gamma)\mathcal{G}_{\text{asym}}(m|\mu_2, \hat{\sigma}_2, \hat{\sigma}_3) \right\}, \quad (1)$$

where γ is a relative normalisation factor and

$$\mathcal{G}_{\text{asym}}(m|\mu_2, \hat{\sigma}_2, \hat{\sigma}_3) = \begin{cases} \frac{1}{\hat{\sigma}_2} \exp\left[-\frac{(m - \mu_2)^2}{2\hat{\sigma}_2^2}\right] & \text{if } m \leq \mu_2 \\ \frac{1}{\hat{\sigma}_3} \exp\left[-\frac{(m - \mu_2)^2}{2\hat{\sigma}_3^2}\right] & \text{if } m > \mu_2. \end{cases}$$

- The combinatorial background \mathcal{F}_c , arising from random combinations of real J/ψ mesons with additional tracks, is modelled by a first-order polynomial

$$\mathcal{F}_c(m|p_0, p_1) = p_0 + p_1 m.$$

All the parameters in Eq. (1) ($\mu_1, \mu_2, \hat{\sigma}_1, \hat{\sigma}_2, \hat{\sigma}_3, \gamma$) are obtained from fits to MC simulations, performed using PYTHIA 8 A14-RB, of $B^\pm \rightarrow J/\psi\pi^\pm$ in bins of the jet p_T and independently of z or p_T^{rel} . The normalisation of this background, $\lambda_{B\pi}$, is fixed relative to the signal as the ratio $\mathcal{R}(\pi, K)$ of the branching fractions of signal and background [74], i.e.

$$\frac{\lambda_{B\pi}}{\lambda_s} = \mathcal{R}(\pi, K) = \frac{\mathcal{B}(B^\pm \rightarrow J/\psi\pi^\pm)}{\mathcal{B}(B^\pm \rightarrow J/\psi K^\pm)} = 3.84\%.$$

The fits are performed individually for each (p_T, z) and (p_T, p_T^{rel}) bin in the mass range [5.0, 5.7] GeV, and each of them has ten free parameters: four for the signal ($\mu, \sigma_1, \sigma_2, \beta$), two for the misreconstructed background (b, s), two for the combinatorial background (p_0, p_1), and two for the free normalisations of each component, λ_i . Figure 2 shows the results of such fits in four representative bins of the longitudinal profile z and transverse profile p_T^{rel} for the lowest and highest jet- p_T selections.

The quality of the fits is quantified using χ^2 functions, defined as $\chi^2 = \sum_i [(x_i - f_i)^2 / (\Delta x_i)^2]$ for each fit. Here, x_i is the value of the data distribution in bin i ; Δx_i is its statistical uncertainty, and f_i is the corresponding value of the fit model. The values of the χ^2 divided by the number of degrees of freedom, $N_{\text{dof}} = 30$, range from 0.6 to 2.2. The fit results are studied as a function of the jet p_T and of the fragmentation variables z and p_T^{rel} . The results show that the signal component dominates the fit models with an average, global purity close to 69%, followed by the misreconstructed background, with a global value of about 15% and the combinatorial background, amounting to 12% of the sample. Finally, the $B^\pm \rightarrow J/\psi\pi^\pm$ background amounts to 3% of the sample. As a general trend, the purity of the sample increases as a function of z , while it is relatively constant as a function of p_T^{rel} , particularly at low p_T . Figure 3 shows the signal purity and the fractions of the different backgrounds resulting from the fit as a function of z and p_T^{rel} , for the lowest and highest jet- p_T selections. The hatched bands include the sum in quadrature of the statistical and systematic uncertainties of the fit, as discussed in Section 7.

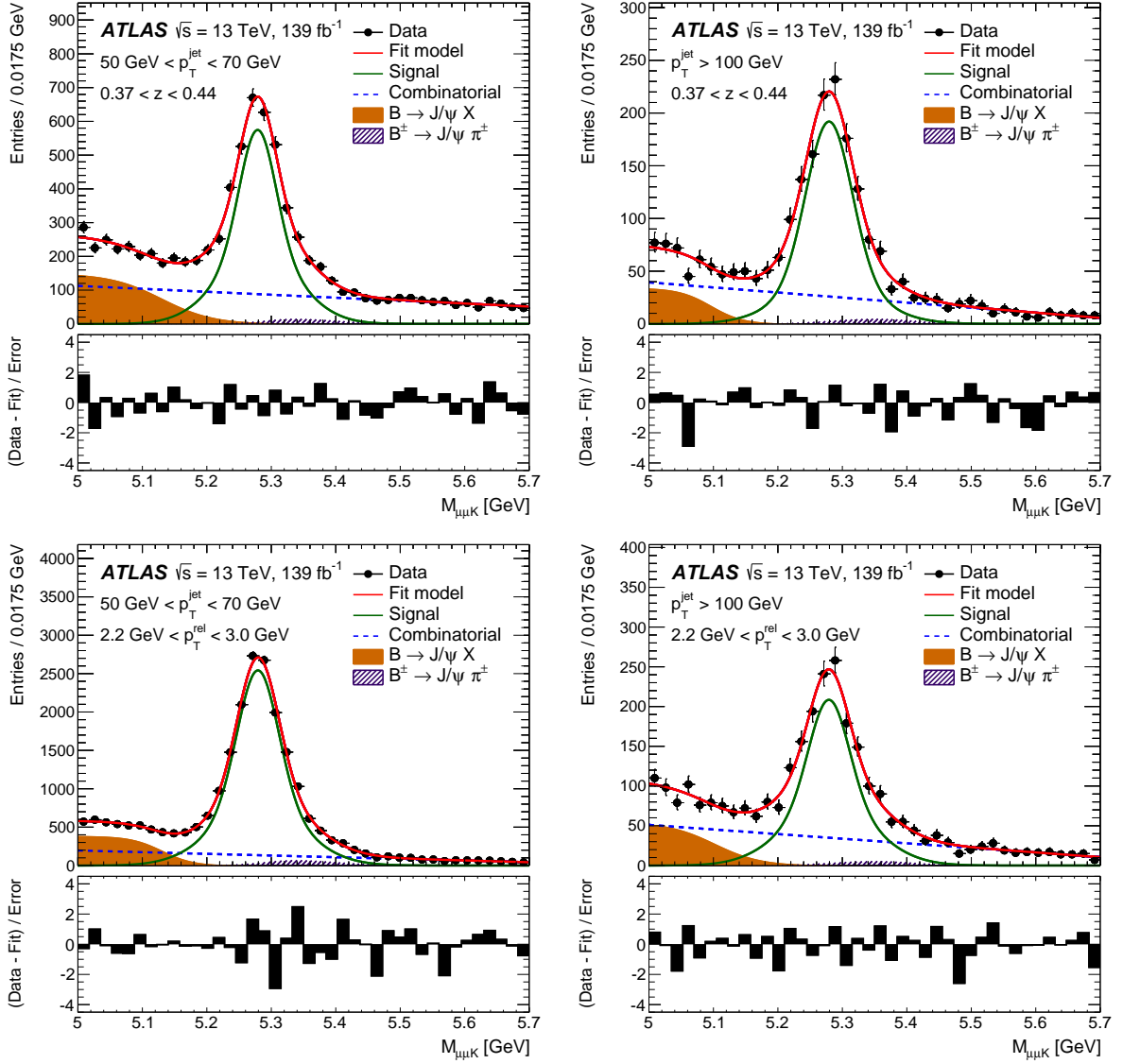


Figure 2: Fits to the invariant mass distributions of B^\pm candidates for $0.37 < z < 0.44$ in the lowest and highest jet- p_T bins (top) and $2.2 \text{ GeV} < p_T^{\text{rel}} < 3.0 \text{ GeV}$ in the lowest and highest jet- p_T bins (bottom). The bottom panels show the difference between the data and the fit, divided by the statistical uncertainty of the data.

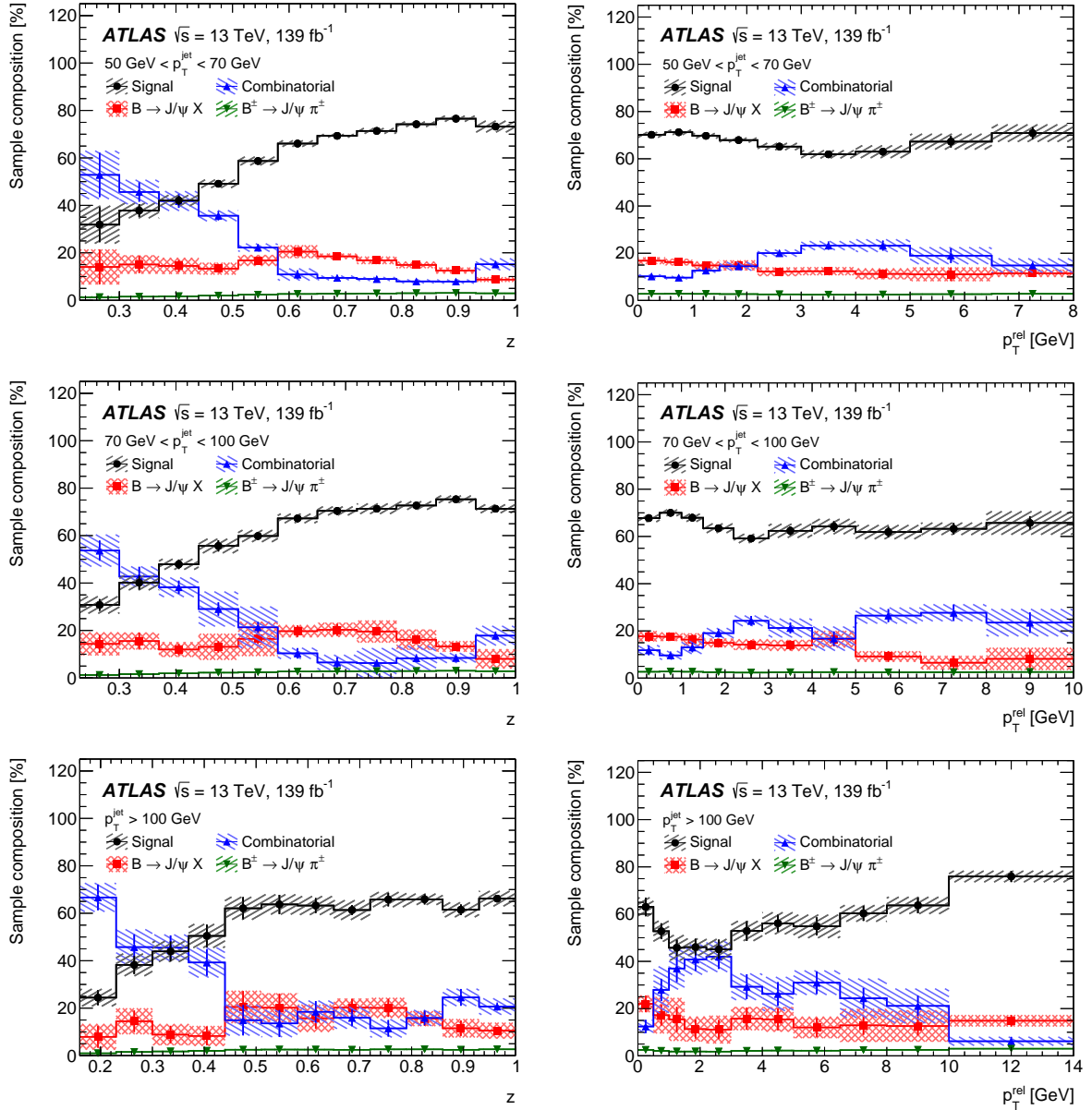


Figure 3: Fit results as a function of z for all jet- p_T bins (left) and as a function of p_T^{rel} (right) for all jet- p_T bins. The black circular markers represent the purity $p(p_T, x)$ for each bin. The error bars represent the statistical uncertainty of the fitted values, while the hatched bands represent the sum in quadrature of the statistical and systematic uncertainties of the fits.

6 Unfolding to particle level

The detector-level distributions, from which the background processes have been subtracted following the methodology described in Section 5, are corrected for detector effects such as inefficiencies and migrations caused by the finite resolution of the detector. The particle-level observables are defined using requirements equivalent to the detector-level selection described in Section 4. Candidate $B^\pm \rightarrow J/\psi K^\pm$ decays are selected if the muons from the J/ψ decay have $p_T > 6$ GeV and the kaon has $p_T > 4$ GeV. The kinematics of the B^\pm hadrons are reconstructed before QED radiation. Jets are reconstructed using the anti- k_r algorithm with $R = 0.4$, using all particles with average lifetime $\tau > 10$ ps, including muons and neutrinos. Jets with $p_T > 20$ GeV and $|\eta| < 2.1$ are selected, and those overlapping with another jet with $p_T > 20$ GeV within $\Delta R = 0.8$ are discarded. While the measurement is performed in the fiducial phase space with $p_T > 50$ GeV, an underflow bin with $35 \text{ GeV} < p_T < 50 \text{ GeV}$ is used to take into account the migrations from phase space regions below the jet p_T threshold.² The B^\pm mesons are matched to jets if the angular distance between them fulfils $\Delta R < 0.4$. Finally, the four-momenta of any decay products of the B^\pm meson lying outside the jet ($\Delta R > 0.4$) are added to the jet four-momentum.

The unfolding procedure can be parameterised using a transfer matrix A_{ij} , which contains the information about the bin-by-bin migrations from the detector-level distribution to the particle-level distributions, and is written as

$$R_i = \sum_{j=1}^N \frac{\mathcal{E}_j}{\mathcal{P}_i} A_{ij} T_j.$$

The unfolding can thus be regarded as a system of linear equations, for which the solution is the particle-level distribution T_j . The transfer matrix A_{ij} , the efficiency \mathcal{E}_j and the purity³ \mathcal{P}_i are determined using the PYTHIA 8 A14-RB MC sample, and R_i are the values of the detector-level distribution. An iterative matrix inversion method based on Bayes' theorem [81] is used, as implemented in the RooUNFOLD program [82]. The number of iterations is chosen so that the sum in quadrature of the statistical uncertainty and the uncertainty associated with the mismodelling in the unfolding, described in Section 7, is minimised. This results in four iterations for the unfolding of both the longitudinal and transverse profiles. The unfolding is performed in such a way that the migrations in both dimensions, between the fragmentation variable (z or p_T^{rel}) and the jet p_T are taken into account. The correlations in the statistical uncertainties, as well as those between the particle-level and detector-level MC distributions, are treated by using pseudo-experiments [83] in the calculation of each component of the unfolding, including matrices, efficiencies and purities as well as in the detector-level data.

The efficiency \mathcal{E} is estimated as the fraction of particle-level jets, associated with a B meson, which are matched within $\Delta R = 0.4$ to a detector-level jet that contains a reconstructed B meson. Its value ranges from 10% to 30% depending on z and p_T^{rel} . The efficiency decreases as a function of z for all p_T bins, although this behaviour is more pronounced for the higher p_T bin. This is due to the fact that, in this boosted regime, the dimuon trigger cannot efficiently separate the trajectories of the two muons produced in the J/ψ decay, and the events containing B^\pm mesons are therefore not recorded efficiently. The values of \mathcal{E} as a function of p_T^{rel} are significantly flatter.

The purity \mathcal{P} is estimated as the fraction of detector-level jets which are matched to a particle-level

² Data falling in this bin are also corrected for background sources as described in Section 5.

³ This purity is unrelated to the purity described in Section 5 and corrected for before the unfolding.

jet within $\Delta R = 0.4$. Its value ranges from 60% to 100%, systematically increasing as a function of both z and the jet p_T . As a function of p_T^{rel} , the purity exhibits a decrease in the low p_T region. This is due to the fact that reconstructed mesons flying in the same direction as the jet, as well as hadrons with high p_T , are more likely to arise from a true B meson. In the high p_T region, \mathcal{P} is constant as a function of p_T^{rel} .

The values of the matrix elements A_{ij} are estimated using particle-level B -meson jets, geometrically matched to the corresponding detector-level objects within $\Delta R = 0.4$. Figure 4 shows the two-dimensional transfer matrices as a function of (p_T, z) and (p_T, p_T^{rel}) .

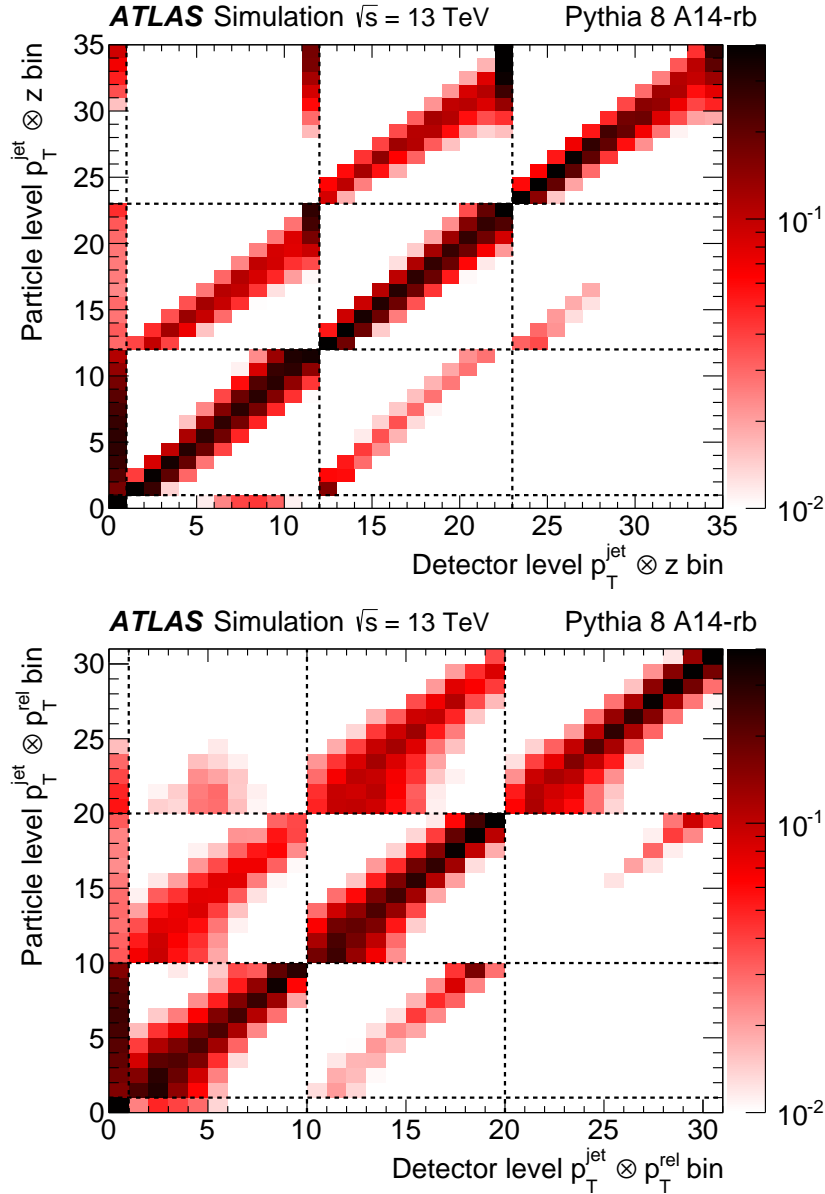


Figure 4: Transfer matrices, obtained using the PYTHIA 8 A14-RB MC sample, as a function of the jet p_T and the longitudinal profile z (top) and the transverse profile p_T^{rel} (bottom). Each small square represents a bin in (p_T, z) or (p_T, p_T^{rel}) , while each large box represents one of the three jet- p_T intervals used in the analysis. The first bin, containing jets with $p_T < 50$ GeV, accounts for the underflow.

7 Systematic uncertainties

The systematic uncertainties in the measurement are classified into four main categories. The first of them concerns the identification of B^\pm mesons, and includes the systematic uncertainties in muon reconstruction as well as the uncertainties in the fit procedure for the determination of the signal purity described in Section 5; the second category concerns jet reconstruction and identification, including the jet energy scale and resolution, the jet angular resolution and the efficiencies of the JVT algorithm. The third category is related to the unfolding procedure, including both the uncertainty in the MC model used for the corrections and the uncertainty due to mismodelling of the data by the nominal MC simulation. The fourth category takes into account systematic effects in the MC description of the pile-up dependence of the measurement.

The systematic uncertainties from all experimental sources are estimated by using the detector-level MC events. The resulting shifted distributions are then corrected for detector effects following the unfolding procedure described in Section 6, normalised to unit area, and compared with the nominal MC distributions, also normalised to unit area. The results of this comparison constitute the systematic uncertainties of the unfolded results for the normalised differential cross sections, and exploit the correlations between the numerator and the denominator when applying the normalisation. The full set of systematic uncertainties are described below, together with a detailed description of how they are estimated.

***B* meson reconstruction uncertainties**

- The uncertainties in the purity corrections for the B^\pm candidates are evaluated by considering other fit models as alternatives to those described in Section 5. The probability density function for each component of the fit is substituted by an alternative function. For the signal model, one of the Gaussian functions in the double-Gaussian pdf is replaced by an asymmetric Gaussian function. The hyperbolic tangent shape in the misreconstructed-background pdf, $1 - \tanh(x)$, is replaced by $1 - \operatorname{erf}(x) = (2/\sqrt{\pi}) \int_x^\infty e^{-t^2} dt$. For the $B^\pm \rightarrow J/\psi\pi^\pm$ background, one of the Gaussian functions in the double-Gaussian shape is replaced by a Crystal Ball function. Finally, the first-order polynomial describing the shape of the combinatorial background is replaced by an exponential function. The total uncertainty in the purity corrections is defined as the sum in quadrature of the deviations of the varied fit results, evaluated separately, from the nominal fit model described in Section 5. The impact of this uncertainty ranges from 1% to a maximum of 17% for the measurement of z , and from 1% to 8% for the measurement of p_T^{rel} , systematically increasing with the jet p_T .
- Muon momentum scale and resolution uncertainties [71] include variations in the smearing of the inner detector and muon spectrometer tracks, variations of the muon momentum scale, and additional charge-dependent variations related to the correction for the sagitta bias. These variations are applied to the muon selection and both when adding the muon four-momenta to the jets using the ghost-association method described in Section 4 and when reconstructing the mass and four-momenta of the B^\pm mesons. These are applied in a fully correlated way. The impact of this uncertainty is below 2% in all regions of the phase space, for both the z and p_T^{rel} measurements.
- Muon identification uncertainties [72] cover variations of the muon efficiency corrections described in Section 4. The variations include 1σ shifts of the statistical and systematic uncertainties in the efficiency corrections. As in the muon reconstruction case, the variations are applied, in a fully correlated way, both when adding muons to the jets and when reconstructing the B hadron momenta. The impact of this uncertainty is small, with values below 3% in all regions of the phase space.

- The uncertainty in the dimuon trigger efficiency [70] is evaluated by using correction factors to take into account the uncertainty in the mismodelling of the trigger efficiency. These correction factors are applied as per-jet weights depending on the p_T and rapidity of the muons, as well as the angular distance ΔR between the two muons in the B^\pm decay. The difference between the weighted distribution and the default one defines the systematic uncertainty. The values of this uncertainty range from a few per mille to a maximum of 4% in the lower tails of the z distribution, and from a few per mille to a maximum of 2% as a function of p_T^{rel} .
- The uncertainty in the kaon reconstruction efficiency is estimated by randomly rejecting 2% of the kaon tracks from the reconstruction, following a uniform random distribution [84]. The impact on the fragmentation properties is at the per mille level for both the z and p_T^{rel} measurements.

Jet-related uncertainties

- The jet energy scale (JES) and jet energy resolution (JER) uncertainties are estimated as described in Ref. [76]. The JES is calibrated on the basis of the simulation and in situ corrections obtained from data. The JES uncertainties are estimated using a correlation scheme comprising a set of 29 independent components, which depend on the jet p_T and η . The total JES uncertainty in the p_T of individual jets ranges from 2% at $p_T = 50$ GeV to approximately 1% at $p_T = 100$ GeV, with a mild dependence on η . The JER uncertainty is estimated using a correlation scheme involving 13 independent variations. Each of these variations ranges from about 0.8% at $p_T = 50$ GeV to about 0.5% at $p_T = 100$ GeV. In this measurement, the JES and JER uncertainties are propagated by varying the energy and p_T of each jet by one standard deviation of each of the independent components. The impact of the JES uncertainty varies from a few per mille for low p_T^{rel} values at high jet- p_T to 10% for medium values of z at low jet- p_T , and typically decreases with increasing jet p_T . The JER has a similar behaviour, varying from approximately 1% for low p_T^{rel} values at high jet p_T to 30% at medium values of z at low jet- p_T .
- The impact of the jet angular resolution (JAR) uncertainty is estimated by smearing the angular coordinates (η, ϕ) of the jets by 10% of the angular resolution of jets reconstructed from topological clusters [85], estimated in MC simulation. The η and ϕ smearing is applied with the p_T component of the jets held constant. The JAR uncertainty is negligible for the measurement of z . On the other hand, due to a linear dependence of p_T^{rel} on the sine of the angle between the B meson and the jet, this uncertainty can have an impact of up to 3% for the measurement of p_T^{rel} .
- The uncertainty from the efficiency corrections for the JVT algorithm described in Section 4, used to mitigate the impact of pile-up jets, is evaluated by using alternative correction factors, shifted by the corresponding uncertainties. This variation has two components, each of which shifts the correction factors in opposite directions. The resulting uncertainty is very small, with values below 0.1%.

Unfolding-related uncertainties

- The effects of the mismodelling of the data by the MC simulation on the unfolding is accounted for as an additional source of uncertainty. This is assessed by reweighting the particle-level distributions so that the detector-level fragmentation variables predicted by the MC samples match those in the data. The modified detector-level distributions are then unfolded using the method described in Section 6. The difference between the modified unfolded distribution and the reweighted particle-level

distribution is taken as the uncertainty. The resulting uncertainty ranges from 0.2% to 10%, and typically increases with increasing values of z and decreasing values of p_T^{rel} .

- The uncertainty due to using a particular MC model in the unfolding is estimated from the impact of two independent variations. The first accounts for the different amounts of gluon splitting in samples generated with different tunes. It is evaluated by comparing the results of the unfolding using the A14 samples with those using the different gluon splitting fractions in the Monash samples. These two particular tunes, which differ in the value of α_s for final-state radiation,⁴ are chosen because fits to the gluon splitting fraction in data are compatible with the uncertainty band spanned by them. The second is related to the description of the measured observables made by different MC models, after disentangling the effect of different gluon splitting fractions. It is evaluated by repeating the unfolding using two alternative samples. While the nominal result is obtained using the PYTHIA 8 A14-RB sample, the alternative samples are simulated using PYTHIA 8 A14 and SHERPA, in which the fragmentation is simulated by the string model. To avoid double counting of the differences arising from the description of the gluon splitting, the SHERPA and PYTHIA 8 A14 samples are reweighted so that the fraction of the selected jets arising from gluon splittings $g \rightarrow b\bar{b}$ is the same as in the PYTHIA 8 A14-RB sample. The envelope of the differences between the results using PYTHIA 8 A14-RB and both alternative samples covers the second source of systematic uncertainty. The total modelling uncertainty is defined by the sum in quadrature of these two variations. This uncertainty ranges from 4% to 30% and it is, together with the JES uncertainty, dominant for these measurements.

Pile-up-related uncertainties

- The uncertainty due to pile-up is derived from the ratios of the unfolded results for low ($\mu < 32$) and high ($\mu \geq 32$) pile-up subsamples to the results for the nominal measurement. The uncertainty is defined as the envelope of the two ratios, and is below 10% for both z and p_T^{rel} .

The total uncertainty is then determined as the sum in quadrature of the all the systematic uncertainties described above. The total uncertainty is larger for low values of the jet p_T , where it can reach values up to 30% in some bins. For the higher p_T bins, the uncertainty is systematically smaller, mainly because of the smaller jet energy scale components. Figure 5 shows the values of the systematic uncertainties as a function of z and p_T^{rel} , for the lowest and highest bins of the jet p_T .

The dependence of the particle-level results on the choice of PDF was tested by using two alternative PDF sets for the SHERPA predictions with the string fragmentation model. Predictions using NNPDF3.0 and MMHT2014 were compared with the nominal prediction, which uses CT14 (see Table 1). A maximum deviation of 2% from the nominal results is observed. Moreover, the CT14 uncertainty, estimated using the full set of eigenvectors, produces a total variation of the order of a few per mille. The effect of varying the PDF is thus much smaller than the experimental uncertainties, and is therefore neglected.

⁴ The value of the strong coupling constant for time-like parton showers in the A14 sample is $\alpha_s = 0.1260$, while the Monash tune uses $\alpha_s = 0.1365$.

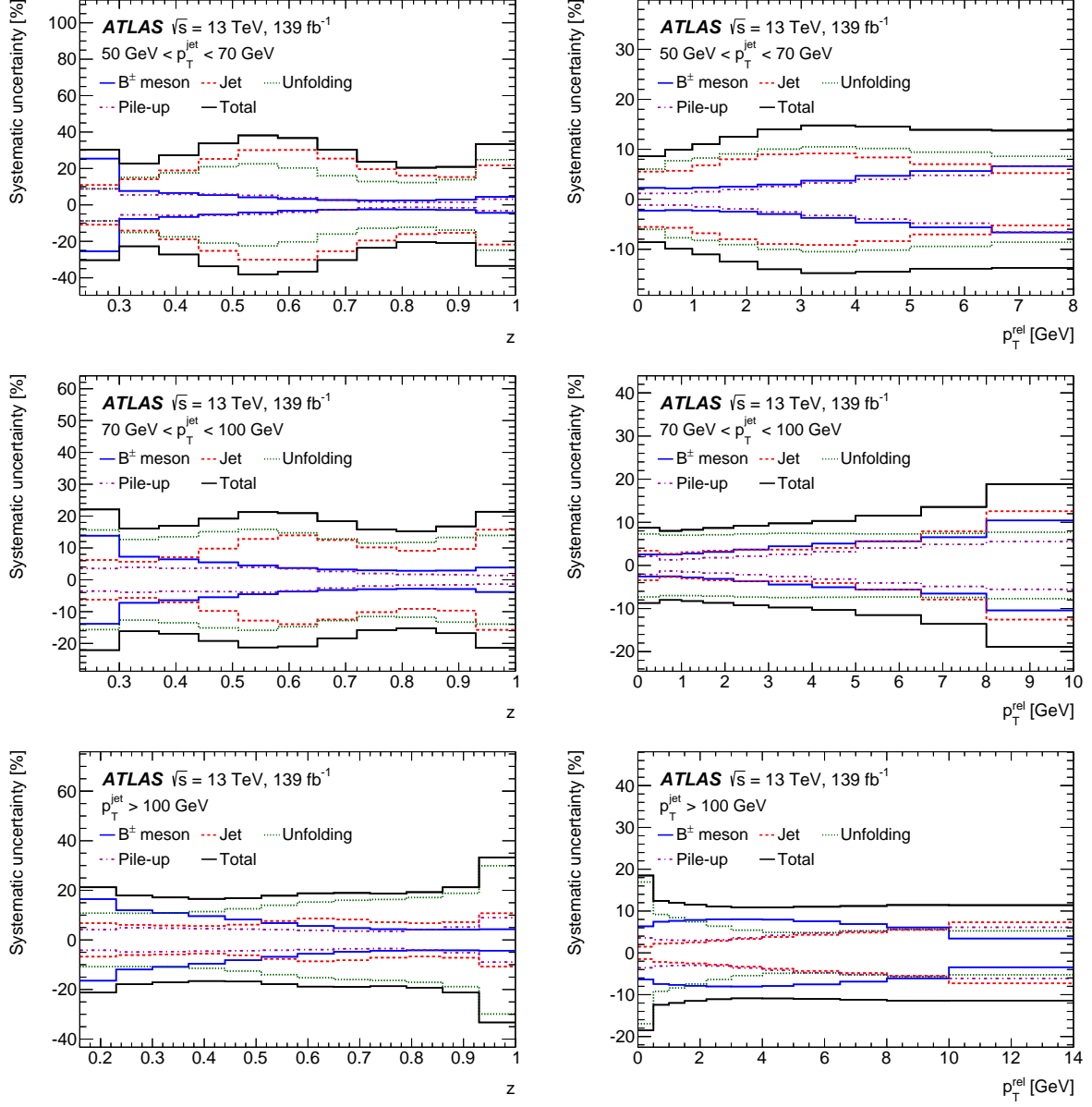


Figure 5: Systematic uncertainties as a function of z for all jet- p_T bins (left) and as a function of p_T^{rel} for all jet- p_T bins (right).

8 Results

The particle-level results are presented and compared with the predictions described in Section 3. Figures 6 to 8 show the distributions of the longitudinal and transverse profiles for each p_T bin.

The results show important differences between the low and high p_T bins. In particular, the lower tails of the z distributions contain a larger fraction of the data at high p_T , which translates into more high- p_T^{rel} events at high p_T . This is understood to be due to the fact that gluon splittings, $g \rightarrow b\bar{b}$, occur with a larger probability at high values of the jet p_T . The resulting b -quarks are reconstructed in the same jet, while the B^\pm meson originates from the fragmentation of one of them, thus leading to smaller values of z and higher values of p_T^{rel} .

The results for the longitudinal profile show reasonable agreement with the HERWIG 7 prediction with the angle-ordered parton shower, while large discrepancies are observed with the dipole parton shower. In particular, the prediction largely overestimates the data in the low z tails at low p_T , with smaller discrepancies for higher values of the jet p_T . This is understood to be a result of the larger fraction of jets arising from gluon splittings in the HERWIG 7 sample with the dipole parton shower.

The SHERPA predictions give a reasonable description of the z distributions in the low and medium p_T bins, although both predictions differ from data for very high values of z , particularly for the cluster model. At high p_T , the description worsens for the cluster model, which tends to underestimate the data at low z and significantly overestimate the data at high z , while the Lund string model confirms the deviation from data at high z .

The PYTHIA 8 samples tend to give descriptions that are qualitatively similar, and these are compatible with data within the systematic uncertainties across the different jet p_T bins. However, the Monash+Peterson model overestimates the data at intermediate z and low p_T , while it tends to conform with the rest at high p_T . The Monash+Lund–Bowler and A14+Lund–Bowler models both overestimate the data at very high values of z in all p_T ranges.

The discrepancies observed for the z distributions have their counterparts in the p_T^{rel} distributions as follows. Due to the larger gluon splitting fractions, the HERWIG 7 sample with the dipole parton shower significantly overestimates the data for p_T^{rel} values between 1.5 and 4.0 GeV at low p_T , while the differences are smaller with increasing p_T . The HERWIG angle-ordered parton shower gives a better description of the p_T^{rel} distributions, although non-negligible discrepancies are also observed.

The SHERPA predictions, particularly the one from the sample interfaced with the cluster hadronisation model, show large discrepancies for low values of p_T^{rel} , which increase when moving towards higher bins of jet p_T . The description of the p_T^{rel} tails is within uncertainties at low p_T , but for higher p_T , both SHERPA samples tend to underestimate the data for high p_T^{rel} . In general, the description from the sample interfaced to the Lund string model is observed to be better than the one provided by the cluster model.

All PYTHIA 8 samples give a good description of the p_T^{rel} distributions across the different jet- p_T bins.

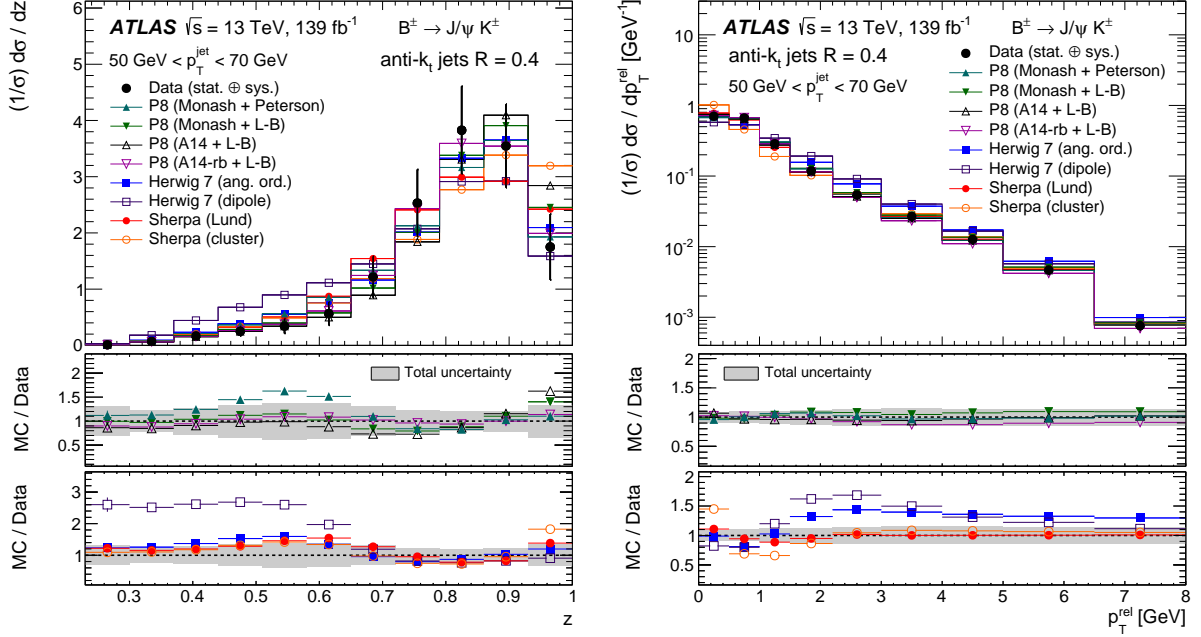


Figure 6: Distributions of the longitudinal profile z and the transverse profile p_T^{rel} for $50 \text{ GeV} < p_T < 70 \text{ GeV}$, together with different predictions from PYTHIA 8, SHERPA and HERWIG 7. The vertical error bars represent the total experimental uncertainties. The lower panels show the ratios of MC predictions to the data, where the gray bands represent the total uncertainties.

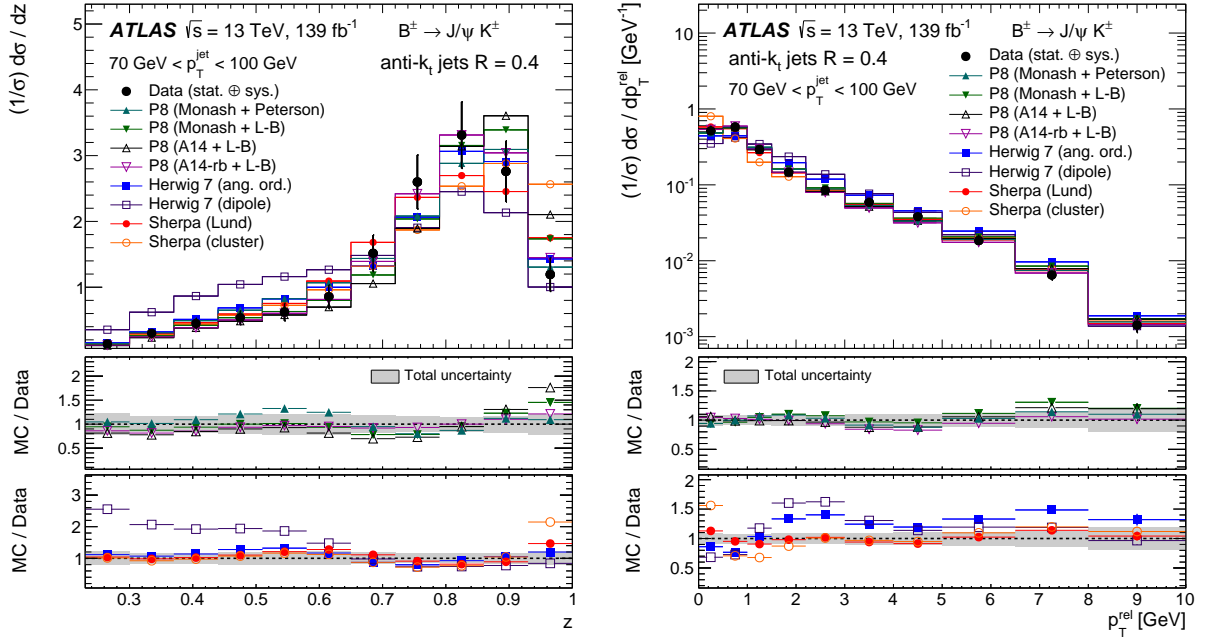


Figure 7: Distributions of the longitudinal profile z and the transverse profile p_T^{rel} for $70 \text{ GeV} < p_T < 100 \text{ GeV}$, together with different predictions from PYTHIA 8, SHERPA and HERWIG 7. The vertical error bars represent the total experimental uncertainties. The lower panels show the ratios of MC predictions to the data, where the gray bands represent the total uncertainties.

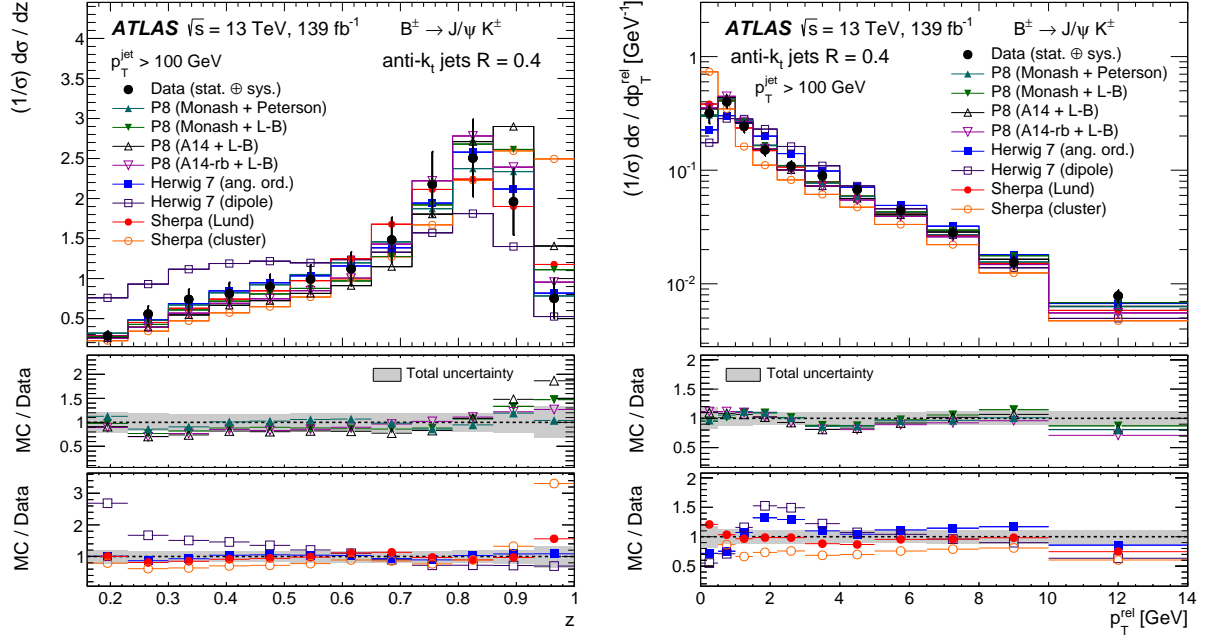


Figure 8: Distributions of the longitudinal profile z and the transverse profile p_T^{rel} for $p_T > 100$ GeV, together with different predictions from PYTHIA 8, SHERPA and HERWIG 7. The vertical error bars represent the total experimental uncertainties. In the first bin of the p_T^{rel} distribution, the prediction by the SHERPA sample using the cluster model is outside the range of the ratio panel. The lower panels show the ratios of MC predictions to the data, where the gray bands represent the total uncertainties.

In order to explicitly test the scale dependence of the longitudinal and transverse profiles, the average values of the longitudinal and transverse profiles, $\langle z \rangle$ and $\langle p_T^{\text{rel}} \rangle$, are studied as a function of the jet p_T . The results, together with the MC predictions, are shown in Figure 9. All PYTHIA samples describe the scale dependence reasonably well for both $\langle z \rangle$ and $\langle p_T^{\text{rel}} \rangle$, although the samples using the A14 and A14-RB tunes predict slightly larger values of $\langle z \rangle$ (and slightly lower values of $\langle p_T^{\text{rel}} \rangle$) than measured in data. The SHERPA sample making use of the cluster hadronisation model fails to describe the $\langle p_T^{\text{rel}} \rangle$ data, disagreeing by 10% to 25%, but describes the $\langle z \rangle$ distribution reasonably well, except at high p_T . The SHERPA sample interfaced to the Lund string hadronisation model describes the $\langle z \rangle$ data well, while showing small discrepancies for $\langle p_T^{\text{rel}} \rangle$, although much smaller than when using the cluster model. The HERWIG 7 sample making use of the angle-ordered parton shower describes the $\langle z \rangle$ scale dependence very well, while showing discrepancies of up to 15% for the $\langle p_T^{\text{rel}} \rangle$ data. Finally, the HERWIG 7 sample implementing the dipole-based parton shower fails to describe both the $\langle z \rangle$ and $\langle p_T^{\text{rel}} \rangle$ profiles, showing discrepancies of up to 10% for the former, and up to 20% for the latter.

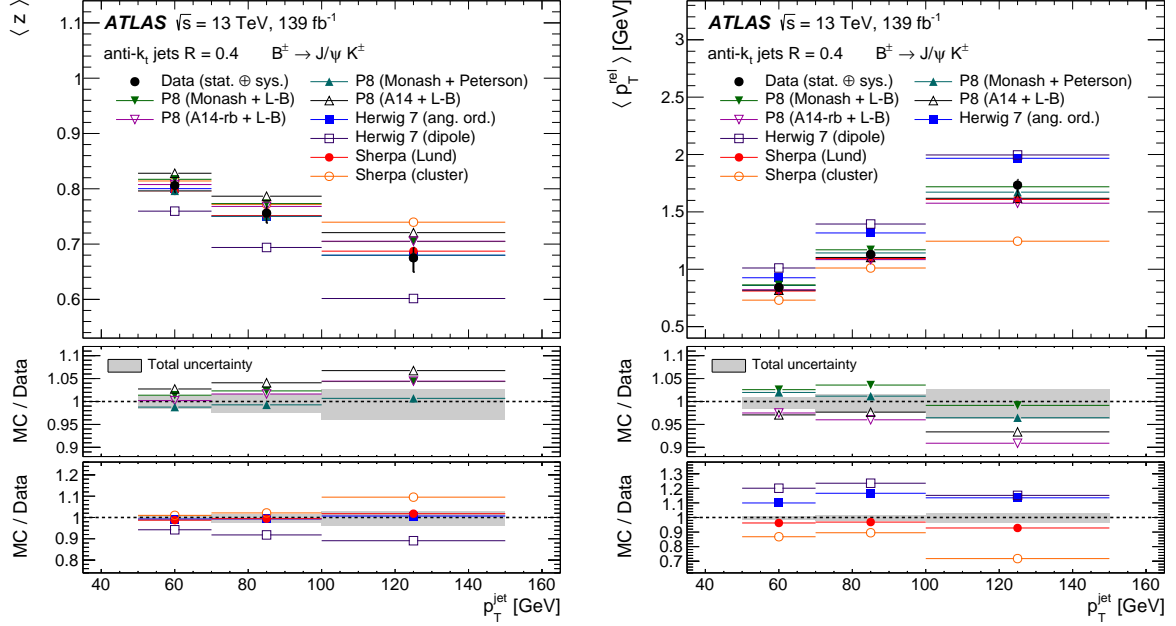


Figure 9: Average values of the longitudinal profile $\langle z \rangle$ and of the transverse profile $\langle p_T^{\text{rel}} \rangle$ as a function of the jet p_T , compared with MC predictions by PYTHIA 8, SHERPA and HERWIG 7. The points are in the bin centre. The vertical error bars represent the total experimental uncertainties. The lower panels show the ratios of MC predictions to the data, where the gray bands represent the total uncertainties.

Some of the discrepancies described above can be traced to the modelling of the gluon splittings $g \rightarrow b\bar{b}$ in the parton shower algorithms. Jets in the MC simulation are considered to contain a gluon splitting into a $b\bar{b}$ pair if they contain two weakly decaying B hadrons within $\Delta R = 0.4$ of the jet axis. Figure 10 shows the fraction of such jets, for each of the MC simulations investigated, as a function of the jet p_T .

As expected, the incidence of gluon splittings in the MC simulation grows as the jet p_T increases. The PYTHIA samples show similar fractions of $g \rightarrow b\bar{b}$ jets, although the samples making use of the Monash tune present a slightly higher fraction due to using a larger value of α_s than the others and, hence, having a larger amount of gluon radiation. Both SHERPA samples present larger fractions than the PYTHIA samples for low and medium p_T . However, for the highest p_T bin, the SHERPA sample using the cluster model presents a lower fraction than PYTHIA. The angle-ordered shower implemented in HERWIG 7 shows an amount of $g \rightarrow b\bar{b}$ splitting very similar to that of SHERPA, while the HERWIG 7 sample making use of the dipole-based parton shower presents a much larger fraction of jets arising from gluon splittings. As pointed out previously, these differences help to explain the discrepancies between this sample and the data, since the lower tails of the z distributions, as well as the higher tails for p_T^{rel} , are strongly influenced by the fraction of gluon splittings.

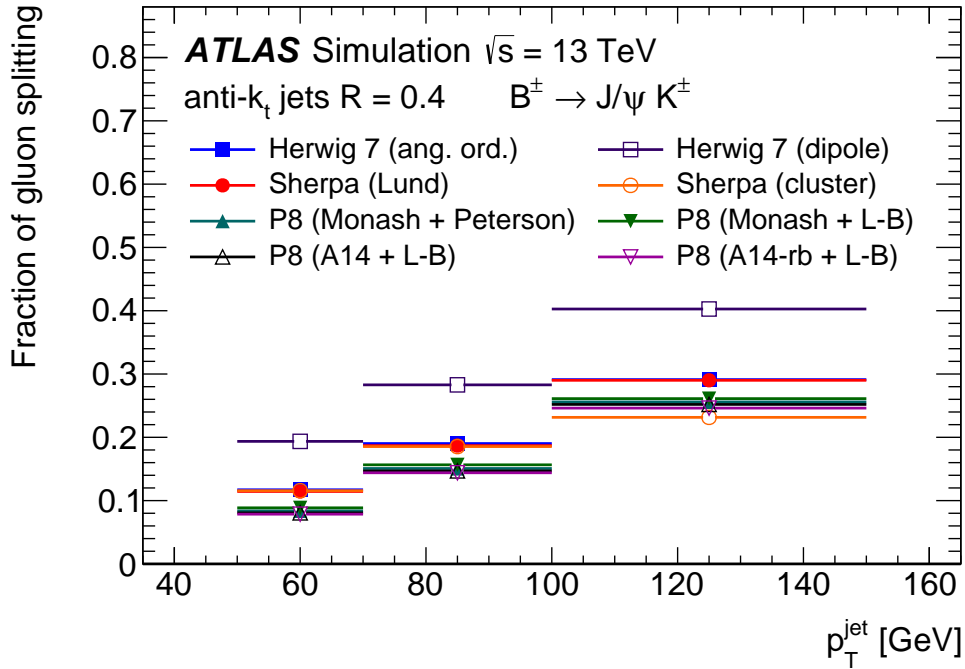


Figure 10: Fraction of jets arising from gluon splittings $g \rightarrow b\bar{b}$ as a function of the jet p_T for different MC models.

9 Summary and conclusions

The fragmentation properties of b -jets have been measured by using the decay of charged B mesons into J/ψ charmonia and charged kaons, using 139 fb^{-1} of pp collisions at $\sqrt{s} = 13 \text{ TeV}$ recorded by the ATLAS detector at the LHC. To this end, the decay channel of the B mesons is fully reconstructed using a three-track fit to a common vertex. The B^\pm candidates are matched to jets, reconstructed using the anti- k_t algorithm with $R = 0.4$, and the longitudinal and transverse profiles of the B mesons over the jet momentum are measured. The measurement spans three bins of the jet transverse momentum, and the yield of B mesons is extracted for each bin of the fragmentation variable (z or p_T^{rel}) and the jet p_T . The results are then corrected for detector resolution effects using an iterative Bayesian algorithm, and the systematic uncertainties due to the muon, jet and event reconstruction properties are evaluated.

The results are compared with different MC predictions, including PYTHIA 8, HERWIG 7 and SHERPA samples using different models for the parton shower and hadronisation. Generally, the best description of the longitudinal profile is provided by the PYTHIA 8 and SHERPA samples making use of the string hadronisation model, which provide similar descriptions for all values of the jet p_T . For medium and high values of the jet p_T , the SHERPA sample with cluster hadronisation shows large deviations from data at very high values of z . The HERWIG 7 sample with the angle-ordered parton shower also gives a good description of the longitudinal profile for all values of the jet p_T . In contrast, the HERWIG 7 samples using the dipole-based parton shower show large deviations from the data in the lower tails of the z distribution. For the transverse profile, similar comments apply. While the PYTHIA 8 and SHERPA samples using the string hadronisation model give fair and similar descriptions of the data for all values of the jet p_T , HERWIG 7 fails to describe the data. The angle-ordered parton shower, however, provides a better description than the

dipole-based parton shower. At medium and high p_T , the SHERPA sample with the cluster hadronisation model gives a poor description for low values of p_T^{rel} .

This analysis provides key measurements which help to better understand the fragmentation functions of heavy quarks. As has been shown, significant differences among different MC models are observed, and also between the models and the data. Some of the discrepancies are understood to arise from poor modelling of the $g \rightarrow b\bar{b}$ splittings, to which the present analysis has substantial sensitivity. Including the present measurements in a future tune of the MC predictions may help to improve the description and reduce the theoretical uncertainties of processes where heavy-flavour quarks are present in the final state, such as top quark pair production or Higgs boson decays into heavy quark pairs.

Acknowledgements

We thank CERN for the very successful operation of the LHC, as well as the support staff from our institutions without whom ATLAS could not be operated efficiently.

We acknowledge the support of ANPCyT, Argentina; YerPhI, Armenia; ARC, Australia; BMWFW and FWF, Austria; ANAS, Azerbaijan; SSTC, Belarus; CNPq and FAPESP, Brazil; NSERC, NRC and CFI, Canada; CERN; ANID, Chile; CAS, MOST and NSFC, China; Minciencias, Colombia; MEYS CR, Czech Republic; D NRF and DNSRC, Denmark; IN2P3-CNRS and CEA-DRF/IRFU, France; SRNSFG, Georgia; BMBF, HGF and MPG, Germany; GSRI, Greece; RGC and Hong Kong SAR, China; ISF and Benozziyo Center, Israel; INFN, Italy; MEXT and JSPS, Japan; CNRST, Morocco; NWO, Netherlands; RCN, Norway; MEiN, Poland; FCT, Portugal; MNE/IFA, Romania; JINR; MES of Russia and NRC KI, Russian Federation; MESTD, Serbia; MSSR, Slovakia; ARRS and MIZŠ, Slovenia; DSI/NRF, South Africa; MICINN, Spain; SRC and Wallenberg Foundation, Sweden; SERI, SNSF and Cantons of Bern and Geneva, Switzerland; MOST, Taiwan; TAEK, Turkey; STFC, United Kingdom; DOE and NSF, United States of America. In addition, individual groups and members have received support from BCKDF, CANARIE, Compute Canada and CRC, Canada; COST, ERC, ERDF, Horizon 2020 and Marie Skłodowska-Curie Actions, European Union; Investissements d’Avenir Labex, Investissements d’Avenir Idex and ANR, France; DFG and AvH Foundation, Germany; Herakleitos, Thales and Aristeia programmes co-financed by EU-ESF and the Greek NSRF, Greece; BSF-NSF and GIF, Israel; Norwegian Financial Mechanism 2014-2021, Norway; NCN and NAWA, Poland; La Caixa Banking Foundation, CERCA Programme Generalitat de Catalunya and PROMETEO and GenT Programmes Generalitat Valenciana, Spain; Göran Gustafssons Stiftelse, Sweden; The Royal Society and Leverhulme Trust, United Kingdom.

The crucial computing support from all WLCG partners is acknowledged gratefully, in particular from CERN, the ATLAS Tier-1 facilities at TRIUMF (Canada), NDGF (Denmark, Norway, Sweden), CC-IN2P3 (France), KIT/GridKA (Germany), INFN-CNAF (Italy), NL-T1 (Netherlands), PIC (Spain), ASGC (Taiwan), RAL (UK) and BNL (USA), the Tier-2 facilities worldwide and large non-WLCG resource providers. Major contributors of computing resources are listed in Ref. [86].

References

- [1] ATLAS Collaboration, *Observation of $H \rightarrow b\bar{b}$ decays and VH production with the ATLAS detector*, *Phys. Lett. B* **786** (2018) 59, arXiv: [1808.08238 \[hep-ex\]](#).
- [2] CMS Collaboration, *Observation of Higgs Boson Decay to Bottom Quarks*, *Phys. Rev. Lett.* **121** (2018) 121801, arXiv: [1808.08242 \[hep-ex\]](#).
- [3] ATLAS Collaboration, *Measurements of inclusive and differential fiducial cross-sections of $t\bar{t}$ production with additional heavy-flavour jets in proton–proton collisions at $\sqrt{s} = 13$ TeV with the ATLAS detector*, *JHEP* **04** (2019) 046, arXiv: [1811.12113 \[hep-ex\]](#).
- [4] CMS Collaboration, *Measurement of the cross section for $t\bar{t}$ production with additional jets and b jets in pp collisions at $\sqrt{s} = 13$ TeV*, *JHEP* **07** (2020) 125, arXiv: [2003.06467 \[hep-ex\]](#).
- [5] ATLAS Collaboration, *Search for the standard model Higgs boson produced in association with top quarks and decaying into a $b\bar{b}$ pair in pp collisions at $\sqrt{s} = 13$ TeV with the ATLAS detector*, *Phys. Rev. D* **97** (2018) 072016, arXiv: [1712.08895 \[hep-ex\]](#).
- [6] CMS Collaboration, *Search for $t\bar{t}H$ production in the $H \rightarrow b\bar{b}$ decay channel with leptonic $t\bar{t}$ decays in proton–proton collisions at $\sqrt{s} = 13$ TeV*, *JHEP* **03** (2019) 026, arXiv: [1804.03682 \[hep-ex\]](#).
- [7] ATLAS Collaboration, *Impact of fragmentation modelling on the jet energy and the top-quark mass measurement using the ATLAS detector*, ATL-PHYS-PUB-2015-042, 2015, URL: <https://cds.cern.ch/record/2054420>.
- [8] ATLAS Collaboration, *Measurement of the top quark mass in the $t\bar{t} \rightarrow$ lepton+jets and $t\bar{t} \rightarrow$ dilepton channels using $\sqrt{s} = 7$ TeV ATLAS data*, *Eur. Phys. J. C* **75** (2015) 330, arXiv: [1503.05427 \[hep-ex\]](#).
- [9] ATLAS Collaboration, *Measurement of the top-quark mass in $t\bar{t} + 1$ -jet events collected with the ATLAS detector in pp collisions at $\sqrt{s} = 8$ TeV*, *JHEP* **11** (2019) 150, arXiv: [1905.02302 \[hep-ex\]](#).
- [10] CMS Collaboration, *Measurement of the mass of the top quark in decays with a J/ψ meson in pp collisions at 8 TeV*, *JHEP* **12** (2016) 123, arXiv: [1608.03560 \[hep-ex\]](#).
- [11] CMS Collaboration, *Measurement of $t\bar{t}$ normalised multi-differential cross sections in pp collisions at $\sqrt{s} = 13$ TeV, and simultaneous determination of the strong coupling strength, top quark pole mass, and parton distribution functions*, *Eur. Phys. J. C* **80** (2020) 658, arXiv: [1904.05237 \[hep-ex\]](#).
- [12] G. Corcella and A. D. Mitov, *Bottom Quark Fragmentation in Top Quark Decay*, *Nucl. Phys. B* **623** (2002) 247, arXiv: [hep-ph/0110319](#).
- [13] G. Corcella and V. Drollinger, *Bottom-quark fragmentation: comparing results from tuned event generators and resummed calculations*, *Nucl. Phys. B* **730** (2005) 82, arXiv: [hep-ph/0508013](#).
- [14] G. Corcella and F. Mescia, *A Phenomenological Study of Bottom Quark Fragmentation in Top Quark Decay*, *Eur. Phys. J. C* **65** (2010) 171, arXiv: [0907.5158 \[hep-ph\]](#).

- [15] G. Corcella, R. Franceschini and D. Kim, *Fragmentation Uncertainties in Hadronic Observables for Top-quark Mass Measurements*, *Nucl. Phys. B* **929** (2018) 485, arXiv: [1712.05801 \[hep-ph\]](#).
- [16] ARGUS Collaboration, *Inclusive production of D^0 , D^+ and D^{*+} (2010) mesons in B decays and nonresonant e^+e^- annihilation at 10.6 GeV*, *Z. Phys. C* **52** (1991) 353.
- [17] OPAL Collaboration, *A measurement of the production of $D^{*\pm}$ mesons on the Z^0 resonance*, *Z. Phys. C* **67** (1995) 27.
- [18] ALEPH Collaboration, *Study of Charm Production in Z Decays*, *Eur. Phys. J. C* **16** (2000) 597, arXiv: [hep-ex/9909032](#).
- [19] CLEO Collaboration, *Charm meson spectra in e^+e^- annihilation at 10.5 GeV center of mass energy*, *Phys. Rev. D* **70** (2004) 112001, arXiv: [hep-ex/0402040](#).
- [20] ALEPH Collaboration, *Study of the fragmentation of b quarks into B mesons at the Z peak*, *Phys. Lett. B* **512** (2001) 30, arXiv: [hep-ex/0106051](#).
- [21] OPAL Collaboration, *Inclusive Analysis of the b Quark Fragmentation Function in Z Decays at LEP*, *Eur. Phys. J. C* **29** (2003) 463, arXiv: [hep-ex/0210031](#).
- [22] DELPHI Collaboration, *A study of the b -quark fragmentation function with the DELPHI detector at LEP I and an averaged distribution obtained at the Z Pole*, *Eur. Phys. J. C* **71** (2011) 1557, arXiv: [1102.4748 \[hep-ex\]](#).
- [23] SLD Collaboration, *Precise Measurement of the b -Quark Fragmentation Function in Z^0 Boson Decays*, *Phys. Rev. Lett.* **84** (2000) 4300, arXiv: [hep-ex/9912058](#).
- [24] SLD Collaboration, *Measurement of the b -quark fragmentation function in Z^0 decays*, *Phys. Rev. D* **65** (2002) 092006, arXiv: [hep-ex/0202031](#).
- [25] UA1 Collaboration, *A study of the D^* content of jets at the CERN pp collider*, *Phys. Lett. B* **244** (1990) 566.
- [26] STAR Collaboration, *Measurement of D^* mesons in jets from $p + p$ collisions at $\sqrt{s} = 200$ GeV*, *Phys. Rev. D* **79** (2009) 112006, arXiv: [0901.0740 \[hep-ex\]](#).
- [27] ATLAS Collaboration, *Measurement of $D^{*\pm}$ meson production in jets from pp collisions at $\sqrt{s} = 7$ TeV with the ATLAS detector*, *Phys. Rev. D* **85** (2012) 052005, arXiv: [1112.4432 \[hep-ex\]](#).
- [28] ALICE Collaboration, *Measurement of the production of charm jets tagged with D^0 mesons in pp collisions at $\sqrt{s} = 7$ TeV*, *JHEP* **08** (2019) 133, arXiv: [1905.02510 \[nucl-ex\]](#).
- [29] LHCb Collaboration, *Study of J/ψ production in jets*, *Phys. Rev. Lett.* **118** (2017) 192001, arXiv: [1701.05116 \[hep-ex\]](#).
- [30] ATLAS Collaboration, *Measurement of the differential cross-section of B^+ meson production in pp collisions at $\sqrt{s} = 7$ TeV at ATLAS*, *JHEP* **10** (2013) 042, arXiv: [1307.0126 \[hep-ph\]](#).
- [31] ATLAS Collaboration, *B^\pm mass reconstruction in $B^\pm \rightarrow J/\psi K^\pm$ decay at ATLAS at 13 TeV pp collisions at the LHC*, ATLAS-CONF-2015-064, 2015, URL: <https://cds.cern.ch/record/2114830>.
- [32] B. Mele and P. Nason, *The fragmentation function for heavy quarks in QCD*, *Nucl. Phys. B* **361** (1991) 626.

- [33] M. Cacciari and E. Gardi, *Heavy-quark fragmentation*, *Nucl. Phys. B* **664** (2003) 299, arXiv: [hep-ph/0301047](https://arxiv.org/abs/hep-ph/0301047).
- [34] ATLAS Collaboration, *The ATLAS Experiment at the CERN Large Hadron Collider*, *JINST* **3** (2008) S08003.
- [35] ATLAS Collaboration, *ATLAS Insertable B-Layer Technical Design Report*, ATLAS-TDR-19; CERN-LHCC-2010-013, 2010, URL: <https://cds.cern.ch/record/1291633>, Addendum: ATLAS-TDR-19-ADD-1; CERN-LHCC-2012-009, 2012, URL: <https://cds.cern.ch/record/1451888>.
- [36] B. Abbott et al., *Production and integration of the ATLAS Insertable B-Layer*, *JINST* **13** (2018) T05008, arXiv: [1803.00844](https://arxiv.org/abs/1803.00844) [[physics.ins-det](#)].
- [37] ATLAS Collaboration, *Performance of the ATLAS trigger system in 2015*, *Eur. Phys. J. C* **77** (2017) 317, arXiv: [1611.09661](https://arxiv.org/abs/1611.09661) [[hep-ex](#)].
- [38] ATLAS Collaboration, *The ATLAS Collaboration Software and Firmware*, ATL-SOFT-PUB-2021-001, 2021, URL: <https://cds.cern.ch/record/2767187>.
- [39] ATLAS Collaboration, *ATLAS data quality operations and performance for 2015–2018 data-taking*, *JINST* **15** (2020) P04003, arXiv: [1911.04632](https://arxiv.org/abs/1911.04632) [[physics.ins-det](#)].
- [40] ATLAS Collaboration, *Luminosity determination in pp collisions at $\sqrt{s} = 13$ TeV using the ATLAS detector at the LHC*, ATLAS-CONF-2019-021, 2019, URL: <https://cds.cern.ch/record/2677054>.
- [41] ATLAS Collaboration, *Luminosity determination in pp collisions at $\sqrt{s} = 8$ TeV using the ATLAS detector at the LHC*, *Eur. Phys. J. C* **76** (2016) 653, arXiv: [1608.03953](https://arxiv.org/abs/1608.03953) [[hep-ex](#)].
- [42] G. Avoni et al., *The new LUCID-2 detector for luminosity measurement and monitoring in ATLAS*, *JINST* **13** (2018) P07017.
- [43] T. Sjöstrand, S. Mrenna and P. Z. Skands, *PYTHIA 6.4 physics and manual*, *JHEP* **05** (2006) 026, arXiv: [hep-ph/0603175](https://arxiv.org/abs/hep-ph/0603175) [[hep-ph](#)].
- [44] T. Sjöstrand et al., *An introduction to PYTHIA 8.2*, *Comput. Phys. Commun.* **191** (2015) 159, arXiv: [1410.3012](https://arxiv.org/abs/1410.3012) [[hep-ph](#)].
- [45] T. Gleisberg et al., *Event generation with SHERPA 1.1*, *JHEP* **02** (2008) 007, arXiv: [0811.4622](https://arxiv.org/abs/0811.4622).
- [46] M. Bahr et al., *Herwig++ physics and manual*, *Eur. Phys. J. C* **58** (2008) 639, arXiv: [0803.0883](https://arxiv.org/abs/0803.0883) [[hep-ph](#)].
- [47] J. Bellm et al., *Herwig 7.0/Herwig++ 3.0 release note*, *Eur. Phys. J. C* **76** (2016) 196, arXiv: [1512.01178](https://arxiv.org/abs/1512.01178) [[hep-ph](#)].
- [48] J. Bellm et al., *Herwig 7.1 Release Note*, (2017), arXiv: [1705.06919](https://arxiv.org/abs/1705.06919) [[hep-ph](#)].
- [49] ATLAS Collaboration, *ATLAS Pythia 8 tunes to 7 TeV data*, ATL-PHYS-PUB-2014-021, 2014, URL: <https://cds.cern.ch/record/1966419>.
- [50] J. Pumplin et al., *Parton Distributions and the Strong Coupling Strength: CTEQ6AB PDFs*, *JHEP* **02** (2006) 032, arXiv: [hep-ph/0512167](https://arxiv.org/abs/hep-ph/0512167).
- [51] P. Skands, S. Carrazza and J. Rojo, *Tuning PYTHIA 8.1: the Monash 2013 Tune*, *Eur. Phys. J. C* **74** (2014) 3024, arXiv: [1404.5630](https://arxiv.org/abs/1404.5630) [[hep-ph](#)].

- [52] R.D. Ball *et al.*, *Parton distributions with LHC data*, [Nucl. Phys. B **867** \(2013\) 244](#), arXiv: [1207.1303 \[hep-ph\]](#).
- [53] B. Andersson, G. Gustafson, G. Ingelman and T. Sjöstrand, *Parton fragmentation and string dynamics*, [Phys. Rept. **97** \(1983\) 31](#).
- [54] T. Sjöstrand, *Jet fragmentation of multiparton configurations in a string framework*, [Nucl. Phys. B **248** \(1984\) 469](#).
- [55] M. G. Bowler, *e^+e^- Production of heavy quarks in the string model.*, [Z. Phys. C **11** \(1981\) 169](#).
- [56] C. Peterson, D. Schlatter, I. Schmitt and P. Zerwas, *Scaling violations in inclusive e^+e^- annihilation spectra*, [Phys. Rev. D **27** \(1983\) 105](#).
- [57] S. Catani, F. Krauss, R. Kuhn and B. R. Webber, *QCD Matrix Elements + Parton Showers*, [JHEP **11** \(2001\) 063](#), arXiv: [hep-ph/0109231 \[hep-ph\]](#).
- [58] F. Krauss, *Matrix Elements and Parton Showers in Hadronic Interactions*, [JHEP **08** \(2002\) 015](#), arXiv: [hep-ph/0205283 \[hep-ph\]](#).
- [59] S. Mandelstam, *Determination of the Pion-Nucleon Scattering Amplitude from Dispersion Relations and Unitarity. General Theory.*, [Phys. Rev. **112** \(1958\) 1344](#).
- [60] S. Dulat *et al.*, *New parton distribution functions from a global analysis of quantum chromodynamics*, [Phys. Rev. D **93** \(2016\) 033006](#), arXiv: [1506.07443 \[hep-ph\]](#).
- [61] J-C. Winter, F. Krauss and G. Soff, *A modified cluster hadronization model*, [Eur. Phys. J. C **36** \(2004\) 381](#), arXiv: [hep-ph/0311085 \[hep-ph\]](#).
- [62] B. R. Webber, *A QCD model for jet fragmentation including soft gluon interference*, [Nucl. Phys. B **238** \(1984\) 492](#).
- [63] E. Bothmann *et al.*, *Event generation with Sherpa 2.2*, [SciPost Phys. **7** \(2019\) 034](#), arXiv: [1905.09127 \[hep-ph\]](#).
- [64] L. A. Harland-Lang, A.D. Martin, P. Motylinski and R.S. Thorne, *Parton distributions in the LHC era: MMHT 2014 PDFs*, [Eur. Phys. J. C **75** \(2015\) 204](#), arXiv: [1412.3989 \[hep-ph\]](#).
- [65] S. Platzer and S. Gieseke, *Dipole showers and automated NLO matching in Herwig++*, [Eur. Phys. J. C **72** \(2012\) 2187](#), arXiv: [1109.6256 \[hep-ph\]](#).
- [66] D. J. Lange, *The EvtGen particle decay simulation package*, [Nucl. Instrum. Meth. A **462** \(2001\) 152](#).
- [67] GEANT4 Collaboration, S. Agostinelli *et al.*, *GEANT4 – a simulation toolkit*, [Nucl. Instrum. Meth. A **506** \(2003\) 250](#).
- [68] ATLAS Collaboration, *The ATLAS Simulation Infrastructure*, [Eur. Phys. J. C **70** \(2010\) 823](#), arXiv: [1005.4568 \[physics.ins-det\]](#).
- [69] ATLAS Collaboration, *The Pythia 8 A3 tune description of ATLAS minimum bias and inelastic measurements incorporating the Donnachie–Landshoff diffractive model*, ATL-PHYS-PUB-2016-017, 2016, URL: <https://cds.cern.ch/record/2206965>.
- [70] ATLAS Collaboration, *Performance of the ATLAS muon triggers in Run 2*, [JINST **15** \(2020\) P09015](#), arXiv: [2004.13447 \[hep-ex\]](#).

- [71] ATLAS Collaboration, *Muon reconstruction performance of the ATLAS detector in proton–proton collision data at $\sqrt{s} = 13$ TeV*, *Eur. Phys. J. C* **76** (2016) 292, arXiv: [1603.05598 \[hep-ex\]](#).
- [72] ATLAS Collaboration, *Muon reconstruction and identification efficiency in ATLAS using the full Run 2 pp collision data set at $\sqrt{s} = 13$ TeV*, *Eur. Phys. J. C* **81** (2021) 578, arXiv: [2012.00578 \[hep-ex\]](#).
- [73] V. Kostyukhin, *VKalVrt - package for vertex reconstruction in ATLAS*, ATL-PHYS-2003-031, 2003, URL: <https://cds.cern.ch/record/685551>.
- [74] M. Tanabashi *et al.* (Particle Data Group), *Review of Particle Physics*, *Phys. Rev. D* **98** (2018) 030001.
- [75] ATLAS Collaboration, *Jet reconstruction and performance using particle flow with the ATLAS Detector*, *Eur. Phys. J. C* **77** (2017) 466, arXiv: [1703.10485 \[hep-ex\]](#).
- [76] ATLAS Collaboration, *Jet energy scale and resolution measured in proton–proton collisions at $\sqrt{s} = 13$ TeV with the ATLAS detector*, *Eur. Phys. J. C* **81** (2020) 689, arXiv: [2007.02645 \[hep-ex\]](#).
- [77] M. Cacciari, G.P. Salam and G. Soyez, *The anti- k_t jet clustering algorithm*, *JHEP* **04** (2008) 063, arXiv: [0802.1189 \[hep-ph\]](#).
- [78] M. Cacciari, G.P. Salam and G. Soyez, *FastJet user manual*, *Eur. Phys. J. C* **72** (2012) 1896, arXiv: [1111.6097 \[hep-ph\]](#).
- [79] M. Cacciari and G. P. Salam, *Pileup subtraction using jet areas*, *Phys. Lett. B* **659** (2008) 119, arXiv: [0707.1378 \[hep-ph\]](#).
- [80] ATLAS Collaboration, *Performance of pile-up mitigation techniques for jets in pp collisions at $\sqrt{s} = 8$ TeV using the ATLAS detector*, *Eur. Phys. J. C* **76** (2016) 581, arXiv: [1510.03823 \[hep-ex\]](#).
- [81] G. D’Agostini, *A multidimensional unfolding method based on Bayes’ theorem*, *Nucl. Instrum. Meth. A* **362** (1995) 487.
- [82] T. Adye, *Unfolding algorithms and tests using RooUnfold*, Proceedings of the PHYSTAT 2011 Workshop, CERN Geneva, Switzerland, CERN-2011-006, 313 (2011), arXiv: [1105.1160 \[physics.data-an\]](#), URL: <http://cdsweb.cern.ch/record/1306523>.
- [83] B. Efron, *An introduction to the bootstrap*, Chapman & Hall, New York (1994).
- [84] ATLAS Collaboration, *Performance of the ATLAS track reconstruction algorithms in dense environments in LHC Run 2*, *Eur. Phys. J. C* **77** (2017) 673, arXiv: [1704.07983 \[hep-ex\]](#).
- [85] ATLAS Collaboration, *Topological cell clustering in the ATLAS calorimeters and its performance in LHC Run 1*, *Eur. Phys. J. C* **77** (2017) 490, arXiv: [1603.02934 \[hep-ex\]](#).
- [86] ATLAS Collaboration, *ATLAS Computing Acknowledgements*, ATL-SOFT-PUB-2021-003, URL: <https://cds.cern.ch/record/2776662>.

The ATLAS Collaboration

G. Aad⁹⁹, B. Abbott¹²⁶, D.C. Abbott¹⁰⁰, A. Abed Abud³⁴, K. Abeling⁵¹, D.K. Abhayasinghe⁹¹, S.H. Abidi²⁷, O.S. AbouZeid³⁸, H. Abramowicz¹⁵⁹, H. Abreu¹⁵⁸, Y. Abulaiti⁵, A.C. Abusleme Hoffman^{144a}, B.S. Acharya^{64a,64b,p}, B. Achkar⁵¹, L. Adam⁹⁷, C. Adam Bourdarios⁴, L. Adamczyk^{81a}, L. Adamek¹⁶⁴, J. Adelman¹¹⁸, A. Adiguzel^{11c,ae}, S. Adorni⁵², T. Adye¹⁴¹, A.A. Affolder¹⁴³, Y. Afik¹⁵⁸, C. Agapopoulou⁶², M.N. Agaras¹², J. Agarwala^{68a,68b}, A. Aggarwal¹¹⁶, C. Agheorghiesei^{25c}, J.A. Aguilar-Saavedra^{137f,137a,ad}, A. Ahmad³⁴, F. Ahmadov⁷⁷, W.S. Ahmed¹⁰¹, X. Ai⁴⁴, G. Aielli^{71a,71b}, S. Akatsuka⁸³, M. Akbiyik⁹⁷, T.P.A. Åkesson⁹⁴, A.V. Akimov¹⁰⁸, K. Al Khoury³⁷, G.L. Alberghi^{21b}, J. Albert¹⁷³, M.J. Alconada Verzini⁸⁶, S. Alderweireldt³⁴, M. Aleksa³⁴, I.N. Aleksandrov⁷⁷, C. Alexa^{25b}, T. Alexopoulos⁹, A. Alfonsi¹¹⁷, F. Alfonsi^{21b,21a}, M. Alhroob¹²⁶, B. Ali¹³⁹, S. Ali¹⁵⁶, M. Aliev¹⁶³, G. Alimonti^{66a}, C. Allaire³⁴, B.M.M. Allbrooke¹⁵⁴, P.P. Allport¹⁹, A. Aloisio^{67a,67b}, F. Alonso⁸⁶, C. Alpigiani¹⁴⁶, E. Alunno Camelia^{71a,71b}, M. Alvarez Estevez⁹⁶, M.G. Alvigi^{67a,67b}, Y. Amaral Coutinho^{78b}, A. Ambler¹⁰¹, L. Ambroz¹³², C. Amelung³⁴, D. Amidei¹⁰³, S.P. Amor Dos Santos^{137a}, S. Amoroso⁴⁴, C.S. Amrouche⁵², C. Anastopoulos¹⁴⁷, N. Andari¹⁴², T. Andeen¹⁰, J.K. Anders¹⁸, S.Y. Andrean^{43a,43b}, A. Andreazza^{66a,66b}, V. Andrei^{59a}, S. Angelidakis⁸, A. Angerami³⁷, A.V. Anisenkov^{119b,119a}, A. Annovi^{69a}, C. Antel⁵², M.T. Anthony¹⁴⁷, E. Antipov¹²⁷, M. Antonelli⁴⁹, D.J.A. Antrim¹⁶, F. Anulli^{70a}, M. Aoki⁷⁹, J.A. Aparisi Pozo¹⁷¹, M.A. Aparo¹⁵⁴, L. Aperio Bella⁴⁴, N. Aranzabal³⁴, V. Araujo Ferraz^{78a}, C. Arcangeletti⁴⁹, A.T.H. Arce⁴⁷, E. Arena⁸⁸, J-F. Arguin¹⁰⁷, S. Argyropoulos⁵⁰, J.-H. Arling⁴⁴, A.J. Armbruster³⁴, A. Armstrong¹⁶⁸, O. Arnaez¹⁶⁴, H. Arnold³⁴, Z.P. Arrubarrena Tame¹¹¹, G. Artoni¹³², H. Asada¹¹⁴, K. Asai¹²⁴, S. Asai¹⁶¹, N.A. Asbah⁵⁷, E.M. Asimakopoulou¹⁶⁹, L. Asquith¹⁵⁴, J. Assahsah^{33d}, K. Assamagan²⁷, R. Astalos^{26a}, R.J. Atkin^{31a}, M. Atkinson¹⁷⁰, N.B. Atlay¹⁷, H. Atmani⁶², P.A. Atmasiddha¹⁰³, K. Augsten¹³⁹, S. Auricchio^{67a,67b}, V.A. Austrup¹⁷⁹, G. Avolio³⁴, M.K. Ayoub^{13c}, G. Azuelos^{107,ak}, D. Babal^{26a}, H. Bachacou¹⁴², K. Bachas¹⁶⁰, F. Backman^{43a,43b}, P. Bagnaia^{70a,70b}, H. Bahrasemani¹⁵⁰, A.J. Bailey¹⁷¹, V.R. Bailey¹⁷⁰, J.T. Baines¹⁴¹, C. Bakalis⁹, O.K. Baker¹⁸⁰, P.J. Bakker¹¹⁷, E. Bakos¹⁴, D. Bakshi Gupta⁷, S. Balaji¹⁵⁵, R. Balasubramanian¹¹⁷, E.M. Baldin^{119b,119a}, P. Balek¹⁴⁰, E. Ballabene^{66a,66b}, F. Balli¹⁴², W.K. Balunas¹³², J. Balz⁹⁷, E. Banas⁸², M. Bandieramonte¹³⁶, A. Bandyopadhyay¹⁷, L. Barak¹⁵⁹, E.L. Barberio¹⁰², D. Barberis^{53b,53a}, M. Barbero⁹⁹, G. Barbour⁹², K.N. Barends^{31a}, T. Barillari¹¹², M-S. Barisits³⁴, J. Barkeloo¹²⁹, T. Barklow¹⁵¹, B.M. Barnett¹⁴¹, R.M. Barnett¹⁶, A. Baroncelli^{58a}, G. Barone²⁷, A.J. Barr¹³², L. Barranco Navarro^{43a,43b}, F. Barreiro⁹⁶, J. Barreiro Guimarães da Costa^{13a}, U. Barron¹⁵⁹, S. Barsov¹³⁵, F. Bartels^{59a}, R. Bartoldus¹⁵¹, G. Bartolini⁹⁹, A.E. Barton⁸⁷, P. Bartos^{26a}, A. Basalaev⁴⁴, A. Basan⁹⁷, I. Bashta^{72a,72b}, A. Bassalat⁶², M.J. Basso¹⁶⁴, C.R. Basson⁹⁸, R.L. Bates⁵⁵, S. Batlamous^{33e}, J.R. Batley³⁰, B. Batool¹⁴⁹, M. Battaglia¹⁴³, M. Baucé^{70a,70b}, F. Bauer^{142,*}, P. Bauer²², H.S. Bawa²⁹, A. Bayirli^{11c}, J.B. Beacham⁴⁷, T. Beau¹³³, P.H. Beauchemin¹⁶⁷, F. Becherer⁵⁰, P. Bechtel²², H.P. Beck^{18,r}, K. Becker¹⁷⁵, C. Becot⁴⁴, A.J. Beddall^{11a}, V.A. Bednyakov⁷⁷, C.P. Bee¹⁵³, T.A. Beermann¹⁷⁹, M. Begalli^{78b}, M. Begel²⁷, A. Behera¹⁵³, J.K. Behr⁴⁴, C. Beirao Da Cruz E Silva³⁴, J.F. Beirer^{51,34}, F. Beisiegel²², M. Belfkir⁴, G. Bella¹⁵⁹, L. Bellagamba^{21b}, A. Bellerive³², P. Bellos¹⁹, K. Beloborodov^{119b,119a}, K. Belotskiy¹⁰⁹, N.L. Belyaev¹⁰⁹, D. Benchekroun^{33a}, Y. Benhammou¹⁵⁹, D.P. Benjamin⁵, M. Benoit²⁷, J.R. Bensinger²⁴, S. Bentvelsen¹¹⁷, L. Beresford¹³², M. Beretta⁴⁹, D. Berge¹⁷, E. Bergeaas Kuutmann¹⁶⁹, N. Berger⁴, B. Bergmann¹³⁹, L.J. Bergsten²⁴, J. Beringer¹⁶, S. Berlendis⁶, G. Bernardi¹³³, C. Bernius¹⁵¹, F.U. Bernlochner²², T. Berry⁹¹, P. Berta⁴⁴, A. Berthold⁴⁶, I.A. Bertram⁸⁷, O. Bessidskaia Bylund¹⁷⁹, S. Bethke¹¹², A. Betti⁴⁰, A.J. Bevan⁹⁰, S. Bhatta¹⁵³, D.S. Bhattacharya¹⁷⁴, P. Bhattarai²⁴, V.S. Bhopatkar⁵, R. Bi¹³⁶, R.M. Bianchi¹³⁶, O. Biebel¹¹¹, R. Bielski³⁴, N.V. Biesuz^{69a,69b}, M. Biglietti^{72a}, T.R.V. Billoud¹³⁹, M. Bindi⁵¹, A. Bingul^{11d}, C. Bini^{70a,70b}, S. Biondi^{21b,21a}, C.J. Birch-sykes⁹⁸, G.A. Bird^{19,141}, M. Birman¹⁷⁷, T. Bisanz³⁴, J.P. Biswal²,

D. Biswas^{178,k}, A. Bitadze⁹⁸, C. Bittrich⁴⁶, K. Bjørke¹³¹, I. Bloch⁴⁴, C. Blocker²⁴, A. Blue⁵⁵,
 U. Blumenschein⁹⁰, J. Blumenthal⁹⁷, G.J. Bobbink¹¹⁷, V.S. Bobrovnikov^{119b,119a}, D. Bogavac¹²,
 A.G. Bogdanchikov^{119b,119a}, C. Bohm^{43a}, V. Boisvert⁹¹, P. Bokan⁴⁴, T. Bold^{81a}, M. Bomben¹³³,
 M. Bona⁹⁰, M. Boonekamp¹⁴², C.D. Booth⁹¹, A.G. Borbély⁵⁵, H.M. Borecka-Bielska¹⁰⁷, L.S. Borgna⁹²,
 G. Borisso⁸⁷, D. Bortoletto¹³², D. Boscherini^{21b}, M. Bosman¹², J.D. Bossio Sola¹⁰¹, K. Bouaouda^{33a},
 J. Boudreau¹³⁶, E.V. Bouhova-Thacker⁸⁷, D. Boumediene³⁶, R. Bouquet¹³³, A. Boveia¹²⁵, J. Boyd³⁴,
 D. Boye²⁷, I.R. Boyko⁷⁷, A.J. Bozson⁹¹, J. Bracinik¹⁹, N. Brahimi^{58d,58c}, G. Brandt¹⁷⁹, O. Brandt³⁰,
 F. Braren⁴⁴, B. Brau¹⁰⁰, J.E. Brau¹²⁹, W.D. Breaden Madden⁵⁵, K. Brendlinger⁴⁴, R. Brenner¹⁷⁷,
 L. Brenner³⁴, R. Brenner¹⁶⁹, S. Bressler¹⁷⁷, B. Brickwedde⁹⁷, D.L. Briglin¹⁹, D. Britton⁵⁵, D. Britzger¹¹²,
 I. Brock²², R. Brock¹⁰⁴, G. Brooijmans³⁷, W.K. Brooks^{144f}, E. Brost²⁷, P.A. Bruckman de Renstrom⁸²,
 B. Brüers⁴⁴, D. Bruncko^{26b}, A. Bruni^{21b}, G. Bruni^{21b}, M. Bruschi^{21b}, N. Brusino^{70a,70b},
 L. Bryngemark¹⁵¹, T. Buanes¹⁵, Q. Buat¹⁵³, P. Buchholz¹⁴⁹, A.G. Buckley⁵⁵, I.A. Budagov⁷⁷,
 M.K. Bugge¹³¹, O. Bulekov¹⁰⁹, B.A. Bullard⁵⁷, T.J. Burch¹¹⁸, S. Burdin⁸⁸, C.D. Burgard⁴⁴,
 A.M. Burger¹²⁷, B. Burghgrave⁷, J.T.P. Burr⁴⁴, C.D. Burton¹⁰, J.C. Burzynski¹⁰⁰, V. Büscher⁹⁷,
 P.J. Bussey⁵⁵, J.M. Butler²³, C.M. Buttar⁵⁵, J.M. Butterworth⁹², W. Buttinger¹⁴¹, C.J. Buxo Vazquez¹⁰⁴,
 A.R. Buzykaev^{119b,119a}, G. Cabras^{21b}, S. Cabrera Urbán¹⁷¹, D. Caforio⁵⁴, H. Cai¹³⁶, V.M.M. Cairo¹⁵¹,
 O. Cakir^{3a}, N. Calace³⁴, P. Calafiura¹⁶, G. Calderini¹³³, P. Calfayan⁶³, G. Callea⁵⁵, L.P. Caloba^{78b},
 A. Caltabiano^{71a,71b}, S. Calvente Lopez⁹⁶, D. Calvet³⁶, S. Calvet³⁶, T.P. Calvet⁹⁹, M. Calvetti^{69a,69b},
 R. Camacho Toro¹³³, S. Camarda³⁴, D. Camarero Munoz⁹⁶, P. Camarri^{71a,71b}, M.T. Camerlingo^{72a,72b},
 D. Cameron¹³¹, C. Camincher¹⁷³, M. Campanelli⁹², A. Camplani³⁸, V. Canale^{67a,67b}, A. Canesse¹⁰¹,
 M. Cano Bret⁷⁵, J. Cantero¹²⁷, Y. Cao¹⁷⁰, M. Capua^{39b,39a}, R. Cardarelli^{71a}, F. Cardillo¹⁷¹,
 G. Carducci^{39b,39a}, T. Carli³⁴, G. Carlino^{67a}, B.T. Carlson¹³⁶, E.M. Carlson^{173,165a}, L. Carminati^{66a,66b},
 M. Carnesale^{70a,70b}, R.M.D. Carney¹⁵¹, S. Caron¹¹⁶, E. Carquin^{144f}, S. Carrá⁴⁴, G. Carratta^{21b,21a},
 J.W.S. Carter¹⁶⁴, T.M. Carter⁴⁸, D. Casadei^{31c}, M.P. Casado^{12,h}, A.F. Casha¹⁶⁴, E.G. Castiglia¹⁸⁰,
 F.L. Castillo¹⁷¹, L. Castillo Garcia¹², V. Castillo Gimenez¹⁷¹, N.F. Castro^{137a,137e}, A. Catinaccio³⁴,
 J.R. Catmore¹³¹, A. Cattai³⁴, V. Cavaliere²⁷, N. Cavalli^{21b,21a}, V. Cavasinni^{69a,69b}, E. Celebi^{11b}, F. Celli¹³²,
 K. Cerny¹²⁸, A.S. Cerqueira^{78a}, A. Cerri¹⁵⁴, L. Cerrito^{71a,71b}, F. Cerutti¹⁶, A. Cervelli^{21b}, S.A. Cetin^{11b},
 Z. Chadi^{33a}, D. Chakraborty¹¹⁸, M. Chala^{137f}, J. Chan¹⁷⁸, W.S. Chan¹¹⁷, W.Y. Chan⁸⁸, J.D. Chapman³⁰,
 B. Chargeishvili^{157b}, D.G. Charlton¹⁹, T.P. Charman⁹⁰, M. Chatterjee¹⁸, C.C. Chau³², S. Chekanov⁵,
 S.V. Chekulaev^{165a}, G.A. Chelkov^{77,ag}, A. Chen¹⁰³, B. Chen⁷⁶, C. Chen^{58a}, C.H. Chen⁷⁶, H. Chen^{13c},
 H. Chen²⁷, J. Chen^{58a}, J. Chen³⁷, J. Chen²⁴, S. Chen¹³⁴, S.J. Chen^{13c}, X. Chen^{13b}, Y. Chen^{58a},
 Y-H. Chen⁴⁴, C.L. Cheng¹⁷⁸, H.C. Cheng^{60a}, H.J. Cheng^{13a}, A. Cheplakov⁷⁷, E. Cheremushkina⁴⁴,
 R. Cherkaoui El Moursli^{33e}, E. Cheu⁶, K. Cheung⁶¹, L. Chevalier¹⁴², V. Chiarella⁴⁹, G. Chiarelli^{69a},
 G. Chiodini^{65a}, A.S. Chisholm¹⁹, A. Chitan^{25b}, I. Chiu¹⁶¹, Y.H. Chiu¹⁷³, M.V. Chizhov^{77,t}, K. Choi¹⁰,
 A.R. Chomont^{70a,70b}, Y. Chou¹⁰⁰, Y.S. Chow¹¹⁷, L.D. Christopher^{31g}, M.C. Chu^{60a}, X. Chu^{13a,13d},
 J. Chudoba¹³⁸, J.J. Chwastowski⁸², D. Cieri¹¹², K.M. Ciesla⁸², V. Cindro⁸⁹, I.A. Cioară^{25b}, A. Ciocio¹⁶,
 F. Ciotto^{67a,67b}, Z.H. Citron^{177,1}, M. Citterio^{66a}, D.A. Ciubotaru^{25b}, B.M. Ciungu¹⁶⁴, A. Clark⁵²,
 P.J. Clark⁴⁸, S.E. Clawson⁹⁸, C. Clement^{43a,43b}, L. Clissa^{21b,21a}, Y. Coadou⁹⁹, M. Cokal^{64a,64c},
 A. Coccaro^{53b}, J. Cochran⁷⁶, R.F. Coelho Barrue^{137a}, R. Coelho Lopes De Sa¹⁰⁰, S. Coelli^{66a}, H. Cohen¹⁵⁹,
 A.E.C. Coimbra³⁴, B. Cole³⁷, J. Collot⁵⁶, P. Conde Muñio^{137a,137h}, S.H. Connell^{31c}, I.A. Connelly⁵⁵,
 E.I. Conroy¹³², F. Conventi^{67a,al}, H.G. Cooke¹⁹, A.M. Cooper-Sarkar¹³², F. Cormier¹⁷², L.D. Corpe⁹²,
 M. Corradi^{70a,70b}, E.E. Corrigan⁹⁴, F. Corriveau^{101,aa}, M.J. Costa¹⁷¹, F. Costanza⁴, D. Costanzo¹⁴⁷,
 B.M. Cote¹²⁵, G. Cowan⁹¹, J.W. Cowley³⁰, J. Crane⁹⁸, K. Cranmer¹²³, R.A. Creager¹³⁴,
 S. Crépe-Renaudin⁵⁶, F. Crescioli¹³³, M. Cristinziani¹⁴⁹, M. Cristoforetti^{73a,73b,b}, V. Croft¹⁶⁷,
 G. Crosetti^{39b,39a}, A. Cueto⁴, T. Cuhadar Donszelmann¹⁶⁸, H. Cui^{13a,13d}, A.R. Cukierman¹⁵¹,
 W.R. Cunningham⁵⁵, S. Czekierda⁸², P. Czodrowski³⁴, M.M. Czurylo^{59b},
 M.J. Da Cunha Sargedas De Sousa^{58a}, J.V. Da Fonseca Pinto^{78b}, C. Da Via⁹⁸, W. Dabrowski^{81a}, T. Dado⁴⁵,

S. Dahbi^{31g}, T. Dai¹⁰³, C. Dallapiccola¹⁰⁰, M. Dam³⁸, G. D'amen²⁷, V. D'Amico^{72a,72b}, J. Damp⁹⁷,
 J.R. Dandoy¹³⁴, M.F. Daneri²⁸, M. Danninger¹⁵⁰, V. Dao³⁴, G. Darbo^{53b}, A. Dattagupta¹²⁹,
 S. D'Auria^{66a,66b}, C. David^{165b}, T. Davidek¹⁴⁰, D.R. Davis⁴⁷, B. Davis-Purcell³², I. Dawson⁹⁰, K. De⁷,
 R. De Asmundis^{67a}, M. De Beurs¹¹⁷, S. De Castro^{21b,21a}, N. De Groot¹¹⁶, P. de Jong¹¹⁷, H. De la Torre¹⁰⁴,
 A. De Maria^{13c}, D. De Pedis^{70a}, A. De Salvo^{70a}, U. De Sanctis^{71a,71b}, M. De Santis^{71a,71b}, A. De Santo¹⁵⁴,
 J.B. De Vivie De Regie⁵⁶, D.V. Dedovich⁷⁷, J. Degens¹¹⁷, A.M. Deiana⁴⁰, J. Del Peso⁹⁶,
 Y. Delabat Diaz⁴⁴, F. Deliot¹⁴², C.M. Delitzsch⁶, M. Della Pietra^{67a,67b}, D. Della Volpe⁵², A. Dell'Acqua³⁴,
 L. Dell'Asta^{66a,66b}, M. Delmastro⁴, P.A. Delsart⁵⁶, S. Demers¹⁸⁰, M. Demichev⁷⁷, S.P. Denisov¹²⁰,
 L. D'Eramo¹¹⁸, D. Derendarz⁸², J.E. Derkaoui^{33d}, F. Derue¹³³, P. Dervan⁸⁸, K. Desch²², K. Dette¹⁶⁴,
 C. Deutsch²², P.O. Deviveiros³⁴, F.A. Di Bello^{70a,70b}, A. Di Ciaccio^{71a,71b}, L. Di Ciaccio⁴,
 C. Di Donato^{67a,67b}, A. Di Girolamo³⁴, G. Di Gregorio^{69a,69b}, A. Di Luca^{73a,73b}, B. Di Micco^{72a,72b},
 R. Di Nardo^{72a,72b}, C. Diaconu⁹⁹, F.A. Dias¹¹⁷, T. Dias Do Vale^{137a}, M.A. Diaz^{144a}, F.G. Diaz Capriles²²,
 J. Dickinson¹⁶, M. Didenko¹⁷¹, E.B. Diehl¹⁰³, J. Dietrich¹⁷, S. Díez Cornell⁴⁴, C. Diez Pardos¹⁴⁹,
 A. Dimitrievska¹⁶, W. Ding^{13b}, J. Dingfelder²², S.J. Dittmeier^{59b}, F. Dittus³⁴, F. Djama⁹⁹, T. Djobava^{157b},
 J.I. Djuvsland¹⁵, M.A.B. Do Vale¹⁴⁵, D. Dodsworth²⁴, C. Doglioni⁹⁴, J. Dolejsi¹⁴⁰, Z. Dolezal¹⁴⁰,
 M. Donadelli^{78c}, B. Dong^{58c}, J. Donini³⁶, A. D'onofrio^{13c}, M. D'Onofrio⁸⁸, J. Dopke¹⁴¹, A. Doria^{67a},
 M.T. Dova⁸⁶, A.T. Doyle⁵⁵, E. Drechsler¹⁵⁰, E. Dreyer¹⁵⁰, T. Dreyer⁵¹, A.S. Drobac¹⁶⁷, D. Du^{58b},
 T.A. du Pree¹¹⁷, F. Dubinin¹⁰⁸, M. Dubovsky^{26a}, A. Dubreuil⁵², E. Duchovni¹⁷⁷, G. Duckeck¹¹¹,
 O.A. Ducu^{34,25b}, D. Duda¹¹², A. Dudarev³⁴, M. D'uffizi⁹⁸, L. Duflo⁶², M. Dührssen³⁴, C. Dülsen¹⁷⁹,
 A.E. Dumitriu^{25b}, M. Dunford^{59a}, S. Dungs⁴⁵, A. Duperrin⁹⁹, H. Duran Yildiz^{3a}, M. Düren⁵⁴,
 A. Durglishvili^{157b}, B. Dutta⁴⁴, D. Duvnjak¹, G.I. Dyckes¹³⁴, M. Dyndal^{81a}, S. Dysch⁹⁸, B.S. Dziedzic⁸²,
 B. Eckerova^{26a}, M.G. Eggleston⁴⁷, E. Egidio Purcino De Souza^{78b}, L.F. Ehrke⁵², T. Eifert⁷, G. Eigen¹⁵,
 K. Einsweiler¹⁶, T. Ekelof¹⁶⁹, Y. El Ghazali^{33b}, H. El Jarrari^{33e}, A. El Moussaouy^{33a}, V. Ellajosyula¹⁶⁹,
 M. Ellert¹⁶⁹, F. Ellinghaus¹⁷⁹, A.A. Elliot⁹⁰, N. Ellis³⁴, J. Elmsheuser²⁷, M. Elsing³⁴, D. Emeliyanov¹⁴¹,
 A. Emerman³⁷, Y. Enari¹⁶¹, J. Erdmann⁴⁵, A. Ereditato¹⁸, P.A. Erland⁸², M. Errenst¹⁷⁹, M. Escalier⁶²,
 C. Escobar¹⁷¹, O. Estrada Pastor¹⁷¹, E. Etzion¹⁵⁹, G. Evans^{137a}, H. Evans⁶³, M.O. Evans¹⁵⁴, A. Ezhilov¹³⁵,
 F. Fabbri⁵⁵, L. Fabbri^{21b,21a}, V. Fabiani¹¹⁶, G. Facini¹⁷⁵, R.M. Fakhrutdinov¹²⁰, S. Falciano^{70a}, P.J. Falke²²,
 S. Falke³⁴, J. Faltova¹⁴⁰, Y. Fan^{13a}, Y. Fang^{13a}, Y. Fang^{13a}, G. Fanourakis⁴², M. Fanti^{66a,66b}, M. Faraj^{58c},
 A. Farbin⁷, A. Farilla^{72a}, E.M. Farina^{68a,68b}, T. Farrow¹⁰⁴, S.M. Farrington⁴⁸, P. Farthouat³⁴, F. Fassi^{33e},
 D. Fassouliotis⁸, M. Faucci Giannelli^{71a,71b}, W.J. Fawcett³⁰, L. Fayard⁶², O.L. Fedin^{135,q}, M. Feickert¹⁷⁰,
 L. Feligioni⁹⁹, A. Fell¹⁴⁷, C. Feng^{58b}, M. Feng^{13b}, M.J. Fenton¹⁶⁸, A.B. Fenyuk¹²⁰, S.W. Ferguson⁴¹,
 J. Ferrando⁴⁴, A. Ferrari¹⁶⁹, P. Ferrari¹¹⁷, R. Ferrari^{68a}, D. Ferrere⁵², C. Ferretti¹⁰³, F. Fiedler⁹⁷,
 A. Filipčić⁸⁹, F. Filthaut¹¹⁶, M.C.N. Fiolhais^{137a,137c,a}, L. Fiorini¹⁷¹, F. Fischer¹¹¹, W.C. Fisher¹⁰⁴,
 T. Fitschen¹⁹, I. Fleck¹⁴⁹, P. Fleischmann¹⁰³, T. Flick¹⁷⁹, B.M. Flierl¹¹¹, L. Flores¹³⁴,
 L.R. Flores Castillo^{60a}, F.M. Follega^{73a,73b}, N. Fomin¹⁵, J.H. Foo¹⁶⁴, G.T. Forcolin^{73a,73b}, B.C. Forland⁶³,
 A. Formica¹⁴², F.A. Förster¹², A.C. Forti⁹⁸, E. Fortin⁹⁹, M.G. Foti¹³², D. Fournier⁶², H. Fox⁸⁷,
 P. Francavilla^{69a,69b}, S. Francescato^{70a,70b}, M. Franchini^{21b,21a}, S. Franchino^{59a}, D. Francis³⁴, L. Franco⁴,
 L. Franconi¹⁸, M. Franklin⁵⁷, G. Frattari^{70a,70b}, A.C. Freegard⁹⁰, P.M. Freeman¹⁹, B. Freund¹⁰⁷,
 W.S. Freund^{78b}, E.M. Freundlich⁴⁵, D. Froidevaux³⁴, J.A. Frost¹³², Y. Fu^{58a}, M. Fujimoto¹²⁴,
 E. Fullana Torregrosa¹⁷¹, T. Fusayasu¹¹³, J. Fuster¹⁷¹, A. Gabrielli^{21b,21a}, A. Gabrielli³⁴, P. Gadow⁴⁴,
 G. Gagliardi^{53b,53a}, L.G. Gagnon¹⁶, G.E. Gallardo¹³², E.J. Gallas¹³², B.J. Gallop¹⁴¹, R. Gamboa Goni⁹⁰,
 K.K. Gan¹²⁵, S. Ganguly¹⁷⁷, J. Gao^{58a}, Y. Gao⁴⁸, Y.S. Gao^{29,n}, F.M. Garay Walls^{144a}, C. García¹⁷¹,
 J.E. García Navarro¹⁷¹, J.A. García Pascual^{13a}, M. Garcia-Sciveres¹⁶, R.W. Gardner³⁵, D. Garg⁷⁵,
 S. Gargiulo⁵⁰, C.A. Garner¹⁶⁴, V. Garonne¹³¹, S.J. Gasirowski¹⁴⁶, P. Gaspar^{78b}, G. Gaudio^{68a},
 P. Gauzzi^{70a,70b}, I.L. Gavrilenko¹⁰⁸, A. Gavriluk¹²¹, C. Gay¹⁷², G. Gaycken⁴⁴, E.N. Gazis⁹,
 A.A. Geanta^{25b}, C.M. Gee¹⁴³, C.N.P. Gee¹⁴¹, J. Geisen⁹⁴, M. Geisen⁹⁷, C. Gemme^{53b}, M.H. Genest⁵⁶,
 S. Gentile^{70a,70b}, S. George⁹¹, T. Gerialis⁴², L.O. Gerlach⁵¹, P. Gessinger-Befurt⁹⁷, G. Gessner⁴⁵,

M. Ghasemi Bostanabad¹⁷³, M. Ghneimat¹⁴⁹, A. Ghosh¹⁶⁸, A. Ghosh⁷⁵, B. Giacobbe^{21b}, S. Giagu^{70a,70b}, N. Giangiacomi¹⁶⁴, P. Giannetti^{69a}, A. Giannini^{67a,67b}, S.M. Gibson⁹¹, M. Gignac¹⁴³, D.T. Gil^{81b}, B.J. Gilbert³⁷, D. Gillberg³², G. Gilles¹⁷⁹, N.E.K. Gillwald⁴⁴, D.M. Gingrich^{2,ak}, M.P. Giordani^{64a,64c}, P.F. Giraud¹⁴², G. Giugliarelli^{64a,64c}, D. Giugni^{66a}, F. Giuli^{71a,71b}, I. Gkialas^{8,i}, E.L. Gkoukousis¹², P. Gkoutoumis⁹, L.K. Gladilin¹¹⁰, C. Glasman⁹⁶, G.R. Gledhill¹²⁹, M. Glisic¹²⁹, I. Gnesi^{39b,d}, M. Goblirsch-Kolb²⁴, D. Godin¹⁰⁷, S. Goldfarb¹⁰², T. Golling⁵², D. Golubkov¹²⁰, J.P. Gombas¹⁰⁴, A. Gomes^{137a,137b}, R. Goncalves Gama⁵¹, R. Gonçalves^{137a,137c}, G. Gonella¹²⁹, L. Gonella¹⁹, A. Gongadze⁷⁷, F. Gonnella¹⁹, J.L. Gonski³⁷, S. González de la Hoz¹⁷¹, S. Gonzalez Fernandez¹², R. Gonzalez Lopez⁸⁸, C. Gonzalez Renteria¹⁶, R. Gonzalez Suarez¹⁶⁹, S. Gonzalez-Sevilla⁵², G.R. Gonzalvo Rodriguez¹⁷¹, R.Y. González Andana^{144a}, L. Goossens³⁴, N.A. Gorasia¹⁹, P.A. Gorbounov¹²¹, H.A. Gordon²⁷, B. Gorini³⁴, E. Gorini^{65a,65b}, A. Gorišek⁸⁹, A.T. Goshaw⁴⁷, M.I. Gostkin⁷⁷, C.A. Gottardo¹¹⁶, M. Goughri^{33b}, V. Goumarre⁴⁴, A.G. Goussiou¹⁴⁶, N. Govender^{31c}, C. Goy⁴, I. Grabowska-Bold^{81a}, K. Graham³², E. Gramstad¹³¹, S. Grancagnolo¹⁷, M. Grandi¹⁵⁴, V. Gratchev¹³⁵, P.M. Gravila^{25f}, F.G. Gravill^{65a,65b}, H.M. Gray¹⁶, C. Grefe²², I.M. Gregor⁴⁴, P. Grenier¹⁵¹, K. Grevtsov⁴⁴, C. Grieco¹², N.A. Grieser¹²⁶, A.A. Grillo¹⁴³, K. Grimm^{29,m}, S. Grinstein^{12,x}, J.-F. Grivaz⁶², S. Groh⁹⁷, E. Gross¹⁷⁷, J. Grosse-Knetter⁵¹, Z.J. Grout⁹², C. Grud¹⁰³, A. Grummer¹¹⁵, J.C. Grundy¹³², L. Guan¹⁰³, W. Guan¹⁷⁸, C. Gubbels¹⁷², J. Guenther³⁴, J.G.R. Guerrero Rojas¹⁷¹, F. Guescini¹¹², D. Guest¹⁷, R. Gugel⁹⁷, A. Guida⁴⁴, T. Guillemin⁴, S. Guindon³⁴, J. Guo^{58c}, L. Guo⁶², Y. Guo¹⁰³, R. Gupta⁴⁴, S. Gurbuz²², G. Gustavino¹²⁶, M. Guth⁵⁰, P. Gutierrez¹²⁶, L.F. Gutierrez Zagazeta¹³⁴, C. Gutschow⁹², C. Guyot¹⁴², C. Gwenlan¹³², C.B. Gwilliam⁸⁸, E.S. Haaland¹³¹, A. Haas¹²³, M. Habedank¹⁷, C. Haber¹⁶, H.K. Hadavand⁷, A. Hadei⁹⁷, M. Haleem¹⁷⁴, J. Haley¹²⁷, J.J. Hall¹⁴⁷, G. Halladjian¹⁰⁴, G.D. Hallewell⁹⁹, L. Halser¹⁸, K. Hamano¹⁷³, H. Hamdaoui^{33e}, M. Hamer²², G.N. Hamity⁴⁸, K. Han^{58a}, L. Han^{13c}, L. Han^{58a}, S. Han¹⁶, Y.F. Han¹⁶⁴, K. Hanagaki^{79,v}, M. Hance¹⁴³, M.D. Hank³⁵, R. Hankache⁹⁸, E. Hansen⁹⁴, J.B. Hansen³⁸, J.D. Hansen³⁸, M.C. Hansen²², P.H. Hansen³⁸, K. Hara¹⁶⁶, T. Harenberg¹⁷⁹, S. Harkusha¹⁰⁵, Y.T. Harris¹³², P.F. Harrison¹⁷⁵, N.M. Hartman¹⁵¹, N.M. Hartmann¹¹¹, Y. Hasegawa¹⁴⁸, A. Hasib⁴⁸, S. Hassani¹⁴², S. Haug¹⁸, R. Hauser¹⁰⁴, M. Havranek¹³⁹, C.M. Hawkes¹⁹, R.J. Hawkings³⁴, S. Hayashida¹¹⁴, D. Hayden¹⁰⁴, C. Hayes¹⁰³, R.L. Hayes¹⁷², C.P. Hays¹³², J.M. Hays⁹⁰, H.S. Hayward⁸⁸, S.J. Haywood¹⁴¹, F. He^{58a}, Y. He¹⁶², Y. He¹³³, M.P. Heath⁴⁸, V. Hedberg⁹⁴, A.L. Heggelund¹³¹, N.D. Hehir⁹⁰, C. Heidegger⁵⁰, K.K. Heidegger⁵⁰, W.D. Heidorn⁷⁶, J. Heilman³², S. Heim⁴⁴, T. Heim¹⁶, B. Heinemann^{44,ai}, J.G. Heinlein¹³⁴, J.J. Heinrich¹²⁹, L. Heinrich³⁴, J. Hejbal¹³⁸, L. Helary⁴⁴, A. Held¹²³, S. Hellesund¹³¹, C.M. Helling¹⁴³, S. Hellman^{43a,43b}, C. Helsen³⁴, R.C.W. Henderson⁸⁷, L. Henkelmann³⁰, A.M. Henriques Correia³⁴, H. Herde¹⁵¹, Y. Hernández Jiménez^{31g}, H. Herr⁹⁷, M.G. Herrmann¹¹¹, T. Herrmann⁴⁶, G. Herten⁵⁰, R. Hertenberger¹¹¹, L. Hervas³⁴, N.P. Hessey^{165a}, H. Hibi⁸⁰, S. Higashino⁷⁹, E. Higón-Rodríguez¹⁷¹, K.K. Hill²⁷, K.H. Hiller⁴⁴, S.J. Hillier¹⁹, M. Hils⁴⁶, I. Hinchliffe¹⁶, F. Hinterkeuser²², M. Hirose¹³⁰, S. Hirose¹⁶⁶, D. Hirschbuehl¹⁷⁹, B. Hiti⁸⁹, O. Hladik¹³⁸, J. Hobbs¹⁵³, R. Hobincu^{25e}, N. Hod¹⁷⁷, M.C. Hodgkinson¹⁴⁷, B.H. Hodgkinson³⁰, A. Hoecker³⁴, J. Hofer⁴⁴, D. Hohn⁵⁰, T. Holm²², T.R. Holmes³⁵, M. Holzbock¹¹², L.B.A.H. Hommels³⁰, B.P. Honan⁹⁸, T.M. Hong¹³⁶, J.C. Honig⁵⁰, A. Hönle¹¹², B.H. Hooberman¹⁷⁰, W.H. Hopkins⁵, Y. Horii¹¹⁴, P. Horn⁴⁶, L.A. Horyn³⁵, S. Hou¹⁵⁶, J. Howarth⁵⁵, J. Hoya⁸⁶, M. Hrabovsky¹²⁸, A. Hrynevich¹⁰⁶, T. Hryn'ova⁴, P.J. Hsu⁶¹, S.-C. Hsu¹⁴⁶, Q. Hu³⁷, S. Hu^{58c}, Y.F. Hu^{13a,13d,am}, D.P. Huang⁹², X. Huang^{13c}, Y. Huang^{58a}, Y. Huang^{13a}, Z. Hubacek¹³⁹, F. Hubaut⁹⁹, M. Huebner²², F. Huegging²², T.B. Huffman¹³², M. Huhtinen³⁴, R. Hulskén⁵⁶, N. Huseynov^{77,ab}, J. Huston¹⁰⁴, J. Huth⁵⁷, R. Hyneman¹⁵¹, S. Hyrych^{26a}, G. Iacobucci⁵², G. Iakovidis²⁷, I. Ibragimov¹⁴⁹, L. Iconomidou-Fayard⁶², P. Iengo³⁴, R. Ignazzi³⁸, R. Iguchi¹⁶¹, T. Iizawa⁵², Y. Ikegami⁷⁹, A. Ilg¹⁸, N. Ilic^{164,164}, H. Imam^{33a}, G. Introzzi^{68a,68b}, M. Iodice^{72a}, K. Iordanidou^{165a}, V. Ippolito^{70a,70b}, M. Ishino¹⁶¹, W. Islam¹²⁷, C. Issever^{17,44}, S. Istin^{11c,an}, J.M. Iturbe Ponce^{60a}, R. Iuppa^{73a,73b}, A. Ivina¹⁷⁷, J.M. Izen⁴¹, V. Izzo^{67a}, P. Jacka¹³⁸, P. Jackson¹, R.M. Jacobs⁴⁴, B.P. Jaeger¹⁵⁰, C.S. Jagfeld¹¹¹, G. Jäkel¹⁷⁹, K.B. Jakobi⁹⁷, K. Jakobs⁵⁰, T. Jakoubek¹⁷⁷, J. Jamieson⁵⁵, K.W. Janas^{81a}, G. Jarlskog⁹⁴, A.E. Jaspán⁸⁸,

N. Javadov^{77,ab}, T. Javûrek³⁴, M. Javurkova¹⁰⁰, F. Jeanneau¹⁴², L. Jeanty¹²⁹, J. Jejelava^{157a,ac}, P. Jenni^{50,e}, S. Jézéquel⁴, J. Jia¹⁵³, Z. Jia^{13c}, Y. Jiang^{58a}, S. Jiggins⁵⁰, J. Jimenez Pena¹¹², S. Jin^{13c}, A. Jinaru^{25b}, O. Jinnouchi¹⁶², H. Jivan^{31g}, P. Johansson¹⁴⁷, K.A. Johns⁶, C.A. Johnson⁶³, E. Jones¹⁷⁵, R.W.L. Jones⁸⁷, T.J. Jones⁸⁸, J. Jovicevic³⁴, X. Ju¹⁶, J.J. Junggeburch¹¹², A. Juste Rozas^{12,x}, A. Kaczmarska⁸², M. Kado^{70a,70b}, H. Kagan¹²⁵, M. Kagan¹⁵¹, A. Kahn³⁷, C. Kahra⁹⁷, T. Kaji¹⁷⁶, E. Kajomovitz¹⁵⁸, C.W. Kalderon²⁷, A. Kaluza⁹⁷, A. Kamenshchikov¹²⁰, M. Kaneda¹⁶¹, N.J. Kang¹⁴³, S. Kang⁷⁶, Y. Kano¹¹⁴, J. Kanzaki⁷⁹, D. Kar^{31g}, K. Karava¹³², M.J. Kareem^{165b}, I. Karkanias¹⁶⁰, S.N. Karpov⁷⁷, Z.M. Karpova⁷⁷, V. Kartvelishvili⁸⁷, A.N. Karyukhin¹²⁰, E. Kasimi¹⁶⁰, C. Kato^{58d}, J. Katzy⁴⁴, K. Kawade¹⁴⁸, K. Kawagoe⁸⁵, T. Kawaguchi¹¹⁴, T. Kawamoto¹⁴², G. Kawamura⁵¹, E.F. Kay¹⁷³, F.I. Kaya¹⁶⁷, S. Kazakos¹², V.F. Kazanin^{119b,119a}, Y. Ke¹⁵³, J.M. Keaveney^{31a}, R. Keeler¹⁷³, J.S. Keller³², D. Kelsey¹⁵⁴, J.J. Kempster¹⁹, J. Kendrick¹⁹, K.E. Kennedy³⁷, O. Kepka¹³⁸, S. Kersten¹⁷⁹, B.P. Kerševan⁸⁹, S. Kitabchi Haghighat¹⁶⁴, M. Khandoga¹³³, A. Khanov¹²⁷, A.G. Kharlamov^{119b,119a}, T. Kharlamova^{119b,119a}, E.E. Khoda¹⁷², T.J. Khoo¹⁷, G. Khoriauli¹⁷⁴, E. Khramov⁷⁷, J. Khubua^{157b}, S. Kido⁸⁰, M. Kiehn³⁴, A. Kilgallon¹²⁹, E. Kim¹⁶², Y.K. Kim³⁵, N. Kimura⁹², A. Kirchhoff⁵¹, D. Kirchmeier⁴⁶, J. Kirk¹⁴¹, A.E. Kiryunin¹¹², T. Kishimoto¹⁶¹, D.P. Kisliuk¹⁶⁴, V. Kitali⁴⁴, C. Kitsaki⁹, O. Kivernyk²², T. Klapdor-Kleingrothaus⁵⁰, M. Klassen^{59a}, C. Klein³², L. Klein¹⁷⁴, M.H. Klein¹⁰³, M. Klein⁸⁸, U. Klein⁸⁸, P. Klimek³⁴, A. Klimentov²⁷, F. Klimpel³⁴, T. Klingl²², T. Klioutchnikova³⁴, F.F. Klitzner¹¹¹, P. Kluit¹¹⁷, S. Kluth¹¹², E. Kneringer⁷⁴, T.M. Knight¹⁶⁴, A. Knue⁵⁰, D. Kobayashi⁸⁵, M. Kobel⁴⁶, M. Kocian¹⁵¹, T. Kodama¹⁶¹, P. Kodys¹⁴⁰, D.M. Koeck¹⁵⁴, P.T. Koenig²², T. Koffas³², N.M. Köhler³⁴, M. Kolb¹⁴², I. Koletsou⁴, T. Komarek¹²⁸, K. Köneke⁵⁰, A.X.Y. Kong¹, T. Kono¹²⁴, V. Konstantinides⁹², N. Konstantinidis⁹², B. Konya⁹⁴, R. Kopeliansky⁶³, S. Koperny^{81a}, K. Korcyl⁸², K. Kordas¹⁶⁰, G. Koren¹⁵⁹, A. Korn⁹², S. Korn⁵¹, I. Korolkov¹², E.V. Korolkova¹⁴⁷, N. Korotkova¹¹⁰, O. Kortner¹¹², S. Kortner¹¹², V.V. Kostyukhin^{147,163}, A. Kotsokechagia⁶², A. Kotwal⁴⁷, A. Koulouris⁸, A. Kourkoumeli-Charalampidi^{68a,68b}, C. Kourkoumelis⁸, E. Kourlitis⁵, R. Kowalewski¹⁷³, W. Kozanecki¹⁴², A.S. Kozhin¹²⁰, V.A. Kramarenko¹¹⁰, G. Kramberger⁸⁹, D. Krasnopevtsev^{58a}, M.W. Krasny¹³³, A. Krasznahorkay³⁴, J.A. Kremer⁹⁷, J. Kretzschmar⁸⁸, K. Kreul¹⁷, P. Krieger¹⁶⁴, F. Krieter¹¹¹, S. Krishnamurthy¹⁰⁰, A. Krishnan^{59b}, M. Krivos¹⁴⁰, K. Krizka¹⁶, K. Kroeninger⁴⁵, H. Kroha¹¹², J. Kroll¹³⁸, J. Kroll¹³⁴, K.S. Krowpman¹⁰⁴, U. Kruchonak⁷⁷, H. Krüger²², N. Krumnack⁷⁶, M.C. Kruse⁴⁷, J.A. Krzysiak⁸², A. Kubota¹⁶², O. Kuchinskaia¹⁶³, S. Kuday^{3b}, D. Kuechler⁴⁴, J.T. Kuechler⁴⁴, S. Kuehn³⁴, T. Kuhl⁴⁴, V. Kukhtin⁷⁷, Y. Kulchitsky^{105,af}, S. Kuleshov^{144d}, M. Kumar^{31g}, N. Kumari⁹⁹, M. Kuna⁵⁶, A. Kupco¹³⁸, T. Kupfer⁴⁵, O. Kuprash⁵⁰, H. Kurashige⁸⁰, L.L. Kurchaninov^{165a}, Y.A. Kurochkin¹⁰⁵, A. Kurova¹⁰⁹, M.G. Kurth^{13a,13d}, E.S. Kuwertz³⁴, M. Kuze¹⁶², A.K. Kvam¹⁴⁶, J. Kvita¹²⁸, T. Kwan¹⁰¹, C. Lacasta¹⁷¹, F. Lacava^{70a,70b}, H. Lacker¹⁷, D. Lacour¹³³, E. Ladygin⁷⁷, R. Lafaye⁴, B. Laforge¹³³, T. Lagouri^{144e}, S. Lai⁵¹, I.K. Lakomic^{81a}, N. Lalloue⁵⁶, J.E. Lambert¹²⁶, S. Lammers⁶³, W. Lampl⁶, C. Lampoudis¹⁶⁰, E. Lançon²⁷, U. Landgraf⁵⁰, M.P.J. Landon⁹⁰, V.S. Lang⁵⁰, J.C. Lange⁵¹, R.J. Langenberg¹⁰⁰, A.J. Lankford¹⁶⁸, F. Lanni²⁷, K. Lantzsch²², A. Lanza^{68a}, A. Lapertosa^{53b,53a}, J.F. Laporte¹⁴², T. Lari^{66a}, F. Lasagni Manghi^{21b}, M. Lassnig³⁴, V. Latonova¹³⁸, T.S. Lau^{60a}, A. Laudrain⁹⁷, A. Laurier³², M. Lavorgna^{67a,67b}, S.D. Lawlor⁹¹, M. Lazzaroni^{66a,66b}, B. Le⁹⁸, A. Lebedev⁷⁶, M. LeBlanc³⁴, T. LeCompte⁵, F. Ledroit-Guillon⁵⁶, A.C.A. Lee⁹², C.A. Lee²⁷, G.R. Lee¹⁵, L. Lee⁵⁷, S.C. Lee¹⁵⁶, S. Lee⁷⁶, L.L. Leeuw^{31c}, B. Lefebvre^{165a}, H.P. Lefebvre⁹¹, M. Lefebvre¹⁷³, C. Leggett¹⁶, K. Lehmann¹⁵⁰, N. Lehmann¹⁸, G. Lehmann Miotto³⁴, W.A. Leight⁴⁴, A. Leisos^{160,w}, M.A.L. Leite^{78c}, C.E. Leitgeb⁴⁴, R. Leitner¹⁴⁰, K.J.C. Leney⁴⁰, T. Lenz²², S. Leone^{69a}, C. Leonidopoulos⁴⁸, A. Leopold¹³³, C. Leroy¹⁰⁷, R. Les¹⁰⁴, C.G. Lester³⁰, M. Levchenko¹³⁵, J. Levêque⁴, D. Levin¹⁰³, L.J. Levinson¹⁷⁷, D.J. Lewis¹⁹, B. Li^{13b}, B. Li¹⁰³, C. Li^{58a}, C-Q. Li^{58c,58d}, H. Li^{58a}, H. Li^{58b}, J. Li^{58c}, K. Li¹⁴⁶, L. Li^{58c}, M. Li^{13a,13d}, Q.Y. Li^{58a}, S. Li^{58d,58c,c}, X. Li⁴⁴, Y. Li⁴⁴, Z. Li^{58b}, Z. Li¹³², Z. Li¹⁰¹, Z. Li⁸⁸, Z. Liang^{13a}, M. Liberatore⁴⁴, B. Liberti^{71a}, K. Lie^{60c}, K. Lin¹⁰⁴, R.A. Linck⁶³, R.E. Lindley⁶, J.H. Lindon², A. Linss⁴⁴, A.L. Lioni⁵², E. Lipeles¹³⁴, A. Lipniacka¹⁵, T.M. Liss^{170,aj},

A. Lister¹⁷², J.D. Little⁷, B. Liu^{13a}, B.X. Liu¹⁵⁰, J.B. Liu^{58a}, J.K.K. Liu³⁵, K. Liu^{58d,58c}, M. Liu^{58a},
 M.Y. Liu^{58a}, P. Liu^{13a}, X. Liu^{58a}, Y. Liu⁴⁴, Y. Liu^{13c,13d}, Y.L. Liu¹⁰³, Y.W. Liu^{58a}, M. Livan^{68a,68b},
 A. Lleres⁵⁶, J. Llorente Merino¹⁵⁰, S.L. Lloyd⁹⁰, E.M. Lobodzinska⁴⁴, P. Loch⁶, S. Loffredo^{71a,71b},
 T. Lohse¹⁷, K. Lohwasser¹⁴⁷, M. Lokajicek¹³⁸, J.D. Long¹⁷⁰, R.E. Long⁸⁷, I. Longarini^{70a,70b}, L. Longo³⁴,
 R. Longo¹⁷⁰, I. Lopez Paz¹², A. Lopez Solis⁴⁴, J. Lorenz¹¹¹, N. Lorenzo Martinez⁴, A.M. Lory¹¹¹,
 A. Lösle⁵⁰, X. Lou^{43a,43b}, X. Lou^{13a}, A. Lounis⁶², J. Love⁵, P.A. Love⁸⁷, J.J. Lozano Bahilo¹⁷¹, G. Lu^{13a},
 M. Lu^{58a}, S. Lu¹³⁴, Y.J. Lu⁶¹, H.J. Lubatti¹⁴⁶, C. Luci^{70a,70b}, F.L. Lucio Alves^{13c}, A. Lucotte⁵⁶,
 F. Luehring⁶³, I. Luise¹⁵³, L. Luminari^{70a}, B. Lund-Jensen¹⁵², N.A. Luongo¹²⁹, M.S. Lutz¹⁵⁹, D. Lynn²⁷,
 H. Lyons⁸⁸, R. Lysak¹³⁸, E. Lytken⁹⁴, F. Lyu^{13a}, V. Lyubushkin⁷⁷, T. Lyubushkina⁷⁷, H. Ma²⁷, L.L. Ma^{58b},
 Y. Ma⁹², D.M. Mac Donell¹⁷³, G. Maccarrone⁴⁹, C.M. Macdonald¹⁴⁷, J.C. MacDonald¹⁴⁷, R. Madar³⁶,
 W.F. Mader⁴⁶, M. Madugoda Ralalage Don¹²⁷, N. Madysa⁴⁶, J. Maeda⁸⁰, T. Maeno²⁷, M. Maerker⁴⁶,
 V. Magerl⁵⁰, J. Magro^{64a,64c}, D.J. Mahon³⁷, C. Maidantchik^{78b}, A. Maio^{137a,137b,137d}, K. Maj^{81a},
 O. Majersky^{26a}, S. Majewski¹²⁹, N. Makovec⁶², B. Malaescu¹³³, Pa. Malecki⁸², V.P. Maleev¹³⁵,
 F. Malek⁵⁶, D. Malito^{39b,39a}, U. Mallik⁷⁵, C. Malone³⁰, S. Maltezos⁹, S. Malyukov⁷⁷, J. Mamuzic¹⁷¹,
 G. Mancini⁴⁹, J.P. Mandalia⁹⁰, I. Mandić⁸⁹, L. Manhaes de Andrade Filho^{78a}, I.M. Maniatis¹⁶⁰,
 M. Manisha¹⁴², J. Manjarres Ramos⁴⁶, K.H. Mankinen⁹⁴, A. Mann¹¹¹, A. Manousos⁷⁴, B. Mansoulie¹⁴²,
 I. Manthos¹⁶⁰, S. Manzoni¹¹⁷, A. Marantis^{160,w}, L. Marchese¹³², G. Marchiori¹³³, M. Marcisovsky¹³⁸,
 L. Marcoccia^{71a,71b}, C. Marcon⁹⁴, M. Marjanovic¹²⁶, Z. Marshall¹⁶, S. Marti-Garcia¹⁷¹, T.A. Martin¹⁷⁵,
 V.J. Martin⁴⁸, B. Martin dit Latour¹⁵, L. Martinelli^{72a,72b}, M. Martinez^{12,x}, P. Martinez Agullo¹⁷¹,
 V.I. Martinez Outschoorn¹⁰⁰, S. Martin-Haugh¹⁴¹, V.S. Martoiu^{25b}, A.C. Martyniuk⁹², A. Marzin³⁴,
 S.R. Maschek¹¹², L. Masetti⁹⁷, T. Mashimo¹⁶¹, R. Mashinistov¹⁰⁸, J. Masik⁹⁸, A.L. Maslennikov^{119b,119a},
 L. Massa^{21b}, P. Massarotti^{67a,67b}, P. Mastrandrea^{69a,69b}, A. Mastroberardino^{39b,39a}, T. Masubuchi¹⁶¹,
 D. Matakias²⁷, T. Mathisen¹⁶⁹, A. Matic¹¹¹, N. Matsuzawa¹⁶¹, J. Maurer^{25b}, B. Maček⁸⁹,
 D.A. Maximov^{119b,119a}, R. Mazini¹⁵⁶, I. Maznas¹⁶⁰, S.M. Mazza¹⁴³, C. Mc Ginn²⁷, J.P. Mc Gowan¹⁰¹,
 S.P. Mc Kee¹⁰³, T.G. McCarthy¹¹², W.P. McCormack¹⁶, E.F. McDonald¹⁰², A.E. McDougall¹¹⁷,
 J.A. Mcfayden¹⁵⁴, G. Mchedlidze^{157b}, M.A. McKay⁴⁰, K.D. McLean¹⁷³, S.J. McMahan¹⁴¹,
 P.C. McNamara¹⁰², R.A. McPherson^{173,aa}, J.E. Mdhluli^{31g}, Z.A. Meadows¹⁰⁰, S. Meehan³⁴, T. Megy³⁶,
 S. Mehlhase¹¹¹, A. Mehta⁸⁸, B. Meirose⁴¹, D. Melini¹⁵⁸, B.R. Mellado Garcia^{31g}, F. Meloni⁴⁴,
 A. Melzer²², E.D. Mendes Gouveia^{137a}, A.M. Mendes Jacques Da Costa¹⁹, H.Y. Meng¹⁶⁴, L. Meng³⁴,
 S. Menke¹¹², M. Mentink³⁴, E. Meoni^{39b,39a}, S.A.M. Merkt¹³⁶, C. Merlassino¹³², P. Mermod^{52,*},
 L. Merola^{67a,67b}, C. Meroni^{66a}, G. Merz¹⁰³, O. Meshkov^{110,108}, J.K.R. Meshreki¹⁴⁹, J. Metcalfe⁵,
 A.S. Mete⁵, C. Meyer⁶³, J-P. Meyer¹⁴², M. Michetti¹⁷, R.P. Middleton¹⁴¹, L. Mijović⁴⁸, G. Mikenberg¹⁷⁷,
 M. Mikestikova¹³⁸, M. Mikuz⁸⁹, H. Mildner¹⁴⁷, A. Milic¹⁶⁴, C.D. Milke⁴⁰, D.W. Miller³⁵, L.S. Miller³²,
 A. Milov¹⁷⁷, D.A. Milstead^{43a,43b}, A.A. Minaenko¹²⁰, I.A. Minashvili^{157b}, L. Mince⁵⁵, A.I. Mincer¹²³,
 B. Mindur^{81a}, M. Mineev⁷⁷, Y. Minegishi¹⁶¹, Y. Mino⁸³, L.M. Mir¹², M. Miralles Lopez¹⁷¹,
 M. Mironova¹³², T. Mitani¹⁷⁶, V.A. Mitsou¹⁷¹, M. Mittal^{58c}, O. Miu¹⁶⁴, P.S. Miyagawa⁹⁰, Y. Miyazaki⁸⁵,
 A. Mizukami⁷⁹, J.U. Mjörnmark⁹⁴, T. Mkrtchyan^{59a}, M. Mlynarikova¹¹⁸, T. Moe^{43a,43b}, S. Mobius⁵¹,
 K. Mochizuki¹⁰⁷, P. Moder⁴⁴, P. Mogg¹¹¹, S. Mohapatra³⁷, G. Mokgatitswane^{31g}, B. Mondal¹⁴⁹,
 S. Mondal¹³⁹, K. Mönig⁴⁴, E. Monnier⁹⁹, A. Montalbano¹⁵⁰, J. Montejo Berlingen³⁴, M. Montella¹²⁵,
 F. Monticelli⁸⁶, N. Morange⁶², A.L. Moreira De Carvalho^{137a}, M. Moreno Llácer¹⁷¹,
 C. Moreno Martinez¹², P. Morettini^{53b}, M. Morgenstern¹⁵⁸, S. Morgenstern¹⁷⁵, D. Mori¹⁵⁰, M. Morii⁵⁷,
 M. Morinaga¹⁷⁶, V. Morisbak¹³¹, A.K. Morley³⁴, A.P. Morris⁹², L. Morvaj³⁴, P. Moschovakos³⁴,
 B. Moser¹¹⁷, M. Mosidze^{157b}, T. Moskalets⁵⁰, P. Moskvitina¹¹⁶, J. Moss^{29,o}, E.J.W. Moyse¹⁰⁰,
 S. Muanza⁹⁹, J. Mueller¹³⁶, D. Muenstermann⁸⁷, G.A. Mullier⁹⁴, J.J. Mullin¹³⁴, D.P. Mungo^{66a,66b},
 J.L. Munoz Martinez¹², F.J. Munoz Sanchez⁹⁸, M. Murin⁹⁸, P. Murin^{26b}, W.J. Murray^{175,141},
 A. Murrone^{66a,66b}, J.M. Muse¹²⁶, M. Muškinja¹⁶, C. Mwewa²⁷, A.G. Myagkov^{120,ag}, A.A. Myers¹³⁶,
 G. Myers⁶³, J. Myers¹²⁹, M. Myska¹³⁹, B.P. Nachman¹⁶, O. Nackenhorst⁴⁵, A.Nag Nag⁴⁶, K. Nagai¹³²,

K. Nagano⁷⁹, J.L. Nagle²⁷, E. Nagy⁹⁹, A.M. Nairz³⁴, Y. Nakahama¹¹⁴, K. Nakamura⁷⁹, H. Nanjo¹³⁰,
 F. Napolitano^{59a}, R.F. Naranjo Garcia⁴⁴, R. Narayan⁴⁰, I. Naryshkin¹³⁵, M. Naseri³², C. Nass²²,
 T. Naumann⁴⁴, G. Navarro^{20a}, J. Navarro-Gonzalez¹⁷¹, P.Y. Nechaeva¹⁰⁸, F. Nechansky⁴⁴, T.J. Neep¹⁹,
 A. Negri^{68a,68b}, M. Negrini^{21b}, C. Nellist¹¹⁶, C. Nelson¹⁰¹, K. Nelson¹⁰³, M.E. Nelson^{43a,43b},
 S. Nemecek¹³⁸, M. Nessi^{34,g}, M.S. Neubauer¹⁷⁰, F. Neuhaus⁹⁷, M. Neumann¹⁷⁹, R. Newhouse¹⁷²,
 P.R. Newman¹⁹, C.W. Ng¹³⁶, Y.S. Ng¹⁷, Y.W.Y. Ng¹⁶⁸, B. Ngair^{33e}, H.D.N. Nguyen⁹⁹,
 T. Nguyen Manh¹⁰⁷, R.B. Nickerson¹³², R. Nicolaidou¹⁴², D.S. Nielsen³⁸, J. Nielsen¹⁴³, M. Niemeyer⁵¹,
 N. Nikiporou¹⁰, V. Nikolaenko^{120,ag}, I. Nikolic-Audit¹³³, K. Nikolopoulos¹⁹, P. Nilsson²⁷, H.R. Nindhito⁵²,
 A. Nisati^{70a}, N. Nishu², R. Nisius¹¹², T. Nitta¹⁷⁶, T. Nobe¹⁶¹, D.L. Noel³⁰, Y. Noguchi⁸³, I. Nomidis¹³³,
 M.A. Nomura²⁷, M.B. Norfolk¹⁴⁷, R.R.B. Norisam⁹², J. Novak⁸⁹, T. Novak⁴⁴, O. Novgorodova⁴⁶,
 L. Novotny¹³⁹, R. Novotny¹¹⁵, L. Nozka¹²⁸, K. Ntekas¹⁶⁸, E. Nurse⁹², F.G. Oakham^{32,ak}, J. Ocariz¹³³,
 A. Ochi⁸⁰, I. Ochoa^{137a}, J.P. Ochoa-Ricoux^{144a}, K. O'Connor²⁴, S. Oda⁸⁵, S. Odaka⁷⁹, S. Oerdek⁵¹,
 A. Ogrodnik^{81a}, A. Oh⁹⁸, C.C. Ohm¹⁵², H. Oide¹⁶², R. Oishi¹⁶¹, M.L. Ojeda¹⁶⁴, Y. Okazaki⁸³,
 M.W. O'Keefe⁸⁸, Y. Okumura¹⁶¹, A. Olariu^{25b}, L.F. Oleiro Seabra^{137a}, S.A. Olivares Pino^{144e},
 D. Oliveira Damazio²⁷, D. Oliveira Goncalves^{78a}, J.L. Oliver¹, M.J.R. Olsson¹⁶⁸, A. Olszewski⁸²,
 J. Olszowska⁸², Ö.O. Öncel¹²², D.C. O'Neil¹⁵⁰, A.P. O'Neill¹³², A. Onofre^{137a,137e}, P.U.E. Onyisi¹⁰,
 H. Oppen¹³¹, R.G. Oreamuno Madriz¹¹⁸, M.J. Oreglia³⁵, G.E. Orellana⁸⁶, D. Orestano^{72a,72b},
 N. Orlando¹², R.S. Orr¹⁶⁴, V. O'Shea⁵⁵, R. Ospanov^{58a}, G. Otero y Garzon²⁸, H. Otono⁸⁵, P.S. Ott^{59a},
 G.J. Ottino¹⁶, M. Ouchrif^{33d}, J. Ouellette²⁷, F. Ould-Saada¹³¹, A. Ouraou^{142,*}, Q. Ouyang^{13a}, M. Owen⁵⁵,
 R.E. Owen¹⁴¹, V.E. Ozcan^{11c}, N. Ozturk⁷, J. Pacalt¹²⁸, H.A. Pacey³⁰, K. Pachal⁴⁷, A. Pacheco Pages¹²,
 C. Padilla Aranda¹², S. Pagan Griso¹⁶, G. Palacino⁶³, S. Palazzo⁴⁸, S. Palestini³⁴, M. Palka^{81b}, P. Palni^{81a},
 D.K. Panchal¹⁰, C.E. Pandini⁵², J.G. Panduro Vazquez⁹¹, P. Pani⁴⁴, G. Panizzo^{64a,64c}, L. Paolozzi⁵²,
 C. Papadatos¹⁰⁷, S. Parajuli⁴⁰, A. Paramonov⁵, C. Paraskevopoulos⁹, D. Paredes Hernandez^{60b},
 S.R. Paredes Saenz¹³², B. Parida¹⁷⁷, T.H. Park¹⁶⁴, A.J. Parker²⁹, M.A. Parker³⁰, F. Parodi^{53b,53a},
 E.W. Parrish¹¹⁸, J.A. Parsons³⁷, U. Parzefall⁵⁰, L. Pascual Dominguez¹³³, V.R. Pascuzzi¹⁶, F. Pasquali¹¹⁷,
 E. Pasqualucci^{70a}, S. Passaggio^{53b}, F. Pastore⁹¹, P. Pasuwan^{43a,43b}, J.R. Pater⁹⁸, A. Pathak^{178,k}, J. Patton⁸⁸,
 T. Pauly³⁴, J. Pearkes¹⁵¹, M. Pedersen¹³¹, L. Pedraza Diaz¹¹⁶, R. Pedro^{137a}, T. Peiffer⁵¹,
 S.V. Peleganchuk^{119b,119a}, O. Penc¹³⁸, C. Peng^{60b}, H. Peng^{58a}, M. Penzin¹⁶³, B.S. Peralva^{78a},
 M.M. Perego⁶², A.P. Pereira Peixoto^{137a}, L. Pereira Sanchez^{43a,43b}, D.V. Perpelitsa²⁷, E. Perez Codina^{165a},
 M. Perganti⁹, L. Perini^{66a,66b}, H. Pernegger³⁴, S. Perrella³⁴, A. Perrevoort¹¹⁷, K. Peters⁴⁴, R.F.Y. Peters⁹⁸,
 B.A. Petersen³⁴, T.C. Petersen³⁸, E. Petit⁹⁹, V. Petousis¹³⁹, C. Petridou¹⁶⁰, P. Petroff⁶², F. Petrucci^{72a,72b},
 M. Pettee¹⁸⁰, N.E. Pettersson¹⁰⁰, K. Petukhova¹⁴⁰, A. Peyaud¹⁴², R. Pezoa^{144f}, L. Pezzotti^{68a,68b},
 G. Pezzullo¹⁸⁰, T. Pham¹⁰², P.W. Phillips¹⁴¹, M.W. Phipps¹⁷⁰, G. Piacquadio¹⁵³, E. Pianori¹⁶,
 F. Piazza^{66a,66b}, A. Picazio¹⁰⁰, R. Piegai²⁸, D. Pietreanu^{25b}, J.E. Pilcher³⁵, A.D. Pilkington⁹⁸,
 M. Pinamonti^{64a,64c}, J.L. Pinfold², C. Pitman Donaldson⁹², D.A. Pizzi³², L. Pizzimento^{71a,71b},
 A. Pizzini¹¹⁷, M.-A. Pleier²⁷, V. Plesanovs⁵⁰, V. Pleskot¹⁴⁰, E. Plotnikova⁷⁷, P. Podberezko^{119b,119a},
 R. Poettgen⁹⁴, R. Poggi⁵², L. Poggioli¹³³, I. Pogrebnyak¹⁰⁴, D. Pohl²², I. Pokharel⁵¹, G. Polesello^{68a},
 A. Poley^{150,165a}, A. Policicchio^{70a,70b}, R. Polifka¹⁴⁰, A. Polini^{21b}, C.S. Pollard⁴⁴, Z.B. Pollock¹²⁵,
 V. Polychronakos²⁷, D. Ponomarenko¹⁰⁹, L. Pontecorvo³⁴, S. Popa^{25a}, G.A. Popeneciu^{25d}, L. Portales⁴,
 D.M. Portillo Quintero⁵⁶, S. Pospisil¹³⁹, P. Postolache^{25c}, K. Potamianos¹³², I.N. Potrap⁷⁷, C.J. Potter³⁰,
 H. Potti¹⁰, T. Poulsen⁴⁴, J. Poveda¹⁷¹, T.D. Powell¹⁴⁷, G. Pownall⁴⁴, M.E. Pozo Astigarraga³⁴,
 A. Prades Ibanez¹⁷¹, P. Pralavorio⁹⁹, M.M. Prapa⁴², S. Prell⁷⁶, D. Price⁹⁸, M. Primavera^{65a},
 M.A. Principe Martin⁹⁶, M.L. Proffitt¹⁴⁶, N. Proklova¹⁰⁹, K. Prokofiev^{60c}, F. Prokoshin⁷⁷,
 S. Protopopescu²⁷, J. Proudfoot⁵, M. Przybycien^{81a}, D. Pudzha¹³⁵, P. Puzo⁶², D. Pyatiizbyantseva¹⁰⁹,
 J. Qian¹⁰³, Y. Qin⁹⁸, A. Quadt⁵¹, M. Queitsch-Maitland³⁴, G. Rabanal Bolanos⁵⁷, F. Ragusa^{66a,66b},
 G. Rahal⁹⁵, J.A. Raine⁵², S. Rajagopalan²⁷, K. Ran^{13a,13d}, D.F. Rassloff^{59a}, D.M. Rauch⁴⁴, S. Rave⁹⁷,
 B. Ravina⁵⁵, I. Ravinovich¹⁷⁷, M. Raymond³⁴, A.L. Read¹³¹, N.P. Readioff¹⁴⁷, M. Reale^{65a,65b},

D.M. Rebuzzi^{68a,68b}, G. Redlinger²⁷, K. Reeves⁴¹, D. Reikher¹⁵⁹, A. Reiss⁹⁷, A. Rej¹⁴⁹, C. Rembser³⁴,
 A. Renardi⁴⁴, M. Renda^{25b}, M.B. Rendel¹¹², A.G. Rennie⁵⁵, S. Resconi^{66a}, E.D. Resseguie¹⁶, S. Rettie⁹²,
 B. Reynolds¹²⁵, E. Reynolds¹⁹, M. Rezaei Estabragh¹⁷⁹, O.L. Rezanova^{119b,119a}, P. Reznicek¹⁴⁰,
 E. Ricci^{73a,73b}, R. Richter¹¹², S. Richter⁴⁴, E. Richter-Was^{81b}, M. Ridel¹³³, P. Rieck¹¹², O. Rifki⁴⁴,
 M. Rijssenbeek¹⁵³, A. Rimoldi^{68a,68b}, M. Rimoldi⁴⁴, L. Rinaldi^{21b,21a}, T.T. Rinn¹⁷⁰, M.P. Rinnagel¹¹¹,
 G. Ripellino¹⁵², I. Riu¹², P. Rivadeneira⁴⁴, J.C. Rivera Vergara¹⁷³, F. Rizatdinova¹²⁷, E. Rizvi⁹⁰, C. Rizzi⁵²,
 S.H. Robertson^{101,aa}, M. Robin⁴⁴, D. Robinson³⁰, C.M. Robles Gajardo^{144f}, M. Robles Manzano⁹⁷,
 A. Robson⁵⁵, A. Rocchi^{71a,71b}, C. Roda^{69a,69b}, S. Rodriguez Bosca^{59a}, A. Rodriguez Rodriguez⁵⁰,
 A.M. Rodríguez Vera^{165b}, S. Roe³⁴, J. Roggel¹⁷⁹, O. Røhne¹³¹, R.A. Rojas^{144f}, B. Roland⁵⁰,
 C.P.A. Roland⁶³, J. Roloff²⁷, A. Romaniouk¹⁰⁹, M. Romano^{21b}, N. Rompotis⁸⁸, M. Ronzani¹²³, L. Roos¹³³,
 S. Rosati^{70a}, G. Rosin¹⁰⁰, B.J. Rosser¹³⁴, E. Rossi¹⁶⁴, E. Rossi⁴, E. Rossi^{67a,67b}, L.P. Rossi^{53b}, L. Rossini⁴⁴,
 R. Rosten¹²⁵, M. Rotaru^{25b}, B. Rottler⁵⁰, D. Rousseau⁶², D. Rouso³⁰, G. Rovelli^{68a,68b}, A. Roy¹⁰,
 A. Rozanov⁹⁹, Y. Rozen¹⁵⁸, X. Ruan^{31g}, A.J. Ruby⁸⁸, T.A. Ruggeri¹, F. Rühr⁵⁰, A. Ruiz-Martinez¹⁷¹,
 A. Rummler³⁴, Z. Rurikova⁵⁰, N.A. Rusakovich⁷⁷, H.L. Russell³⁴, L. Rustige³⁶, J.P. Rutherford⁶,
 E.M. Rüttinger¹⁴⁷, M. Rybar¹⁴⁰, E.B. Rye¹³¹, A. Ryzhov¹²⁰, J.A. Sabater Iglesias⁴⁴, P. Sabatini¹⁷¹,
 L. Sabetta^{70a,70b}, H.F.W. Sadrozinski¹⁴³, R. Sadykov⁷⁷, F. Safai Tehrani^{70a}, B. Safarzadeh Samani¹⁵⁴,
 M. Safdari¹⁵¹, P. Saha¹¹⁸, S. Saha¹⁰¹, M. Sahinsoy¹¹², A. Sahu¹⁷⁹, M. Saimpert³⁴, M. Saito¹⁶¹, T. Saito¹⁶¹,
 D. Salamani⁵², G. Salamanna^{72a,72b}, A. Salnikov¹⁵¹, J. Salt¹⁷¹, A. Salvador Salas¹², D. Salvatore^{39b,39a},
 F. Salvatore¹⁵⁴, A. Salzburger³⁴, D. Sammel⁵⁰, D. Sampsonidis¹⁶⁰, D. Sampsonidou^{58d,58c}, J. Sánchez¹⁷¹,
 A. Sanchez Pineda⁴, V. Sanchez Sebastian¹⁷¹, H. Sandaker¹³¹, C.O. Sander⁴⁴, I.G. Sanderswood⁸⁷,
 J.A. Sandesara¹⁰⁰, M. Sandhoff¹⁷⁹, C. Sandoval^{20b}, D.P.C. Sankey¹⁴¹, M. Sannino^{53b,53a}, Y. Sano¹¹⁴,
 A. Sansoni⁴⁹, C. Santoni³⁶, H. Santos^{137a,137b}, S.N. Santpur¹⁶, A. Santra¹⁷⁷, K.A. Saoucha¹⁴⁷,
 A. Saprionov⁷⁷, J.G. Saraiva^{137a,137d}, J. Sardain⁹⁹, O. Sasaki⁷⁹, K. Sato¹⁶⁶, C. Sauer^{59b}, F. Sauerburger⁵⁰,
 E. Sauvan⁴, P. Savard^{164,ak}, R. Sawada¹⁶¹, C. Sawyer¹⁴¹, L. Sawyer⁹³, I. Sayago Galvan¹⁷¹, C. Sbarra^{21b},
 A. Sbrizzi^{64a,64c}, T. Scanlon⁹², J. Schaarschmidt¹⁴⁶, P. Schacht¹¹², D. Schaefer³⁵, L. Schaefer¹³⁴,
 U. Schäfer⁹⁷, A.C. Schaffer⁶², D. Schaile¹¹¹, R.D. Schamberger¹⁵³, E. Schanet¹¹¹, C. Scharf¹⁷,
 N. Scharmberg⁹⁸, V.A. Schegelsky¹³⁵, D. Scheirich¹⁴⁰, F. Schenck¹⁷, M. Schernau¹⁶⁸, C. Schiavi^{53b,53a},
 L.K. Schildgen²², Z.M. Schillaci²⁴, E.J. Schioppa^{65a,65b}, M. Schioppa^{39b,39a}, B. Schlag⁹⁷,
 K.E. Schleicher⁵⁰, S. Schlenker³⁴, K. Schmieden⁹⁷, C. Schmitt⁹⁷, S. Schmitt⁴⁴, L. Schoeffel¹⁴²,
 A. Schoening^{59b}, P.G. Scholer⁵⁰, E. Schopf¹³², M. Schott⁹⁷, J. Schovancova³⁴, S. Schramm⁵²,
 F. Schroeder¹⁷⁹, H-C. Schultz-Coulon^{59a}, M. Schumacher⁵⁰, B.A. Schumm¹⁴³, Ph. Schune¹⁴²,
 A. Schwartzman¹⁵¹, T.A. Schwarz¹⁰³, Ph. Schwemling¹⁴², R. Schwienhorst¹⁰⁴, A. Sciandra¹⁴³,
 G. Sciolla²⁴, F. Scuri^{69a}, F. Scutti¹⁰², C.D. Sebastiani⁸⁸, K. Sedlaczek⁴⁵, P. Seema¹⁷, S.C. Seidel¹¹⁵,
 A. Seiden¹⁴³, B.D. Seidlitz²⁷, T. Seiss³⁵, C. Seitz⁴⁴, J.M. Seixas^{78b}, G. Sekhniaidze^{67a}, S.J. Sekula⁴⁰,
 L.P. Selem⁴, N. Semprini-Cesari^{21b,21a}, S. Sen⁴⁷, C. Serfon²⁷, L. Serin⁶², L. Serkin^{64a,64b}, M. Sessa^{58a},
 H. Severini¹²⁶, S. Sevova¹⁵¹, F. Sforza^{53b,53a}, A. Sfyrta⁵², E. Shabalina⁵¹, J.D. Shahinian¹³⁴,
 N.W. Shaikh^{43a,43b}, D. Shaked Renous¹⁷⁷, L.Y. Shan^{13a}, M. Shapiro¹⁶, A. Sharma³⁴, A.S. Sharma¹,
 S. Sharma⁴⁴, P.B. Shatalov¹²¹, K. Shaw¹⁵⁴, S.M. Shaw⁹⁸, M. Shehade¹⁷⁷, P. Sherwood⁹², L. Shi⁹²,
 C.O. Shimmin¹⁸⁰, Y. Shimogama¹⁷⁶, M. Shimojima¹¹³, J.D. Shinner⁹¹, I.P.J. Shipsey¹³², S. Shirabe⁵²,
 M. Shiyakova⁷⁷, J. Shlomi¹⁷⁷, M.J. Shochet³⁵, J. Shojaii¹⁰², D.R. Shope¹⁵², S. Shrestha¹²⁵, E.M. Shrif^{31g},
 M.J. Shroff¹⁷³, E. Shulga¹⁷⁷, P. Sicho¹³⁸, A.M. Sickles¹⁷⁰, E. Sideras Haddad^{31g}, O. Sidiropoulou³⁴,
 A. Sidoti^{21b}, F. Siegert⁴⁶, Dj. Sijacki¹⁴, M.V. Silva Oliveira³⁴, S.B. Silverstein^{43a}, S. Simion⁶²,
 R. Simoniello³⁴, S. Simsek^{11b}, P. Sinervo¹⁶⁴, V. Sinetkii¹¹⁰, S. Singh¹⁵⁰, S. Sinha^{31g}, M. Sioli^{21b,21a},
 I. Siral¹²⁹, S. Yu. Sivoklov¹¹⁰, J. Sjölin^{43a,43b}, A. Skaf⁵¹, E. Skorda⁹⁴, P. Skubic¹²⁶, M. Slawinska⁸²,
 K. Sliwa¹⁶⁷, V. Smakhtin¹⁷⁷, B.H. Smart¹⁴¹, J. Smiesko¹⁴⁰, S. Yu. Smirnov¹⁰⁹, Y. Smirnov¹⁰⁹,
 L.N. Smirnova^{110,s}, O. Smirnova⁹⁴, E.A. Smith³⁵, H.A. Smith¹³², M. Smizanska⁸⁷, K. Smolek¹³⁹,
 A. Smykiewicz⁸², A.A. Snesev¹⁰⁸, H.L. Snoek¹¹⁷, I.M. Snyder¹²⁹, S. Snyder²⁷, R. Sobie^{173,aa},

A. Soffer¹⁵⁹, A. Søgaaard⁴⁸, F. Sohns⁵¹, C.A. Solans Sanchez³⁴, E.Yu. Soldatov¹⁰⁹, U. Soldevila¹⁷¹,
 A.A. Solodkov¹²⁰, S. Solomon⁵⁰, A. Soloshenko⁷⁷, O.V. Solovyanov¹²⁰, V. Solovyev¹³⁵, P. Sommer¹⁴⁷,
 H. Son¹⁶⁷, A. Sonay¹², W.Y. Song^{165b}, A. Sopczak¹³⁹, A.L. Sopio⁹², F. Sopkova^{26b}, S. Sottocornola^{68a,68b},
 R. Soualah^{64a,64c}, A.M. Soukharev^{119b,119a}, Z. Soumami^{33e}, D. South⁴⁴, S. Spagnolo^{65a,65b}, M. Spalla¹¹²,
 M. Spangenberg¹⁷⁵, F. Spanò⁹¹, D. Sperlich⁵⁰, T.M. Spieker^{59a}, G. Spigo³⁴, M. Spina¹⁵⁴, D.P. Spiteri⁵⁵,
 M. Spousta¹⁴⁰, A. Stabile^{66a,66b}, B.L. Stamas¹¹⁸, R. Stamen^{59a}, M. Stamenkovic¹¹⁷, A. Stampekis¹⁹,
 M. Standke²², E. Stanecka⁸², B. Stanislaus³⁴, M.M. Stanitzki⁴⁴, M. Stankaityte¹³², B. Stapf⁴⁴,
 E.A. Starchenko¹²⁰, G.H. Stark¹⁴³, J. Stark⁹⁹, D.M. Starko^{165b}, P. Staroba¹³⁸, P. Starovoitov^{59a}, S. Stärz¹⁰¹,
 R. Staszewski⁸², G. Stavropoulos⁴², P. Steinberg²⁷, A.L. Steinhebel¹²⁹, B. Stelzer^{150,165a}, H.J. Stelzer¹³⁶,
 O. Stelzer-Chilton^{165a}, H. Stenzel⁵⁴, T.J. Stevenson¹⁵⁴, G.A. Stewart³⁴, M.C. Stockton³⁴, G. Stoicea^{25b},
 M. Stolarski^{137a}, S. Stonjek¹¹², A. Straessner⁴⁶, J. Strandberg¹⁵², S. Strandberg^{43a,43b}, M. Strauss¹²⁶,
 T. Strebler⁹⁹, P. Strizenc^{26b}, R. Ströhmer¹⁷⁴, D.M. Strom¹²⁹, L.R. Strom⁴⁴, R. Stroynowski⁴⁰,
 A. Strubig^{43a,43b}, S.A. Stucci²⁷, B. Stugu¹⁵, J. Stupak¹²⁶, N.A. Styles⁴⁴, D. Su¹⁵¹, S. Su^{58a}, W. Su^{58d,146,58c},
 X. Su^{58a}, N.B. Suarez¹³⁶, K. Sugizaki¹⁶¹, V.V. Sulin¹⁰⁸, M.J. Sullivan⁸⁸, D.M.S. Sultan⁵², S. Sultansoy^{3c},
 T. Sumida⁸³, S. Sun¹⁰³, S. Sun¹⁷⁸, X. Sun⁹⁸, O. Sunneborn Gudnadottir¹⁶⁹, C.J.E. Suster¹⁵⁵,
 M.R. Sutton¹⁵⁴, M. Svatos¹³⁸, M. Swiatlowski^{165a}, T. Swirski¹⁷⁴, I. Sykora^{26a}, M. Sykora¹⁴⁰, T. Sykora¹⁴⁰,
 D. Ta⁹⁷, K. Tackmann^{44,y}, A. Taffard¹⁶⁸, R. Tafirout^{165a}, E. Tagiev¹²⁰, R.H.M. Taibah¹³³, R. Takashima⁸⁴,
 K. Takeda⁸⁰, T. Takeshita¹⁴⁸, E.P. Takeva⁴⁸, Y. Takubo⁷⁹, M. Talby⁹⁹, A.A. Talyshev^{119b,119a}, K.C. Tam^{60b},
 N.M. Tamir¹⁵⁹, J. Tanaka¹⁶¹, R. Tanaka⁶², Z. Tao¹⁷², S. Tapia Araya¹⁷⁰, S. Tapprogge⁹⁷,
 A. Tarek Abouelfadl Mohamed¹⁰⁴, S. Tarem¹⁵⁸, K. Tariq^{58b}, G. Tarna^{25b,f}, G.F. Tartarelli^{66a}, P. Tas¹⁴⁰,
 M. Tasevsky¹³⁸, E. Tassi^{39b,39a}, G. Tateno¹⁶¹, Y. Tayalati^{33e}, G.N. Taylor¹⁰², W. Taylor^{165b}, H. Teagle⁸⁸,
 A.S. Tee⁸⁷, R. Teixeira De Lima¹⁵¹, P. Teixeira-Dias⁹¹, H. Ten Kate³⁴, J.J. Teoh¹¹⁷, K. Terashi¹⁶¹,
 J. Terron⁹⁶, S. Terzo¹², M. Testa⁴⁹, R.J. Teuscher^{164,aa}, N. Themistokleous⁴⁸, T. Thevenaux-Pelzer¹⁷,
 D.W. Thomas⁹¹, J.P. Thomas¹⁹, E.A. Thompson⁴⁴, P.D. Thompson¹⁹, E. Thomson¹³⁴, E.J. Thorpe⁹⁰,
 Y. Tian⁵¹, V.O. Tikhomirov^{108,ah}, Yu.A. Tikhonov^{119b,119a}, S. Timoshenko¹⁰⁹, P. Tipton¹⁸⁰, S. Tisserant⁹⁹,
 S.H. Tlou^{31g}, A. Tnourji³⁶, K. Todome^{21b,21a}, S. Todorova-Nova¹⁴⁰, S. Todt⁴⁶, M. Togawa⁷⁹, J. Tojo⁸⁵,
 S. Tokár^{26a}, K. Tokushuku⁷⁹, E. Tolley¹²⁵, R. Tombs³⁰, M. Tomoto^{79,114}, L. Tompkins¹⁵¹, P. Tornambe¹⁰⁰,
 E. Torrence¹²⁹, H. Torres⁴⁶, E. Torró Pastor¹⁷¹, M. Toscani²⁸, C. Toscirì³⁵, J. Toth^{99,z}, D.R. Tovey¹⁴⁷,
 A. Traet¹⁵, C.J. Treado¹²³, T. Trefzger¹⁷⁴, A. Tricoli²⁷, I.M. Trigger^{165a}, S. Trincaz-Duvoid¹³³,
 D.A. Trischuk¹⁷², W. Trischuk¹⁶⁴, B. Trocmé⁵⁶, A. Trofymov⁶², C. Troncon^{66a}, F. Trovato¹⁵⁴, L. Truong^{31c},
 M. Trzebinski⁸², A. Trzupek⁸², F. Tsai¹⁵³, A. Tsiamis¹⁶⁰, P.V. Tsiarehka^{105,af}, A. Tsirigotis^{160,w},
 V. Tsiskaridze¹⁵³, E.G. Tskhadadze^{157a}, M. Tsopoulou¹⁶⁰, I.I. Tsukerman¹²¹, V. Tsulaia¹⁶, S. Tsuno⁷⁹,
 O. Tsur¹⁵⁸, D. Tsybychev¹⁵³, Y. Tu^{60b}, A. Tudorache^{25b}, V. Tudorache^{25b}, A.N. Tuna³⁴, S. Turchikhin⁷⁷,
 D. Turgeman¹⁷⁷, I. Turk Cakir^{3b,u}, R.J. Turner¹⁹, R. Turra^{66a}, P.M. Tuts³⁷, S. Tzamarias¹⁶⁰, P. Tzani⁹,
 E. Tzovara⁹⁷, K. Uchida¹⁶¹, F. Ukegawa¹⁶⁶, G. Unal³⁴, M. Unal¹⁰, A. Undrus²⁷, G. Unel¹⁶⁸,
 F.C. Ungaro¹⁰², K. Uno¹⁶¹, J. Urban^{26b}, P. Urquijo¹⁰², G. Usai⁷, R. Ushioda¹⁶², Z. Uysal^{11d}, V. Vacek¹³⁹,
 B. Vachon¹⁰¹, K.O.H. Vadla¹³¹, T. Vafeiadis³⁴, C. Valderanis¹¹¹, E. Valdes Santurio^{43a,43b}, M. Valente^{165a},
 S. Valentinetti^{21b,21a}, A. Valero¹⁷¹, L. Valéry⁴⁴, R.A. Vallance¹⁹, A. Vallier⁹⁹, J.A. Valls Ferrer¹⁷¹,
 T.R. Van Daalen¹², P. Van Gemmeren⁵, S. Van Stroud⁹², I. Van Vulpen¹¹⁷, M. Vanadia^{71a,71b},
 W. Vandelli³⁴, M. Vandenbroucke¹⁴², E.R. Vandewall¹²⁷, D. Vannicola^{70a,70b}, L. Vannoli^{53b,53a}, R. Vari^{70a},
 E.W. Varnes⁶, C. Varni^{53b,53a}, T. Varol¹⁵⁶, D. Varouchas⁶², K.E. Varvell¹⁵⁵, M.E. Vasile^{25b}, L. Vaslin³⁶,
 G.A. Vasquez¹⁷³, F. Vazeille³⁶, D. Vazquez Furelos¹², T. Vazquez Schroeder³⁴, J. Veatch⁵¹, V. Vecchio⁹⁸,
 M.J. Veen¹¹⁷, I. Veliscek¹³², L.M. Veloce¹⁶⁴, F. Veloso^{137a,137c}, S. Veneziano^{70a}, A. Ventura^{65a,65b},
 A. Verbytskyi¹¹², M. Verducci^{69a,69b}, C. Vergis²², M. Verissimo De Araujo^{78b}, W. Verkerke¹¹⁷,
 A.T. Vermeulen¹¹⁷, J.C. Vermeulen¹¹⁷, C. Vernieri¹⁵¹, P.J. Verschuuren⁹¹, M.L. Vesterbacka¹²³,
 M.C. Vetterli^{150,ak}, N. Viaux Maira^{144f}, T. Vickey¹⁴⁷, O.E. Vickey Boeriu¹⁴⁷, G.H.A. Viehhauser¹³²,
 L. Vigani^{59b}, M. Villa^{21b,21a}, M. Villaplana Perez¹⁷¹, E.M. Villhauer⁴⁸, E. Vilucchi⁴⁹, M.G. Vincter³²,

G.S. Virdee¹⁹, A. Vishwakarma⁴⁸, C. Vittori^{21b,21a}, I. Vivarelli¹⁵⁴, V. Vladimirov¹⁷⁵, E. Voevodina¹¹², M. Vogel¹⁷⁹, P. Vokac¹³⁹, J. Von Ahnen⁴⁴, S.E. von Buddenbrock^{31g}, E. Von Toerne²², V. Vorobel¹⁴⁰, K. Vorobev¹⁰⁹, M. Vos¹⁷¹, J.H. Vosseveld⁸⁸, M. Vozak⁹⁸, N. Vranjes¹⁴, M. Vranjes Milosavljevic¹⁴, V. Vrba^{139,*}, M. Vreeswijk¹¹⁷, N.K. Vu⁹⁹, R. Vuillermet³⁴, I. Vukotic³⁵, S. Wada¹⁶⁶, C. Wagner¹⁰⁰, P. Wagner²², W. Wagner¹⁷⁹, S. Wahdan¹⁷⁹, H. Wahlberg⁸⁶, R. Wakasa¹⁶⁶, M. Wakida¹¹⁴, V.M. Walbrecht¹¹², J. Walder¹⁴¹, R. Walker¹¹¹, S.D. Walker⁹¹, W. Walkowiak¹⁴⁹, A.M. Wang⁵⁷, A.Z. Wang¹⁷⁸, C. Wang^{58a}, C. Wang^{58c}, H. Wang¹⁶, J. Wang^{60a}, P. Wang⁴⁰, R.-J. Wang⁹⁷, R. Wang⁵⁷, R. Wang¹¹⁸, S.M. Wang¹⁵⁶, S. Wang^{58b}, T. Wang^{58a}, W.T. Wang^{58a}, W.X. Wang^{58a}, X. Wang¹⁷⁰, Y. Wang^{58a}, Z. Wang¹⁰³, C. Wanotayaroj³⁴, A. Warburton¹⁰¹, C.P. Ward³⁰, R.J. Ward¹⁹, N. Warrack⁵⁵, A.T. Watson¹⁹, M.F. Watson¹⁹, G. Watts¹⁴⁶, B.M. Waugh⁹², A.F. Webb¹⁰, C. Weber²⁷, M.S. Weber¹⁸, S.A. Weber³², S.M. Weber^{59a}, C. Wei^{58a}, Y. Wei¹³², A.R. Weidberg¹³², J. Weingarten⁴⁵, M. Weirich⁹⁷, C. Weiser⁵⁰, T. Wenaus²⁷, B. Wendland⁴⁵, T. Wengler³⁴, S. Wenig³⁴, N. Vermes²², M. Wessels^{59a}, K. Whalen¹²⁹, A.M. Wharton⁸⁷, A.S. White⁵⁷, A. White⁷, M.J. White¹, D. Whiteson¹⁶⁸, W. Wiedenmann¹⁷⁸, C. Wiel⁴⁶, M. Wielers¹⁴¹, N. Wieseotte⁹⁷, C. Wiglesworth³⁸, L.A.M. Wiik-Fuchs⁵⁰, D.J. Wilbern¹²⁶, H.G. Wilkens³⁴, L.J. Wilkins⁹¹, D.M. Williams³⁷, H.H. Williams¹³⁴, S. Williams³⁰, S. Willocq¹⁰⁰, P.J. Windischhofer¹³², I. Wingerter-Seez⁴, F. Winklmeier¹²⁹, B.T. Winter⁵⁰, M. Wittgen¹⁵¹, M. Wobisch⁹³, A. Wolf⁹⁷, R. Wölker¹³², J. Wollrath¹⁶⁸, M.W. Wolter⁸², H. Wolters^{137a,137c}, V.W.S. Wong¹⁷², A.F. Wongel⁴⁴, S.D. Worm⁴⁴, B.K. Wosiek⁸², K.W. Woźniak⁸², K. Wraight⁵⁵, J. Wu^{13a,13d}, S.L. Wu¹⁷⁸, X. Wu⁵², Y. Wu^{58a}, Z. Wu^{142,58a}, J. Wuerzinger¹³², T.R. Wyatt⁹⁸, B.M. Wynne⁴⁸, S. Xella³⁸, J. Xiang^{60c}, X. Xiao¹⁰³, X. Xie^{58a}, I. Xiolidis¹⁵⁴, D. Xu^{13a}, H. Xu^{58a}, H. Xu^{58a}, L. Xu^{58a}, R. Xu¹³⁴, T. Xu^{58a}, W. Xu¹⁰³, Y. Xu^{13b}, Z. Xu^{58b}, Z. Xu¹⁵¹, B. Yabsley¹⁵⁵, S. Yacoob^{31a}, N. Yamaguchi⁸⁵, Y. Yamaguchi¹⁶², M. Yamatani¹⁶¹, H. Yamauchi¹⁶⁶, T. Yamazaki¹⁶, Y. Yamazaki⁸⁰, J. Yan^{58c}, Z. Yan²³, H.J. Yang^{58c,58d}, H.T. Yang¹⁶, S. Yang^{58a}, T. Yang^{60c}, X. Yang^{58a}, X. Yang^{13a}, Y. Yang¹⁶¹, Z. Yang^{103,58a}, W.-M. Yao¹⁶, Y.C. Yap⁴⁴, H. Ye^{13c}, J. Ye⁴⁰, S. Ye²⁷, I. Yeletsikh⁷⁷, M.R. Yexley⁸⁷, P. Yin³⁷, K. Yorita¹⁷⁶, K. Yoshihara⁷⁶, C.J.S. Young³⁴, C. Young¹⁵¹, R. Yuan^{58b,j}, X. Yue^{59a}, M. Zaazoua^{33c}, B. Zabinski⁸², G. Zacharis⁹, E. Zaffaroni⁵², A.M. Zaitsev^{120,ag}, T. Zakareishvili^{157b}, N. Zakharchuk³², S. Zambito³⁴, D. Zanzi⁵⁰, S.V. ZeiBner⁴⁵, C. Zeitnitz¹⁷⁹, G. Zemaityte¹³², J.C. Zeng¹⁷⁰, O. Zenin¹²⁰, T. Ženiš^{26a}, S. Zenz⁹⁰, S. Zerradi^{33a}, D. Zerwas⁶², M. Zgubic¹³², B. Zhang^{13c}, D.F. Zhang^{13b}, G. Zhang^{13b}, J. Zhang⁵, K. Zhang^{13a}, L. Zhang^{13c}, M. Zhang¹⁷⁰, R. Zhang¹⁷⁸, S. Zhang¹⁰³, X. Zhang^{58c}, X. Zhang^{58b}, Z. Zhang⁶², P. Zhao⁴⁷, Y. Zhao¹⁴³, Z. Zhao^{58a}, A. Zhemchugov⁷⁷, Z. Zheng¹⁰³, D. Zhong¹⁷⁰, B. Zhou¹⁰³, C. Zhou¹⁷⁸, H. Zhou⁶, M. Zhou¹⁵³, N. Zhou^{58c}, Y. Zhou⁶, C.G. Zhu^{58b}, C. Zhu^{13a,13d}, H.L. Zhu^{58a}, H. Zhu^{13a}, J. Zhu¹⁰³, Y. Zhu^{58a}, X. Zhuang^{13a}, K. Zhukov¹⁰⁸, V. Zhulanov^{119b,119a}, D. Ziemska⁶³, N.I. Zimine⁷⁷, S. Zimmermann^{50,*}, M. Ziolkowski¹⁴⁹, L. Živković¹⁴, A. Zoccoli^{21b,21a}, K. Zoch⁵², T.G. Zorbas¹⁴⁷, W. Zou³⁷, L. Zwalinski³⁴.

¹Department of Physics, University of Adelaide, Adelaide; Australia.

²Department of Physics, University of Alberta, Edmonton AB; Canada.

³(^a)Department of Physics, Ankara University, Ankara; (^b)Istanbul Aydin University, Application and Research Center for Advanced Studies, Istanbul; (^c)Division of Physics, TOBB University of Economics and Technology, Ankara; Turkey.

⁴LAPP, Univ. Savoie Mont Blanc, CNRS/IN2P3, Annecy ; France.

⁵High Energy Physics Division, Argonne National Laboratory, Argonne IL; United States of America.

⁶Department of Physics, University of Arizona, Tucson AZ; United States of America.

⁷Department of Physics, University of Texas at Arlington, Arlington TX; United States of America.

⁸Physics Department, National and Kapodistrian University of Athens, Athens; Greece.

⁹Physics Department, National Technical University of Athens, Zografou; Greece.

¹⁰Department of Physics, University of Texas at Austin, Austin TX; United States of America.

- ¹¹(*a*) Bahcesehir University, Faculty of Engineering and Natural Sciences, Istanbul; (*b*) Istanbul Bilgi University, Faculty of Engineering and Natural Sciences, Istanbul; (*c*) Department of Physics, Bogazici University, Istanbul; (*d*) Department of Physics Engineering, Gaziantep University, Gaziantep; (*e*) Department of Physics, Istanbul University, Istanbul; (*f*) Istinye University, Sariyer, Istanbul; Turkey.
- ¹²Institut de Física d'Altes Energies (IFAE), Barcelona Institute of Science and Technology, Barcelona; Spain.
- ¹³(*a*) Institute of High Energy Physics, Chinese Academy of Sciences, Beijing; (*b*) Physics Department, Tsinghua University, Beijing; (*c*) Department of Physics, Nanjing University, Nanjing; (*d*) University of Chinese Academy of Science (UCAS), Beijing; China.
- ¹⁴Institute of Physics, University of Belgrade, Belgrade; Serbia.
- ¹⁵Department for Physics and Technology, University of Bergen, Bergen; Norway.
- ¹⁶Physics Division, Lawrence Berkeley National Laboratory and University of California, Berkeley CA; United States of America.
- ¹⁷Institut für Physik, Humboldt Universität zu Berlin, Berlin; Germany.
- ¹⁸Albert Einstein Center for Fundamental Physics and Laboratory for High Energy Physics, University of Bern, Bern; Switzerland.
- ¹⁹School of Physics and Astronomy, University of Birmingham, Birmingham; United Kingdom.
- ²⁰(*a*) Facultad de Ciencias y Centro de Investigaciones, Universidad Antonio Nariño, Bogotá; (*b*) Departamento de Física, Universidad Nacional de Colombia, Bogotá; Colombia.
- ²¹(*a*) Dipartimento di Fisica e Astronomia A. Righi, Università di Bologna, Bologna; (*b*) INFN Sezione di Bologna; Italy.
- ²²Physikalisches Institut, Universität Bonn, Bonn; Germany.
- ²³Department of Physics, Boston University, Boston MA; United States of America.
- ²⁴Department of Physics, Brandeis University, Waltham MA; United States of America.
- ²⁵(*a*) Transilvania University of Brasov, Brasov; (*b*) Horia Hulubei National Institute of Physics and Nuclear Engineering, Bucharest; (*c*) Department of Physics, Alexandru Ioan Cuza University of Iasi, Iasi; (*d*) National Institute for Research and Development of Isotopic and Molecular Technologies, Physics Department, Cluj-Napoca; (*e*) University Politehnica Bucharest, Bucharest; (*f*) West University in Timisoara, Timisoara; Romania.
- ²⁶(*a*) Faculty of Mathematics, Physics and Informatics, Comenius University, Bratislava; (*b*) Department of Subnuclear Physics, Institute of Experimental Physics of the Slovak Academy of Sciences, Kosice; Slovak Republic.
- ²⁷Physics Department, Brookhaven National Laboratory, Upton NY; United States of America.
- ²⁸Departamento de Física (FCEN) and IFIBA, Universidad de Buenos Aires and CONICET, Buenos Aires; Argentina.
- ²⁹California State University, CA; United States of America.
- ³⁰Cavendish Laboratory, University of Cambridge, Cambridge; United Kingdom.
- ³¹(*a*) Department of Physics, University of Cape Town, Cape Town; (*b*) iThemba Labs, Western Cape; (*c*) Department of Mechanical Engineering Science, University of Johannesburg, Johannesburg; (*d*) National Institute of Physics, University of the Philippines Diliman (Philippines); (*e*) University of South Africa, Department of Physics, Pretoria; (*f*) University of Zululand, KwaDlangezwa; (*g*) School of Physics, University of the Witwatersrand, Johannesburg; South Africa.
- ³²Department of Physics, Carleton University, Ottawa ON; Canada.
- ³³(*a*) Faculté des Sciences Ain Chock, Réseau Universitaire de Physique des Hautes Energies - Université Hassan II, Casablanca; (*b*) Faculté des Sciences, Université Ibn-Tofail, Kénitra; (*c*) Faculté des Sciences Semlalia, Université Cadi Ayyad, LPHEA-Marrakech; (*d*) LPMR, Faculté des Sciences, Université

- Mohamed Premier, Oujda;^(e) Faculté des sciences, Université Mohammed V, Rabat;^(f) Mohammed VI Polytechnic University, Ben Guerir; Morocco.
- ³⁴CERN, Geneva; Switzerland.
- ³⁵Enrico Fermi Institute, University of Chicago, Chicago IL; United States of America.
- ³⁶LPC, Université Clermont Auvergne, CNRS/IN2P3, Clermont-Ferrand; France.
- ³⁷Nevis Laboratory, Columbia University, Irvington NY; United States of America.
- ³⁸Niels Bohr Institute, University of Copenhagen, Copenhagen; Denmark.
- ³⁹(^a) Dipartimento di Fisica, Università della Calabria, Rende;^(b) INFN Gruppo Collegato di Cosenza, Laboratori Nazionali di Frascati; Italy.
- ⁴⁰Physics Department, Southern Methodist University, Dallas TX; United States of America.
- ⁴¹Physics Department, University of Texas at Dallas, Richardson TX; United States of America.
- ⁴²National Centre for Scientific Research "Demokritos", Agia Paraskevi; Greece.
- ⁴³(^a) Department of Physics, Stockholm University;^(b) Oskar Klein Centre, Stockholm; Sweden.
- ⁴⁴Deutsches Elektronen-Synchrotron DESY, Hamburg and Zeuthen; Germany.
- ⁴⁵Lehrstuhl für Experimentelle Physik IV, Technische Universität Dortmund, Dortmund; Germany.
- ⁴⁶Institut für Kern- und Teilchenphysik, Technische Universität Dresden, Dresden; Germany.
- ⁴⁷Department of Physics, Duke University, Durham NC; United States of America.
- ⁴⁸SUPA - School of Physics and Astronomy, University of Edinburgh, Edinburgh; United Kingdom.
- ⁴⁹INFN e Laboratori Nazionali di Frascati, Frascati; Italy.
- ⁵⁰Physikalisches Institut, Albert-Ludwigs-Universität Freiburg, Freiburg; Germany.
- ⁵¹II. Physikalisches Institut, Georg-August-Universität Göttingen, Göttingen; Germany.
- ⁵²Département de Physique Nucléaire et Corpusculaire, Université de Genève, Genève; Switzerland.
- ⁵³(^a) Dipartimento di Fisica, Università di Genova, Genova;^(b) INFN Sezione di Genova; Italy.
- ⁵⁴II. Physikalisches Institut, Justus-Liebig-Universität Giessen, Giessen; Germany.
- ⁵⁵SUPA - School of Physics and Astronomy, University of Glasgow, Glasgow; United Kingdom.
- ⁵⁶LPSC, Université Grenoble Alpes, CNRS/IN2P3, Grenoble INP, Grenoble; France.
- ⁵⁷Laboratory for Particle Physics and Cosmology, Harvard University, Cambridge MA; United States of America.
- ⁵⁸(^a) Department of Modern Physics and State Key Laboratory of Particle Detection and Electronics, University of Science and Technology of China, Hefei;^(b) Institute of Frontier and Interdisciplinary Science and Key Laboratory of Particle Physics and Particle Irradiation (MOE), Shandong University, Qingdao;^(c) School of Physics and Astronomy, Shanghai Jiao Tong University, Key Laboratory for Particle Astrophysics and Cosmology (MOE), SKLPPC, Shanghai;^(d) Tsung-Dao Lee Institute, Shanghai; China.
- ⁵⁹(^a) Kirchhoff-Institut für Physik, Ruprecht-Karls-Universität Heidelberg, Heidelberg;^(b) Physikalisches Institut, Ruprecht-Karls-Universität Heidelberg, Heidelberg; Germany.
- ⁶⁰(^a) Department of Physics, Chinese University of Hong Kong, Shatin, N.T., Hong Kong;^(b) Department of Physics, University of Hong Kong, Hong Kong;^(c) Department of Physics and Institute for Advanced Study, Hong Kong University of Science and Technology, Clear Water Bay, Kowloon, Hong Kong; China.
- ⁶¹Department of Physics, National Tsing Hua University, Hsinchu; Taiwan.
- ⁶²IJCLab, Université Paris-Saclay, CNRS/IN2P3, 91405, Orsay; France.
- ⁶³Department of Physics, Indiana University, Bloomington IN; United States of America.
- ⁶⁴(^a) INFN Gruppo Collegato di Udine, Sezione di Trieste, Udine;^(b) ICTP, Trieste;^(c) Dipartimento Politecnico di Ingegneria e Architettura, Università di Udine, Udine; Italy.
- ⁶⁵(^a) INFN Sezione di Lecce;^(b) Dipartimento di Matematica e Fisica, Università del Salento, Lecce; Italy.
- ⁶⁶(^a) INFN Sezione di Milano;^(b) Dipartimento di Fisica, Università di Milano, Milano; Italy.
- ⁶⁷(^a) INFN Sezione di Napoli;^(b) Dipartimento di Fisica, Università di Napoli, Napoli; Italy.
- ⁶⁸(^a) INFN Sezione di Pavia;^(b) Dipartimento di Fisica, Università di Pavia, Pavia; Italy.

- ^{69(a)}INFN Sezione di Pisa;^(b)Dipartimento di Fisica E. Fermi, Università di Pisa, Pisa; Italy.
- ^{70(a)}INFN Sezione di Roma;^(b)Dipartimento di Fisica, Sapienza Università di Roma, Roma; Italy.
- ^{71(a)}INFN Sezione di Roma Tor Vergata;^(b)Dipartimento di Fisica, Università di Roma Tor Vergata, Roma; Italy.
- ^{72(a)}INFN Sezione di Roma Tre;^(b)Dipartimento di Matematica e Fisica, Università Roma Tre, Roma; Italy.
- ^{73(a)}INFN-TIFPA;^(b)Università degli Studi di Trento, Trento; Italy.
- ⁷⁴Institut für Astro- und Teilchenphysik, Leopold-Franzens-Universität, Innsbruck; Austria.
- ⁷⁵University of Iowa, Iowa City IA; United States of America.
- ⁷⁶Department of Physics and Astronomy, Iowa State University, Ames IA; United States of America.
- ⁷⁷Joint Institute for Nuclear Research, Dubna; Russia.
- ^{78(a)}Departamento de Engenharia Elétrica, Universidade Federal de Juiz de Fora (UFJF), Juiz de Fora;^(b)Universidade Federal do Rio De Janeiro COPPE/EE/IF, Rio de Janeiro;^(c)Instituto de Física, Universidade de São Paulo, São Paulo;^(d)Rio de Janeiro State University, Rio de Janeiro; Brazil.
- ⁷⁹KEK, High Energy Accelerator Research Organization, Tsukuba; Japan.
- ⁸⁰Graduate School of Science, Kobe University, Kobe; Japan.
- ^{81(a)}AGH University of Science and Technology, Faculty of Physics and Applied Computer Science, Krakow;^(b)Marian Smoluchowski Institute of Physics, Jagiellonian University, Krakow; Poland.
- ⁸²Institute of Nuclear Physics Polish Academy of Sciences, Krakow; Poland.
- ⁸³Faculty of Science, Kyoto University, Kyoto; Japan.
- ⁸⁴Kyoto University of Education, Kyoto; Japan.
- ⁸⁵Research Center for Advanced Particle Physics and Department of Physics, Kyushu University, Fukuoka ; Japan.
- ⁸⁶Instituto de Física La Plata, Universidad Nacional de La Plata and CONICET, La Plata; Argentina.
- ⁸⁷Physics Department, Lancaster University, Lancaster; United Kingdom.
- ⁸⁸Oliver Lodge Laboratory, University of Liverpool, Liverpool; United Kingdom.
- ⁸⁹Department of Experimental Particle Physics, Jožef Stefan Institute and Department of Physics, University of Ljubljana, Ljubljana; Slovenia.
- ⁹⁰School of Physics and Astronomy, Queen Mary University of London, London; United Kingdom.
- ⁹¹Department of Physics, Royal Holloway University of London, Egham; United Kingdom.
- ⁹²Department of Physics and Astronomy, University College London, London; United Kingdom.
- ⁹³Louisiana Tech University, Ruston LA; United States of America.
- ⁹⁴Fysiska institutionen, Lunds universitet, Lund; Sweden.
- ⁹⁵Centre de Calcul de l'Institut National de Physique Nucléaire et de Physique des Particules (IN2P3), Villeurbanne; France.
- ⁹⁶Departamento de Física Teórica C-15 and CIAFF, Universidad Autónoma de Madrid, Madrid; Spain.
- ⁹⁷Institut für Physik, Universität Mainz, Mainz; Germany.
- ⁹⁸School of Physics and Astronomy, University of Manchester, Manchester; United Kingdom.
- ⁹⁹CPPM, Aix-Marseille Université, CNRS/IN2P3, Marseille; France.
- ¹⁰⁰Department of Physics, University of Massachusetts, Amherst MA; United States of America.
- ¹⁰¹Department of Physics, McGill University, Montreal QC; Canada.
- ¹⁰²School of Physics, University of Melbourne, Victoria; Australia.
- ¹⁰³Department of Physics, University of Michigan, Ann Arbor MI; United States of America.
- ¹⁰⁴Department of Physics and Astronomy, Michigan State University, East Lansing MI; United States of America.
- ¹⁰⁵B.I. Stepanov Institute of Physics, National Academy of Sciences of Belarus, Minsk; Belarus.
- ¹⁰⁶Research Institute for Nuclear Problems of Byelorussian State University, Minsk; Belarus.

- ¹⁰⁷Group of Particle Physics, University of Montreal, Montreal QC; Canada.
- ¹⁰⁸P.N. Lebedev Physical Institute of the Russian Academy of Sciences, Moscow; Russia.
- ¹⁰⁹National Research Nuclear University MEPhI, Moscow; Russia.
- ¹¹⁰D.V. Skobeltsyn Institute of Nuclear Physics, M.V. Lomonosov Moscow State University, Moscow; Russia.
- ¹¹¹Fakultät für Physik, Ludwig-Maximilians-Universität München, München; Germany.
- ¹¹²Max-Planck-Institut für Physik (Werner-Heisenberg-Institut), München; Germany.
- ¹¹³Nagasaki Institute of Applied Science, Nagasaki; Japan.
- ¹¹⁴Graduate School of Science and Kobayashi-Maskawa Institute, Nagoya University, Nagoya; Japan.
- ¹¹⁵Department of Physics and Astronomy, University of New Mexico, Albuquerque NM; United States of America.
- ¹¹⁶Institute for Mathematics, Astrophysics and Particle Physics, Radboud University/Nikhef, Nijmegen; Netherlands.
- ¹¹⁷Nikhef National Institute for Subatomic Physics and University of Amsterdam, Amsterdam; Netherlands.
- ¹¹⁸Department of Physics, Northern Illinois University, DeKalb IL; United States of America.
- ¹¹⁹(^a)Budker Institute of Nuclear Physics and NSU, SB RAS, Novosibirsk; (^b)Novosibirsk State University Novosibirsk; Russia.
- ¹²⁰Institute for High Energy Physics of the National Research Centre Kurchatov Institute, Protvino; Russia.
- ¹²¹Institute for Theoretical and Experimental Physics named by A.I. Alikhanov of National Research Centre "Kurchatov Institute", Moscow; Russia.
- ¹²²(^a)New York University Abu Dhabi, Abu Dhabi; (^b)United Arab Emirates University, Al Ain; (^c)University of Sharjah, Sharjah; United Arab Emirates.
- ¹²³Department of Physics, New York University, New York NY; United States of America.
- ¹²⁴Ochanomizu University, Otsuka, Bunkyo-ku, Tokyo; Japan.
- ¹²⁵Ohio State University, Columbus OH; United States of America.
- ¹²⁶Homer L. Dodge Department of Physics and Astronomy, University of Oklahoma, Norman OK; United States of America.
- ¹²⁷Department of Physics, Oklahoma State University, Stillwater OK; United States of America.
- ¹²⁸Palacký University, Joint Laboratory of Optics, Olomouc; Czech Republic.
- ¹²⁹Institute for Fundamental Science, University of Oregon, Eugene, OR; United States of America.
- ¹³⁰Graduate School of Science, Osaka University, Osaka; Japan.
- ¹³¹Department of Physics, University of Oslo, Oslo; Norway.
- ¹³²Department of Physics, Oxford University, Oxford; United Kingdom.
- ¹³³LPNHE, Sorbonne Université, Université de Paris, CNRS/IN2P3, Paris; France.
- ¹³⁴Department of Physics, University of Pennsylvania, Philadelphia PA; United States of America.
- ¹³⁵Konstantinov Nuclear Physics Institute of National Research Centre "Kurchatov Institute", PNPI, St. Petersburg; Russia.
- ¹³⁶Department of Physics and Astronomy, University of Pittsburgh, Pittsburgh PA; United States of America.
- ¹³⁷(^a)Laboratório de Instrumentação e Física Experimental de Partículas - LIP, Lisboa; (^b)Departamento de Física, Faculdade de Ciências, Universidade de Lisboa, Lisboa; (^c)Departamento de Física, Universidade de Coimbra, Coimbra; (^d)Centro de Física Nuclear da Universidade de Lisboa, Lisboa; (^e)Departamento de Física, Universidade do Minho, Braga; (^f)Departamento de Física Teórica y del Cosmos, Universidad de Granada, Granada (Spain); (^g)Dep Física and CEFITEC of Faculdade de Ciências e Tecnologia, Universidade Nova de Lisboa, Caparica; (^h)Instituto Superior Técnico, Universidade de Lisboa, Lisboa; Portugal.

- ¹³⁸Institute of Physics of the Czech Academy of Sciences, Prague; Czech Republic.
- ¹³⁹Czech Technical University in Prague, Prague; Czech Republic.
- ¹⁴⁰Charles University, Faculty of Mathematics and Physics, Prague; Czech Republic.
- ¹⁴¹Particle Physics Department, Rutherford Appleton Laboratory, Didcot; United Kingdom.
- ¹⁴²IRFU, CEA, Université Paris-Saclay, Gif-sur-Yvette; France.
- ¹⁴³Santa Cruz Institute for Particle Physics, University of California Santa Cruz, Santa Cruz CA; United States of America.
- ¹⁴⁴^(a)Departamento de Física, Pontificia Universidad Católica de Chile, Santiago;^(b)Millennium Institute for Subatomic physics at high energy frontier (SAPHIR), Santiago;^(c)Universidad de la Serena, La Serena;^(d)Universidad Andres Bello, Department of Physics, Santiago;^(e)Instituto de Alta Investigación, Universidad de Tarapacá, Arica;^(f)Departamento de Física, Universidad Técnica Federico Santa María, Valparaíso; Chile.
- ¹⁴⁵Universidade Federal de São João del Rei (UFSJ), São João del Rei; Brazil.
- ¹⁴⁶Department of Physics, University of Washington, Seattle WA; United States of America.
- ¹⁴⁷Department of Physics and Astronomy, University of Sheffield, Sheffield; United Kingdom.
- ¹⁴⁸Department of Physics, Shinshu University, Nagano; Japan.
- ¹⁴⁹Department Physik, Universität Siegen, Siegen; Germany.
- ¹⁵⁰Department of Physics, Simon Fraser University, Burnaby BC; Canada.
- ¹⁵¹SLAC National Accelerator Laboratory, Stanford CA; United States of America.
- ¹⁵²Department of Physics, Royal Institute of Technology, Stockholm; Sweden.
- ¹⁵³Departments of Physics and Astronomy, Stony Brook University, Stony Brook NY; United States of America.
- ¹⁵⁴Department of Physics and Astronomy, University of Sussex, Brighton; United Kingdom.
- ¹⁵⁵School of Physics, University of Sydney, Sydney; Australia.
- ¹⁵⁶Institute of Physics, Academia Sinica, Taipei; Taiwan.
- ¹⁵⁷^(a)E. Andronikashvili Institute of Physics, Iv. Javakhishvili Tbilisi State University, Tbilisi;^(b)High Energy Physics Institute, Tbilisi State University, Tbilisi; Georgia.
- ¹⁵⁸Department of Physics, Technion, Israel Institute of Technology, Haifa; Israel.
- ¹⁵⁹Raymond and Beverly Sackler School of Physics and Astronomy, Tel Aviv University, Tel Aviv; Israel.
- ¹⁶⁰Department of Physics, Aristotle University of Thessaloniki, Thessaloniki; Greece.
- ¹⁶¹International Center for Elementary Particle Physics and Department of Physics, University of Tokyo, Tokyo; Japan.
- ¹⁶²Department of Physics, Tokyo Institute of Technology, Tokyo; Japan.
- ¹⁶³Tomsk State University, Tomsk; Russia.
- ¹⁶⁴Department of Physics, University of Toronto, Toronto ON; Canada.
- ¹⁶⁵^(a)TRIUMF, Vancouver BC;^(b)Department of Physics and Astronomy, York University, Toronto ON; Canada.
- ¹⁶⁶Division of Physics and Tomonaga Center for the History of the Universe, Faculty of Pure and Applied Sciences, University of Tsukuba, Tsukuba; Japan.
- ¹⁶⁷Department of Physics and Astronomy, Tufts University, Medford MA; United States of America.
- ¹⁶⁸Department of Physics and Astronomy, University of California Irvine, Irvine CA; United States of America.
- ¹⁶⁹Department of Physics and Astronomy, University of Uppsala, Uppsala; Sweden.
- ¹⁷⁰Department of Physics, University of Illinois, Urbana IL; United States of America.
- ¹⁷¹Instituto de Física Corpuscular (IFIC), Centro Mixto Universidad de Valencia - CSIC, Valencia; Spain.
- ¹⁷²Department of Physics, University of British Columbia, Vancouver BC; Canada.
- ¹⁷³Department of Physics and Astronomy, University of Victoria, Victoria BC; Canada.

- ¹⁷⁴Fakultät für Physik und Astronomie, Julius-Maximilians-Universität Würzburg, Würzburg; Germany.
- ¹⁷⁵Department of Physics, University of Warwick, Coventry; United Kingdom.
- ¹⁷⁶Waseda University, Tokyo; Japan.
- ¹⁷⁷Department of Particle Physics and Astrophysics, Weizmann Institute of Science, Rehovot; Israel.
- ¹⁷⁸Department of Physics, University of Wisconsin, Madison WI; United States of America.
- ¹⁷⁹Fakultät für Mathematik und Naturwissenschaften, Fachgruppe Physik, Bergische Universität Wuppertal, Wuppertal; Germany.
- ¹⁸⁰Department of Physics, Yale University, New Haven CT; United States of America.
- ^a Also at Borough of Manhattan Community College, City University of New York, New York NY; United States of America.
- ^b Also at Bruno Kessler Foundation, Trento; Italy.
- ^c Also at Center for High Energy Physics, Peking University; China.
- ^d Also at Centro Studi e Ricerche Enrico Fermi; Italy.
- ^e Also at CERN, Geneva; Switzerland.
- ^f Also at CPPM, Aix-Marseille Université, CNRS/IN2P3, Marseille; France.
- ^g Also at Département de Physique Nucléaire et Corpusculaire, Université de Genève, Genève; Switzerland.
- ^h Also at Departament de Física de la Universitat Autònoma de Barcelona, Barcelona; Spain.
- ⁱ Also at Department of Financial and Management Engineering, University of the Aegean, Chios; Greece.
- ^j Also at Department of Physics and Astronomy, Michigan State University, East Lansing MI; United States of America.
- ^k Also at Department of Physics and Astronomy, University of Louisville, Louisville, KY; United States of America.
- ^l Also at Department of Physics, Ben Gurion University of the Negev, Beer Sheva; Israel.
- ^m Also at Department of Physics, California State University, East Bay; United States of America.
- ⁿ Also at Department of Physics, California State University, Fresno; United States of America.
- ^o Also at Department of Physics, California State University, Sacramento; United States of America.
- ^p Also at Department of Physics, King's College London, London; United Kingdom.
- ^q Also at Department of Physics, St. Petersburg State Polytechnical University, St. Petersburg; Russia.
- ^r Also at Department of Physics, University of Fribourg, Fribourg; Switzerland.
- ^s Also at Faculty of Physics, M.V. Lomonosov Moscow State University, Moscow; Russia.
- ^t Also at Faculty of Physics, Sofia University, 'St. Kliment Ohridski', Sofia; Bulgaria.
- ^u Also at Giresun University, Faculty of Engineering, Giresun; Turkey.
- ^v Also at Graduate School of Science, Osaka University, Osaka; Japan.
- ^w Also at Hellenic Open University, Patras; Greece.
- ^x Also at Institutio Catalana de Recerca i Estudis Avancats, ICREA, Barcelona; Spain.
- ^y Also at Institut für Experimentalphysik, Universität Hamburg, Hamburg; Germany.
- ^z Also at Institute for Particle and Nuclear Physics, Wigner Research Centre for Physics, Budapest; Hungary.
- ^{aa} Also at Institute of Particle Physics (IPP); Canada.
- ^{ab} Also at Institute of Physics, Azerbaijan Academy of Sciences, Baku; Azerbaijan.
- ^{ac} Also at Institute of Theoretical Physics, Iliia State University, Tbilisi; Georgia.
- ^{ad} Also at Instituto de Física Teórica, IFT-UAM/CSIC, Madrid; Spain.
- ^{ae} Also at Istanbul University, Dept. of Physics, Istanbul; Turkey.
- ^{af} Also at Joint Institute for Nuclear Research, Dubna; Russia.
- ^{ag} Also at Moscow Institute of Physics and Technology State University, Dolgoprudny; Russia.
- ^{ah} Also at National Research Nuclear University MEPhI, Moscow; Russia.

ai Also at Physikalisches Institut, Albert-Ludwigs-Universität Freiburg, Freiburg; Germany.

aj Also at The City College of New York, New York NY; United States of America.

ak Also at TRIUMF, Vancouver BC; Canada.

al Also at Università di Napoli Parthenope, Napoli; Italy.

am Also at University of Chinese Academy of Sciences (UCAS), Beijing; China.

an Also at Yeditepe University, Physics Department, Istanbul; Turkey.

* Deceased